

University of Windsor

## Scholarship at UWindor

---

Electronic Theses and Dissertations

Theses, Dissertations, and Major Papers

---

1-1-2007

### Integrated Assessment and Improvement of the Quality Assurance System for the Cosworth Casting Process.

Dilon Yousif  
*University of Windsor*

Follow this and additional works at: <https://scholar.uwindsor.ca/etd>

---

#### Recommended Citation

Yousif, Dilon, "Integrated Assessment and Improvement of the Quality Assurance System for the Cosworth Casting Process." (2007). *Electronic Theses and Dissertations*. 7175.  
<https://scholar.uwindsor.ca/etd/7175>

This online database contains the full-text of PhD dissertations and Masters' theses of University of Windsor students from 1954 forward. These documents are made available for personal study and research purposes only, in accordance with the Canadian Copyright Act and the Creative Commons license—CC BY-NC-ND (Attribution, Non-Commercial, No Derivative Works). Under this license, works must always be attributed to the copyright holder (original author), cannot be used for any commercial purposes, and may not be altered. Any other use would require the permission of the copyright holder. Students may inquire about withdrawing their dissertation and/or thesis from this database. For additional inquiries, please contact the repository administrator via email ([scholarship@uwindsor.ca](mailto:scholarship@uwindsor.ca)) or by telephone at 519-253-3000ext. 3208.

Integrated Assessment and Improvement of the Quality Assurance System for the Cosworth  
Casting Process

By  
Dilon Yousif

A Thesis Submitted to the  
Faculty  
of Graduate Studies  
Through Engineering Materials  
in Partial Fulfillment of the Requirements for the  
Degree of Master of Applied Science at the  
University of Windsor

Windsor, Ontario, Canada  
2007  
© 2007, Dilon Yousif



Library and Archives  
Canada

Published Heritage  
Branch

395 Wellington Street  
Ottawa ON K1A 0N4  
Canada

Bibliothèque et  
Archives Canada

Direction du  
Patrimoine de l'édition

395, rue Wellington  
Ottawa ON K1A 0N4  
Canada

*Your file* *Votre référence*  
ISBN: 978-0-494-70597-1  
*Our file* *Notre référence*  
ISBN: 978-0-494-70597-1

**NOTICE:**

The author has granted a non-exclusive license allowing Library and Archives Canada to reproduce, publish, archive, preserve, conserve, communicate to the public by telecommunication or on the Internet, loan, distribute and sell theses worldwide, for commercial or non-commercial purposes, in microform, paper, electronic and/or any other formats.

The author retains copyright ownership and moral rights in this thesis. Neither the thesis nor substantial extracts from it may be printed or otherwise reproduced without the author's permission.

---

In compliance with the Canadian Privacy Act some supporting forms may have been removed from this thesis.

While these forms may be included in the document page count, their removal does not represent any loss of content from the thesis.

**AVIS:**

L'auteur a accordé une licence non exclusive permettant à la Bibliothèque et Archives Canada de reproduire, publier, archiver, sauvegarder, conserver, transmettre au public par télécommunication ou par l'Internet, prêter, distribuer et vendre des thèses partout dans le monde, à des fins commerciales ou autres, sur support microforme, papier, électronique et/ou autres formats.

L'auteur conserve la propriété du droit d'auteur et des droits moraux qui protègent cette thèse. Ni la thèse ni des extraits substantiels de celle-ci ne doivent être imprimés ou autrement reproduits sans son autorisation.

---

Conformément à la loi canadienne sur la protection de la vie privée, quelques formulaires secondaires ont été enlevés de cette thèse.

Bien que ces formulaires aient inclus dans la pagination, il n'y aura aucun contenu manquant.

  
**Canada**

## ABSTRACT

The purpose of this study was to improve the Quality Assurance (QA) System at the Nemak Windsor Aluminum Plant (WAP). The project used Six Sigma method based on Define, Measure, Analyze, Improve, and Control (DMAIC). Analysis of in process melt at WAP was based on chemical, thermal, and mechanical testing. The control limits for the W319 Al Alloy were statistically recalculated using the composition measured under stable conditions. The “Chemistry Viewer” software was developed for statistical analysis of alloy composition. This software features the Silicon Equivalency ( $Si_{EQ}$ ) developed by the IRC. The Melt Sampling Device (MSD) was designed and evaluated at WAP to overcome traditional sampling limitations. The Thermal Analysis “Filters” software was developed for cooling curve analysis of the 3XX Al Alloy(s) using IRC techniques. The impact of low melting point impurities on the start of melting was evaluated using the Universal Metallurgical Simulator and Analyzer (UMSA).

## **DEDICATION**

I dedicate this thesis to my parents, my family, and friends for their great support and encouragement during the course of this project.

## ACKNOWLEDGEMENTS

I would like to thank my supervisor, Dr. Jerry H. Sokolowski, for his support and guidance during my time as a graduate student and a team member of the NSERC/Ford-Nemak/University of Windsor Industrial Research Chair (IRC) in Light Metals Casting Technology. I greatly appreciate the valuable opportunities and assistance received from the Ford Motor Company, Nemak of Canada Corporation, Natural Sciences and Engineering Research Council of Canada (NSERC), Foundry Educational Foundation (FEF), and American Foundry Society (AFS).

I would like to extend my thanks to the outside program reader Dr. N. Zamani, program reader Dr. D. Northwood, and Dr. H. Henry as the chair of examination committee.

I wish to express my appreciation to Ellen Moosberger for her invaluable support during my studies. My thanks to the IRC team members for sharing a great experience during the years of work and for all of their support.

Thanks to the WAP engineers, especially John Burford, Dr. Azita Ariapour, Dr. G. E. Byczynski, and the Canadian Auto Workers (CAW) who made it possible to complete this work. Thanks to the staff at the Nemak Engineering Centre (NEC) and Technical Support Centre (TSC) at the University of Windsor for their efforts.

Thanks to Drs. Wojciech Kasprzak and Robin Francis for their invaluable partnership and to Dr. W. T. Kierkus, as well as Dr. M. Djurdjevic for their support and technical guidance.

Thanks to my family and friends for their great support and encouragement.

## TABLE OF CONTENTS

<b>ABSTRACT.....</b>	<b>iii</b>
<b>DEDICATION.....</b>	<b>iv</b>
<b>ACKNOWLEDGMENT.....</b>	<b>v</b>
<b>TABLE OF CONTENTS.....</b>	<b>vi</b>
<b>LIST OF TABLES.....</b>	<b>vii</b>
<b>LIST OF FIGURES.....</b>	<b>viii</b>
<b>LIST OF APPENDECIS.....</b>	<b>xi</b>
<b>LIST OF INTELLECTUAL PROPERTY CLAIMS.....</b>	<b>xii</b>
<b>NOMENCLATUTRE.....</b>	<b>xiii</b>
<b>1 INTRODUCTION.....</b>	<b>1</b>
1.1 The Ford - Nematik Windsor Aluminum Plant.....	2
1.2 Cosworth Precision Sand Casting Process.....	2
1.3 Research Objectives.....	15
<b>2 REVIEW OF THE LITERATURE .....</b>	<b>16</b>
2.1 Ten Rules for Good Casting .....	16
2.2 Hypoeutectic Aluminum Silicon Alloys.....	25
2.3 Heat Treatment.....	36
2.4 Cooling Curve Analysis.....	39
2.5 Chemical Spectroscopy Analysis.....	40
2.6 Gas Comparative Analysis.....	42
2.7 Radiography Analysis .....	42
2.8 Brinell Hardness Analysis.....	43
2.9 Six Sigma DMAIC Method for Process Improvement.....	45
2.10 Statistical Quality Control.....	45
<b>3 METHODOLOGY OF EXPERIMENTS .....</b>	<b>49</b>
3.1 Introduction.....	49
3.2 Chemical Analysis .....	49
3.3 Dissolved Hydrogen Gas Analysis .....	53
3.4 Radiography Analysis .....	53
3.5 Hardness Analysis.....	53
3.6 Heating Curve Analysis .....	56
3.7 Cooling Curve Analysis.....	60
<b>4 RESULTS AND DISCUSSION .....</b>	<b>66</b>
4.1 Recalculation of the W319 Al Alloy Control Limits.....	66
4.2 Development of “Chemistry Viewer” Software for 3XX Al Alloy(s) .....	76
4.3 Development of Thermal Analysis “Filters” Software for 3XX Al Alloy(s) ...	82
4.4 Development of Melt Sampling Device .....	89
4.5 Results Summary .....	91
<b>5 CONCLUSIONS .....</b>	<b>92</b>
<b>APPENDIX.....</b>	<b>93</b>
<b>REFERENCES.....</b>	<b>94</b>

**VITA AUCTORIS.....97**



## LIST OF TABLES

Table 2.1. Heat treatment codes (Matweb, 2005).....	28
Table 2.2. Mechanical properties of common Al alloys (Matweb, 2005).....	28
Table 2.3. Chemical specification limits for common Al alloys (Matweb, 2005).....	28
Table 2.4. Relative Characteristics of Common Al Alloys (Matweb, 2005).....	29
Table 2.5. Algorithm to calculate $Si_{EQ}$ in multi component hypoeutectic Al alloys (Djurdjevic, et al., 2003). .....	31
Table 2.6. 3XX Al Alloy Solidification Characteristics and As Cast Mechanical Properties Predicted Using $Si_{EQ}$ (Djurdjevic, et al., 1998).....	32
Table 3.1. Summary of data collected from the WAP production process.....	50
Table 3.2. Cooling curve characteristics for the W319 Al alloy ().....	61
Table 4.1. Evaluation Analysis of the WAP Chemical Control Limits. ....	69
Table 4.2. Evaluation analysis of the proposed WAP chemical control limits.....	74
Table 4.3. Statistical analysis of the WAP brinell hardness and porosity. ....	74

## LIST OF FIGURES

Figure 1.1 Cosworth Low Pressure Sand Casting Process Flow Diagram.....	4
Figure 1.2 The ford 3.0L V6 duratec engine (WAP, 2003).....	5
Figure 1.3. Thermal expansions of zircon, chromite, olivine, and silica (Dupont, 2006)..	5
Figure 1.4. WAP 3.0L V6 engine block sand mold package (WAP, 2004).....	5
Figure 1.5. CPSCP quiescent melt flow through the melt processing stages. ....	8
Figure 1.6. Reverbratory melt holding furnace.....	8
Figure 1.7. Argon rotary impeller degassing unit (Pyrotek, 2005).....	9
Figure 1.8. Cosworth electromagnetic pump.....	9
Figure 1.9. Mold fill profile analysis pump voltage vs. fill time plot.....	10
Figure 1.10. WAP casting pump carousal system. ....	12
Figure 1.11. Mold rollover, TSR, and partial solution treatment. ....	12
Figure 1.12. WAP quality inspection tests and process operations. ....	14
Figure 2.1. Hydrogen solubility in Al (Campbell, 2004).....	17
Figure 2.2. Effect of melt filtering on al alloy(s) mechanical properties (Campbell, 2004). .....	17
Figure 2.3. Turbulence avoided using bottom gating instead of top gating (Campbell, 2004).....	18
Figure 2.4. Excessive melt velocity results in folded oxides in the casting (Campbell, 2004).....	18
Figure 2.5. Slow moving melt results in undesired horizontal flow (Campbell, 2004)....	20
Figure 2.6. Bubble damage caused by a badly designed fill system (Campbell, 2004)..	20
Figure 2.7. Bubble damage caused by core out gassing (Campbell, 2004).....	21
Figure 2.8. Software used to identify distinct feeding areas (Cast Solutions, 2006).....	21
Figure 2.9. Software used to determine the proper size of risers (Cast Solutions, 2006).	21
Figure 2.10. Convection loops re-melt casting during solidification (Campbell, 2004)..	23
Figure 2.11. Convection loops eliminated by oversized risers (Campbell, 2004).....	23
Figure 2.12. Segregation in different areas due to a slow or fast cooling rate (Campbell, 2004).....	24
Figure 2.13. Effect of cooling rate from the solution treatment temperature on the ductility of the as cast Al bar (Campbell, 2004). ....	24
Figure 2.14. Micrographs of typical as-cast W319 Al sample (Kasprzak, et al., 2001)...	29
Figure 2.15. Modified and unmodified Silicon in 319 and 380 Al alloys (Guthy, 2002).	29
Figure 2.16. Micrographs of Copper rich phases in a W319 sample (Djurdjevic, et al., 2001).....	31
Figure 2.17. Micrographs of Iron phases in a W319 sample (Djurdjevic, et al., 2001)..	31
Figure 2.18. Micrographs of various types of porosity in the w319 al alloy sample (Triveño, et al., 2003).....	34
Figure 2.19. a) Schematic of a shrinkage pore in 3D and.....	34
Figure 2.20. Effect of porosity on Al alloys ultimate tensile strength (Monroe, 2004)....	35
Figure 2.21. Effect of dissolved hydrogen on casting porosity (Monroe, 2004).....	35
Figure 2.22. WAP Melt Thermal Treatment and Cast Component Heat Treatment T7 Temperature Time Schedule. ....	37
Figure 2.23. Phase Diagram and TTT Diagram for Aluminum Copper Alloy (Roberts, 2006).....	37

Figure 2.24. Effect of Artificial Aging on Hardness of Al-Cu Alloy (b), and schematic diagram of Al-Cu precipitates (a) and (c) (Roberts, 2006). .....	38
Figure 2.25. Phase diagram (a) correlation to the cooling curve (b) for Al-Si Alloys (Sparkman, et. al., 1994). .....	41
Figure 2.26. Increase of sensitivity using a 16 bit instead of a 12 bit AD converter (Sparkman, et. al., 1994). .....	41
Figure 2.27. Spark emissions represent precise element concentrations (ARL, 2006). ...	41
Figure 2.28. Reduced pressure test or Straube-Pfeiffer test used for hydrogen analysis..	44
Figure 2.29. X-Ray radiographs of Al alloy solidified under 0.01 atm (left), and 1 atm (right) (Campbell, 2004). .....	44
Figure 2.30. Calculation of BHN for the brinell hardness test (Instron, 2006). .....	44
Figure 2.31. Define Measure Analyze Improve Control (DMAIC) road map (i Six Sigma, 2006).....	47
Figure 2.32. Control charts using individual moving average XmR and Tukey method.	47
Figure 2.33. Advantage of using tukey control charts (i Six Sigma 2005).....	48
Figure 2.34. Danger of using fixed limits instead of statistically calculated limits (i Six Sigma 2005). .....	48
Figure 3.1. Design of experiments for WAP plant wide quality assessment.....	50
Figure 3.2. Sampling plan for OES analysis and Hydrogen analysis at WAP. ....	51
Figure 3.3. ARL 3460 Metal Analyzer Spectrometer for Metal Analysis (ARL, 2006)..	52
Figure 3.4. ASTM Type B Mold and OES Test Sample (ARL, 2006).....	52
Figure 3.5. Visual Rating Standard for the Reduced Pressure Test (WAP, 2004). .....	54
Figure 3.6. X-Radiography Porosity Analysis of Engine Block Bulkhead Sections.....	55
Figure 3.7. Hardness Brinell Analysis of Engine Block Bulkhead Sections. ....	55
Figure 3.8. Heating and cooling curve analysis using UMSA (Kasprzak, et al. 2002). ...	57
Figure 3.9. Heating / cooling curves and 1 <sup>st</sup> derivative for the W319 Al alloy sample (Kasprzak, et al., 2002). .....	58
Figure 3.10. Description of UMSA Samples Extracted from Ingots, Melts, and Castings (Kasprzak, et al., 2002). .....	59
Figure 3.11. Cooling curve analysis temperature – time with baseline plot and temperature 1 <sup>st</sup> derivative – time plot for the W319 Al alloy Sample from WAP. ....	62
Figure 3.12. Cooling curve analysis - temperature 1 <sup>st</sup> derivative - temperature with baseline plot and fraction solid – temperature plot for the W319 Al alloy Sample from WAP. ....	62
Figure 3.13. Schematic diagram of the MSD. ....	63
Figure 3.14. Cooling curve analysis using the MSD. ....	64
Figure 3.15. Sand cup used for cooling curve analysis with the Alu-Delta equipment... ..	65
Figure 4.1. Run Chart for Tin in the W319 Al Alloy Processed at WAP.....	69
Figure 4.2 Hardness Analysis of the Engine Block Bulkheads Cast at WAP. ....	70
Figure 4.3. Normal Probability of Tin in the W319 Al Alloy Processed at WAP.....	70
Figure 4.4. Histogram Plot of Tin in the W319 Al Alloy Processed at WAP. ....	71
Figure 4.5. Box Plot of Tin in the W319 Al Alloy Processed at WAP. ....	71
Figure 4.6. Heating Curve Analysis Featuring Temperature – Time Plot. ....	72
Figure 4.7. Heating curve analysis featuring temperature 1 <sup>st</sup> derivative – temperature plot. ....	72

Figure 4.8. Effect of different levels of tin in W319 Al alloy on the start of melting temperature measured by UMSA heating curve analysis. ....	73
Figure 4.9. Run chart for brinell hardness of engine blocks cast at WAP. ....	75
Figure 4.10. Run chart for porosity analysis of engine blocks cast at WAP. ....	75
Figure 4.11. 2003 WAP Original OES Chemical Analysis Procedure. ....	77
Figure 4.12. Proposed New Chemical Analysis Procedure for the in Process W319 Al Alloy. ....	78
Figure 4.13. Screen Shot of the Control Window in the “Chemistry Viewer” Software. ....	79
Figure 4.14. “Chemistry Viewer” Example of the Tukey Control Chart. ....	79
Figure 4.15. “Chemistry Viewer” Example of Histogram Plot. ....	80
Figure 4.16. “Chemistry Viewer” Example of Box and Whisker Plot. ....	80
Figure 4.17. “Chemistry Viewer” Example of Histogram Plot. ....	81
Figure 4.18. “Chemistry Viewer” Example of Running Variance Plot. ....	81
Figure 4.19. Procedure for Cooling Curve Analysis of Al-Si Alloys. ....	83
Figure 4.20. Quick Reference User Guide for “Filters” Software. ....	84
Figure 4.21. Control Window for SPC Analysis of Archived Cooling Curve Characteristics. ....	85
Figure 4.22. Cooling Curve Analysis Featuring Temperature – Time Plot (Left Y Axis) and Temperature 1 <sup>st</sup> Derivative – Time Plot with Baseline (Right Y Axis), and Summary of the Solidification Characteristics. ....	86
Figure 4.23. Cooling Curve Analysis Featuring Temperature 1 <sup>st</sup> Derivative – Time Plot with Baseline and Fraction Solid – Time Plot. ....	86
Figure 4.24. Cooling Curve Analysis Featuring Temperature 1 <sup>st</sup> Derivative – Temperature Plot with Baseline and Fraction Solid – Temperature Plot. ....	87
Figure 4.25. Cooling Curve Analysis Featuring Temperature - Time Plot. ....	87
Figure 4.26. Cooling Curve Analysis with Time, Temperature, and Temperature Derivative. ....	88
Figure 4.27. Comparison of the Cooling Curve Sensitivity Between the Alu-Delta TA System, the MSD developed by IRC, and the 3.0L Engine Block In-Situ TA. ....	90

LIST OF APPENDICES

Appendix I WAP Experimental Data (on attached CD)

## LIST OF INTELLECTUAL PROPERTY CLAIMS

The author claims the ownership of the following original ideas as Intellectual Properties that were developed within the scope of this thesis.

- Development of a stand alone executable software called “Chemistry Viewer” for analysis of the chemical composition for multi-component alloys. The software could be used to plot statistical analysis charts and calculate a descriptive statistical summary for any selected element measured during a specified period of time. The software could be used to predict as cast material properties for 3XX Al Alloy(s) using the  $Si_{EQ}$  technique.
- Development of a Melt Sampling Device (MSD), to collect melt samples for online cooling curve analysis, was conducted with Mr. J. Burford, Drs. J. Sokolowski and M. Djurdjevic. The unbiased melt sample could be taken from any depth in the furnace without any detrimental melt disturbance. The device features a low thermal mass hollow steel test cup with a separate end cap.
- Development of a stand alone executable software called “Filters” for cooling curve analysis of 3XX Al Alloy(s). The built in algorithms include Savitsky-Golay noise and differentiation filters, which was used in the cooling curve processing procedures developed by the IRC team (Kierkus, et al., 1999).

## NOMENCLATURE

AD Converter	Analog to Digital Converter
AFS	American Foundry Society
AITAP	Aluminum Thermal Analysis Platform
ASTM	American Society for Testing and Materials
BCT	Body Centered Tetragonal
CAW	Canadian Auto Workers
CMM	Computerized Measurement Machine
CPSCP	Cosworth Precision Sand Casting Process
CTQ	Critical To Quality
DMAIC	Define Measure Analyze Improve Control
EM	Electromagnetic
FCC	Face Centered Cubic
FEF	Foundry Educational Foundation
GUI	Graphical User Interface
BHN	Brinell Hardness Number
IRC	NSERC/Ford-Nemak/University of Windsor Industrial Research Chair in Light Metals Casting Technology
LCL	Lower Control Limit
MSD	Melt Sampling Device
NEC	Nemak Engineering Centre
NSERC	Natural Sciences and Engineering Research Council of Canada
OES	Optical Emission Spectroscopy
PI	Performance Index
QA	Quality Assurance
QC	Quality Control
Si <sub>EQ</sub>	Silicon Equivalency
SiML	Silicon Modification Level
SPC	Statistical Process Control
SSSS	Super Saturated Solid Solution
TA	Thermal Analysis
TSC	Technical Support Centre – University of Windsor
TSR	Thermal Sand Reclamation
TTT	Time Temperature Transformation
UCL	Upper Control Limit
UMSA	Universal Metallurgical Simulator and Analyzer
WAP	Windsor Aluminum Plant - Nemak of Canada Corporation
XmR	Individuals and Moving Range

# 1 INTRODUCTION

A continuous improvement in quality is required to ensure that metal casting will continue to play a vital role in today's manufacturing industry. The need for high quality castings requires the use of more complex processes like the Cosworth Precision Sand Process (CPSCP). Comprehensive and effective QA must be enforced to closely control the known critical-to-quality parameters. This study focused on the development of analysis software and testing equipment for QA of the W319 Al Alloy. The Six Sigma DMAIC methodology was followed to conduct experiments at WAP for improvement of the QA system. Known critical to quality parameters were monitored through analysis of ingots, melts, and castings. Valid process control limits for the W319 Al Alloy composition were established based on the statistical analysis of data collected at WAP. The proposed solutions developed in this study are ready to be commercially implemented at any other Al foundry facility. Two software applications were developed during this study for 3XX Al Alloy(s) OES melt composition analysis and cooling curve analysis. The first software called "Chemistry Viewer" was developed for statistical analysis of the multi-component alloy composition. The  $Si_{EQ}$  method developed by the IRC was integrated into the "Chemistry Viewer" to predict as cast material properties for the 3XX Al Alloy(s). The second software called "Filters" was developed for the data post processing required to perform 3XX Al Alloy(s) cooling curve analysis. The IRC analysis techniques to determine the baseline equation were integrated into the "Filters" software to determine the fraction solid and the latent heat. The experimental literature data from the IRC and from other sources was integrated into the "Filters" software to predict as cast material properties for the 3XX Al Alloy(s). Heating curve experiments were conducted using the UMSA to determine the effect of the alloy chemical composition at the start of the melting temperature. The approach used in this study for conducting experiments and data analysis could be implemented at any foundry to improve the QC system.



## **1.1 The Ford - Nematik Windsor Aluminum Plant**

WAP is a joint venture between the Nematik of Canada Corporation and the Ford Motor Company, and is a state of the art foundry producing a variety of V6 and V8 engine blocks. This plant uses one of the first applications of the CPSCP in North America. The original process was improved by Ford engineers after using the roll over technique to reduce casting cycle time. The casting process at WAP is described in Figure 1.1. Originally the Electromagnetic (EM) pump filled the mold from bottom to top, and then maintained pressure until solidification was complete. The improved process is based on the rollover technique where the filled mold is rotated 180° along the axis of the runner system. This allows for the transfer of the mold away from the casting station while solidification continues just like a traditional casting. The mold assembly at is automated with robots except for a few delicate manual assemblies. WAP was the first casting plant in the world to achieve certification for the ISO 14001 Environmental Management Standard. Many environmental initiatives have been included such as 99.8% sand recycling, and dry machining without coolant (WAP, 2004). The Duratec 3.0L V6 casting is the most produced product at WAP, see Figure 1.2 (WAP, 2004).

## **1.2 Cosworth Precision Sand Casting Process**

The CPSCP is a low pressure process developed for production of premium quality Al Alloy(s) castings for the automotive industry. The sand precision casting term implies a near net shape designed to minimize machining. This process grew as a result of problems in the car racing industry during the 1970s such as porosity, random dimensional errors, and early fatigue failures, which limited design performance and reliability. After achieving success in the racing industry, the CPSCP process was extended into high volume production. This section further describes the CPSCP process.

### **1.2.1 Sand Core Making**

Zircon Sand is used instead of traditional Silica sand due to low thermal expansion, resistance to metal reactions, reduced cleaning of the casting, low binder requirements, high thermal conductivity, and high bulk density. Low thermal expansion results in less core movement during casting as shown in Figure 1.3 (Dupont, 2006). The high bulk density of Zircon is much closer to Al than Silica requiring less core glue and allowing for ability to cast thin walls (Cosworth, 2005). More than 99% of recycled sand is used for making new cores. Sand quality is controlled through the American Society for Testing and Materials (ASTM) sieve test to determine grain size distribution. The sand particles are mixed with a two part binder and formed into a core shape in the cold box process at room temperature to form cores with good tensile strength, hot strength, and dimensional stability. Ashland Specialty Chemical Company produces a patented two part binder called ISOCURE, which is used at WAP. The typical blend is 55% of Part I Phenol-Formaldehyde, and Part II Polymeric Isocyanate with solvents and additives. The sand binder mixture hardens instantly after purging Triethyl-Amine as a catalyst gas to produce Phenolic Urethane polymer (Bakhtiyarov, 2000). This is followed by air purging to distribute and remove the residual catalyst gas.

### **1.2.2 Mold Package Assembly**

Molding consists of the operations necessary to prepare the mold to receive the melt such as the assembly of internal cores, adding in-mold grain refiners, adding cast in components, and closing the mold. Sand cores placed inside the mold cavity form the casting interior surfaces. A fully assembled mold consists of several interlocked cores as shown in Figure 1.4 (WAP, 2004). The mold is designed to eliminate pressure build up during filling by venting air out through the clearance between the cores. In mold liners made of cast iron are integrated as part of the complete mold package. These liners must be carefully handled to avoid surface contamination (CMI, 2005). The liner shot blasting strengthens the liner to casting surface interface. It is important to add new shot media to avoid liner surface contamination caused by fine shot. The grain size distribution of the Shot blast media could be controlled through the ASTM sieve analysis. The liners are preheated just before casting to reduce the effects of thermal shock on the melt.

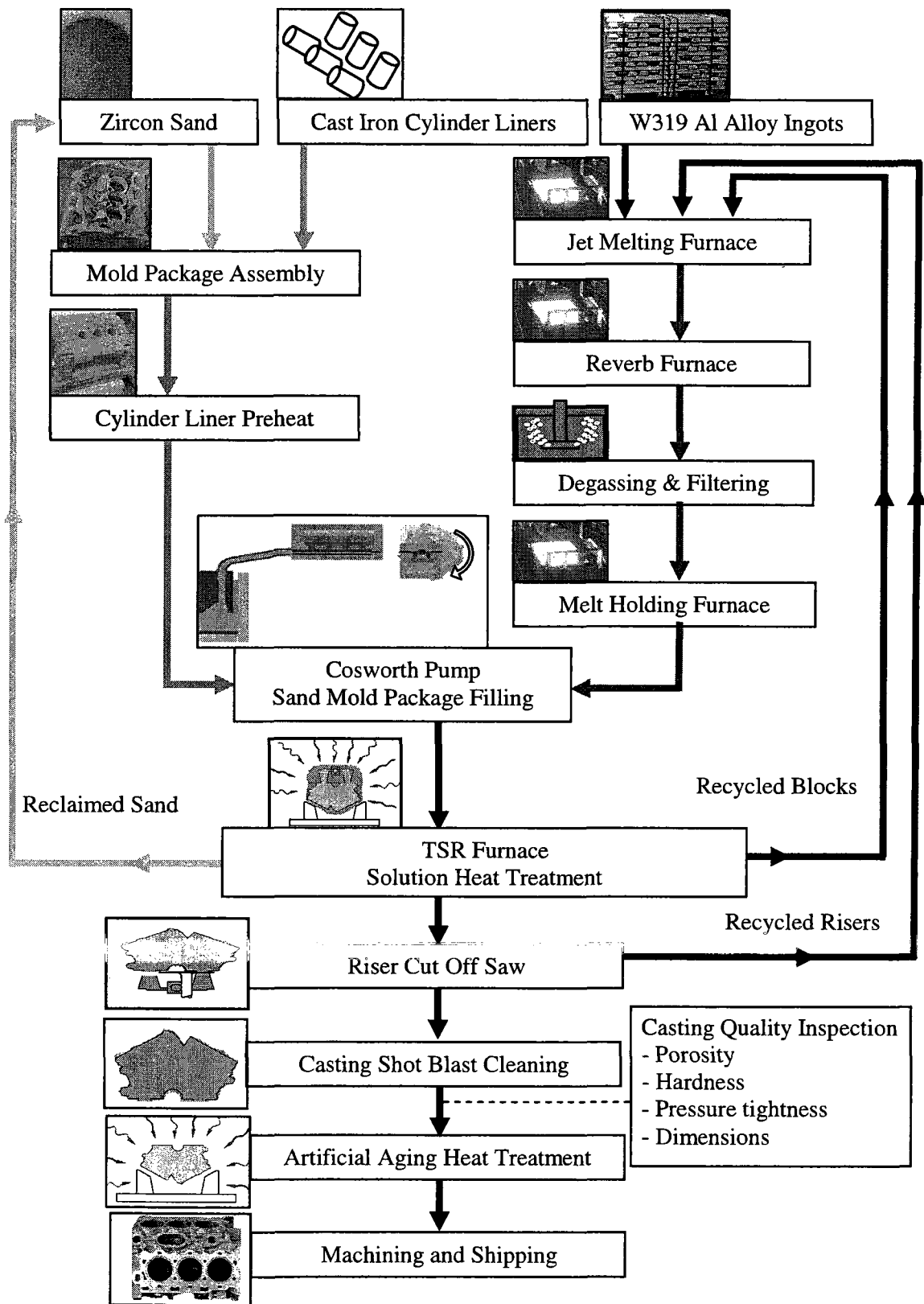


Figure 1.1 Cosworth Low Pressure Sand Casting Process Flow Diagram

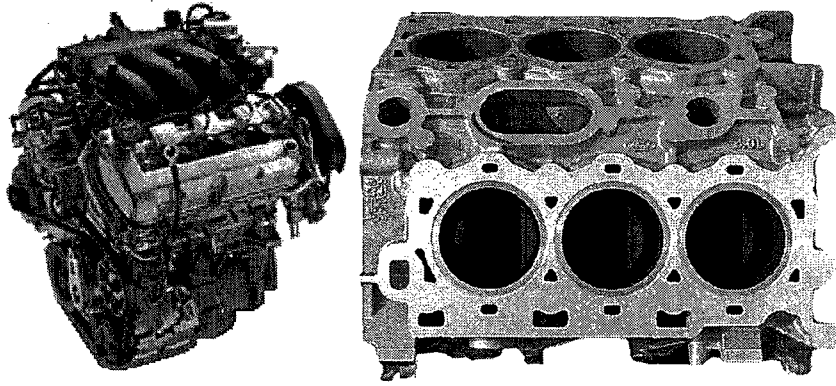


Figure 1.2 The Ford 3.0L V6 Duratec engine (WAP, 2003).  
 (left) the assembled Ford's 3.0L V6 Duratec engine  
 (right) the WAP engine block casting for Ford's 3.0L V6 Duratec engine

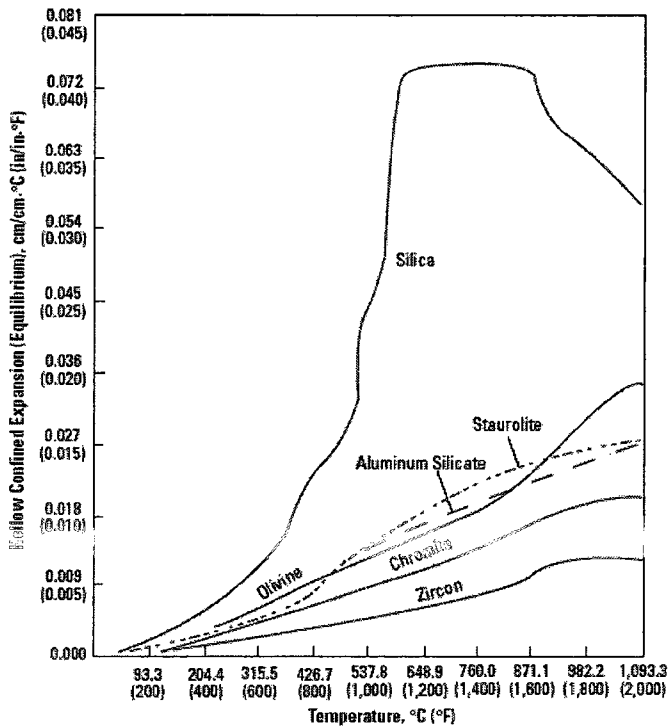


Figure 1.3. Thermal expansions of zircon, chromite, olivine, and silica (Dupont, 2006).

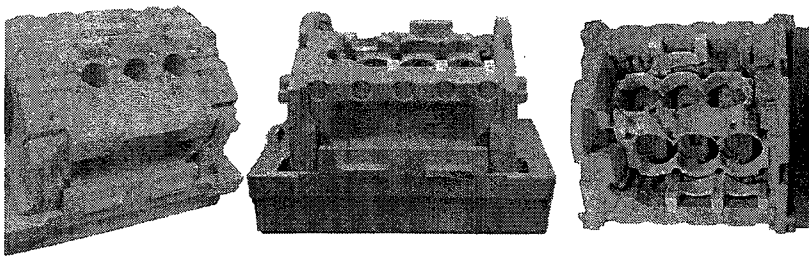


Figure 1.4. WAP 3.0L V6 engine block sand mold package (WAP, 2004).

### 1.2.3 W319 Al Alloy Melt Processing

The important advantage of using the CPSCP melt process is the quiescent flow that avoids unnecessary disturbances of the melt as shown in Figure 1.5 and Figure 1.6. The dry charges of solid metal consisting of ingots and casting returns are positioned on a sloping hearth above the level of molten metal so that the entire charge is completely enveloped by hot gases. The solid metal rapidly absorbs the melting heat and drains from the sloping hearth into the wet holding basin. Although reverberatory furnaces normally rely on fuel for heating, dry hearth furnaces may use electric energy instead. The melt is protected against oxidation and thermal shock by using a blanket of inert Nitrogen gas that allows longer times for furnace melt holding. There is no limit on the type or size of melt holding furnace since the system is not pressurized, and could be easily accessed for cleaning, and analysis. Holding the melt for several hours in a large furnace allows for sufficient time for suspended oxides and other insoluble inclusions to either float or sink. The separation process occurs very slowly as oxides with entrapped air have small differences in density. A significant proportion of inclusions may have, by chance, neutral buoyancy and may never separate. Therefore, effective removal of the residual inclusions is achieved by melt filtering and degassing. Melt degassing with an inert gas such as Argon is used to remove the dissolved Hydrogen that forms gas porosity and exaggerates shrinkage porosity. The most common degassing method is rotary impeller degassing using Argon gas as shown in Figure 1.7 (Pyrotek, 2005). Mono-atomic dissolved hydrogen either diffuses into the gas bubbles or forms diatomic hydrogen gas at the bubble surface. The diffusion occurs due to a difference in partial pressure between the melt and the Argon bubbles. At the same time, oxides are captured by the rising bubbles and float to the top surface.

### 1.2.4 Electromagnetic Pump

The EM pump is used to inject the cleanest melt into the mold from the middle depth of the furnace as shown in Figure 1.9 **Figure 1.8**. The EM pump is based on Faradays principle to pump the melt without using any moving parts. The melt is drawn from the middle depth of the furnace to avoid the risk of oxide transfer into the mold. A ceramic porous disk placed at the base of the pump filters the melt before entering the

pump intake opening. The melt flow rate must be controlled to reduce turbulence inside the mold and eliminate the formation of harmful oxide films (Cosworth, 2005). The IRC researched root causes of pump clogging and developed practical solutions to avoid problems in production (Sokolowski, et al., 2005). The computerized pump control system adjusts pump power based on the fill level inside the mold, which is indirectly detected by a capacitive antenna placed on the top of the mold. The fill profile analysis of the pump voltage and the level signal voltage can be performed for each produced casting, see Figure 1.10. The fill level signal is affected by the initial contact between the rising melt and the in-mold cast iron liners. The roll over operation of the mold is automated by the rotating carousel station positioned in front of the pump station. The carousel has four rotating cages that perform the following steps shown in Figure 1.11 and Figure 1.12.

1. Mold Receive:

- A robot loads the empty mold package inside the mold cage.
- A level antenna plate is pressed on top to lock the mold in position.
- A carousel rotates 90° to position the mold in front of the pump station.

2. Mold Fill and Roll Over:

- A launder system is pressed against the mold to eliminate leaks during filling.
- A pump injects the melt into the mold until the full level is reached.
- The mold is overturned by rotating the cage 180° along the axis of the runner system, which reduces the damaging effects of the convection loops.
- The pump pressure is maintained to achieve pressure assisted feeding.
- The pump is turned off to allow for drain back of the melt in the runner system, which reduces the amount of scrap metal and simplifies the riser cut off.
- The carousel rotates 90° degrees to index the filled mold.

3. Mold Index:

- The filled mold continues to solidify with the hottest metal at the top section just like a traditional gravity casting with a riser feeding system.

4. Mold Remove:

- A robot removes the filled mold from the cage.
- A carousel rotates 90° degrees to position the mold cage for the next cycle.

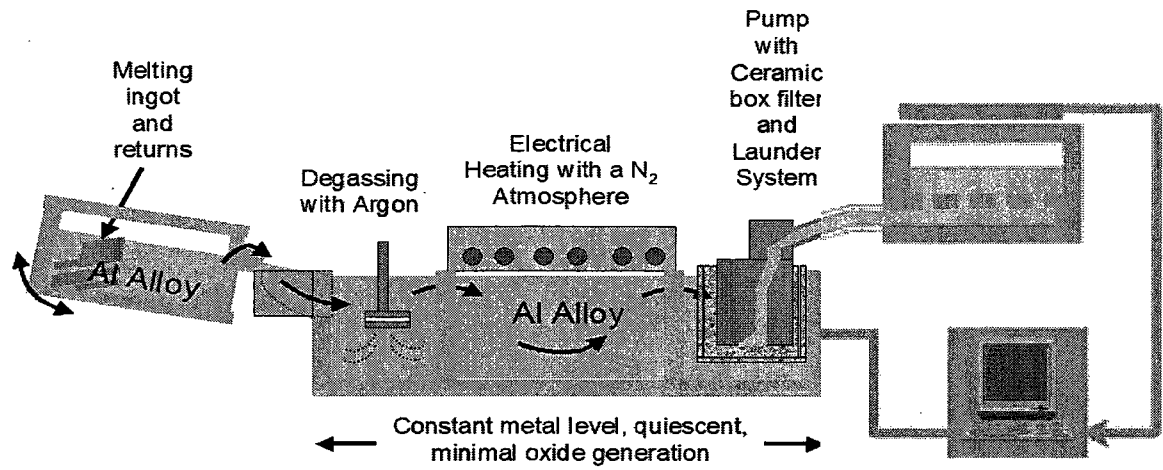


Figure 1.5. CPSCP quiescent melt flow through the melt processing stages.

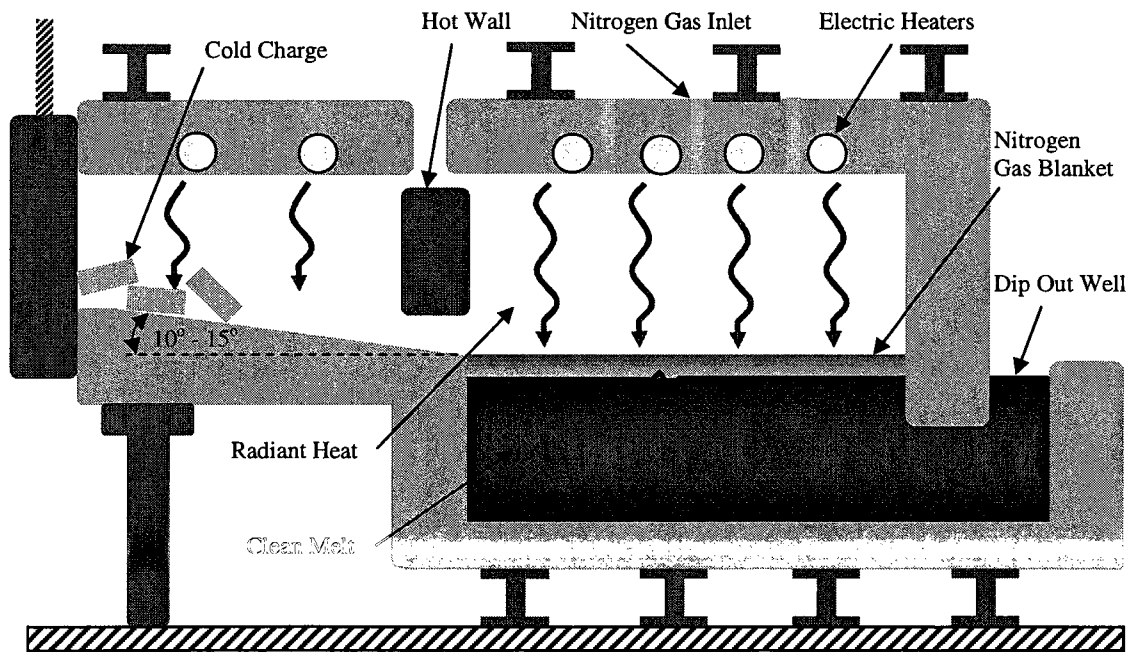


Figure 1.6. Reverbatory melt holding furnace.

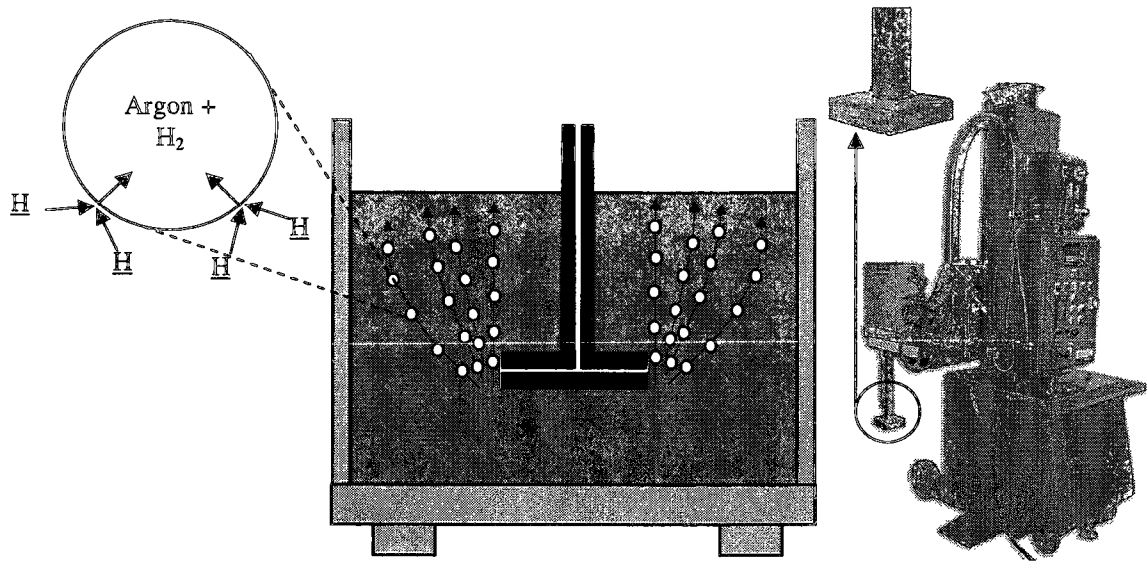


Figure 1.7. Argon rotary impeller degassing unit (Pyrotek, 2005).

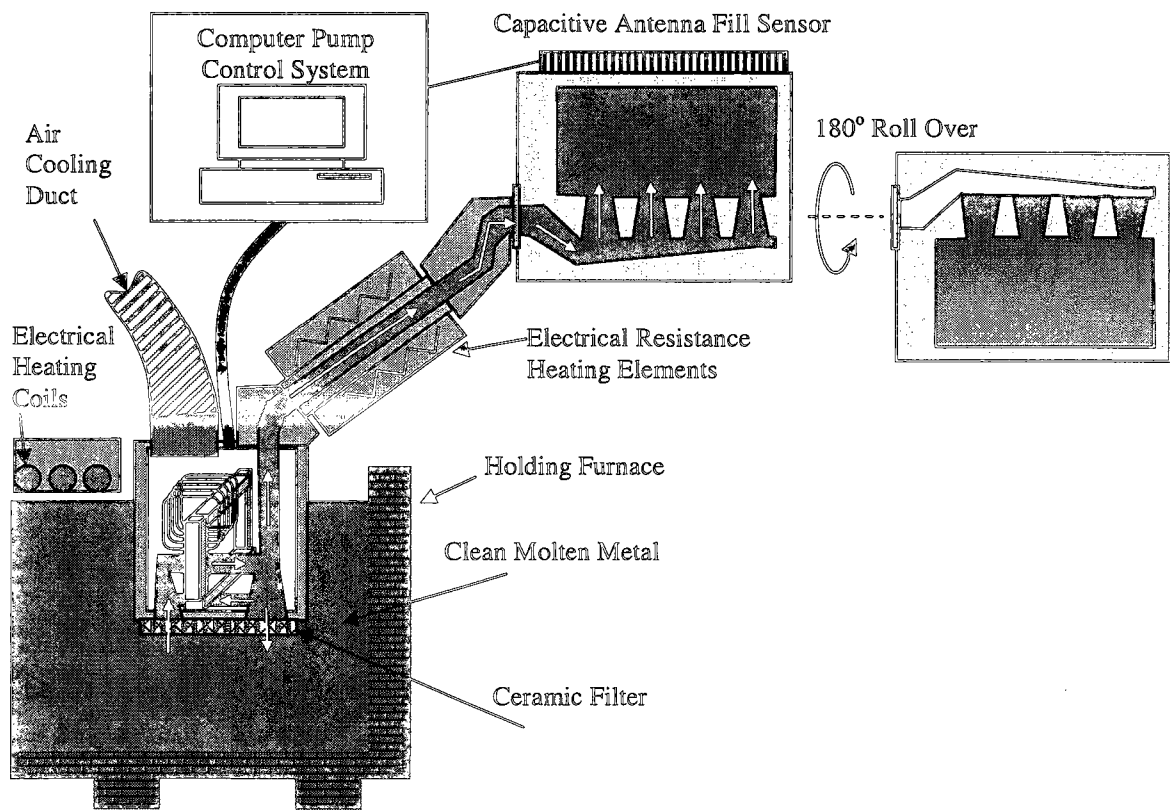
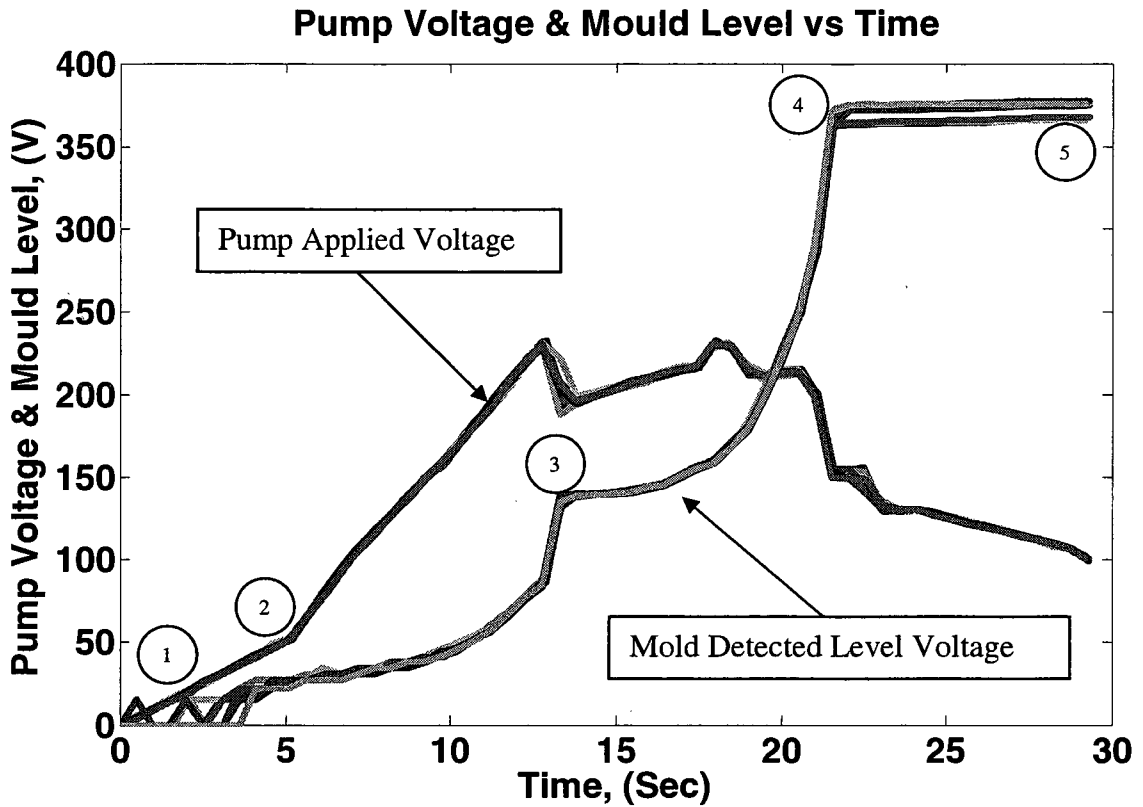


Figure 1.8. Cosworth electromagnetic pump.





Fill Stage #	Description
1	Mold Fill begins using fixed ramp up rate for pump voltage
2	Pump switches to automatic fill based on level capacitor sensor signal
3	Mold fill level sensor sharp increase due to effect of initial contact between the rising liquid metal and the in-mold cast iron liners
4	Fill level complete and mold fixture starts to roll over the mold
5	Mold completes roll over rotation and is moved away from the pump

Figure 1.9. Mold fill profile analysis pump voltage vs. fill time plot.

### **1.2.5 Thermal Sand Removal (TSR)**

The casting solidifies in the sand mold package that is transferred to the TSR continuous furnace set at 500°C for 6 hours. The casting goes through partial solution treatment in the TSR furnace while the sand is thermally separated from the casting. The applied heat breaks down the resin holding the sand particles together. The fallen sand is collected using a conveyer belt system and then reconditioned by removing fine particles and burning off residual resin. New cores are made using 99% of the reconditioned sand mixed with 1% new sand. The castings exit the TSR furnace with an air quench. Air quench is used to eliminate concerns about residual stresses and dimensional variations caused by using a more severe quench media like water. The furnace heat allows Cu rich phases to partially dissolve into the Al matrix (Djurdjevic, et al., 2001). The risers on each casting are cut with a band saw. The castings go through cleaning by shot blasting to remove any sand from the internal passages. The cut risers along with production scrap castings are returned to the melting furnace.

### **1.2.6 Heat Treatment**

Aluminum casting alloys develop their properties as a result of heat treatment that generally involves solution treatment, quench, and aging. In solution treatment, the casting is heated into the single-phase zone on the phase diagram without exceeding the eutectic temperature. Segregation must be avoided to take the most advantage of the solution treatment to avoid local melting of low melting point segregation pockets. These areas melt during heat treatment but do not re-solidify with the proper structure, thereby substantially decreasing casting properties. After solution heat treatment, the castings are quenched to retain strengthening alloying elements in a supersaturated solution. The quenched castings go through an aging treatment at intermediate temperatures. The aging treatment could be varied to control specific properties to a desired specification. The reheating during aging results in precipitation of Super Saturated Solid Solution (SSSS) phases that strengthen the casting. An annealing treatment could be employed to remove residual stresses; however, annealing destroys the effects of the aging treatment. The final properties developed depend on the cast component chemical composition, structure and heat treatment settings.

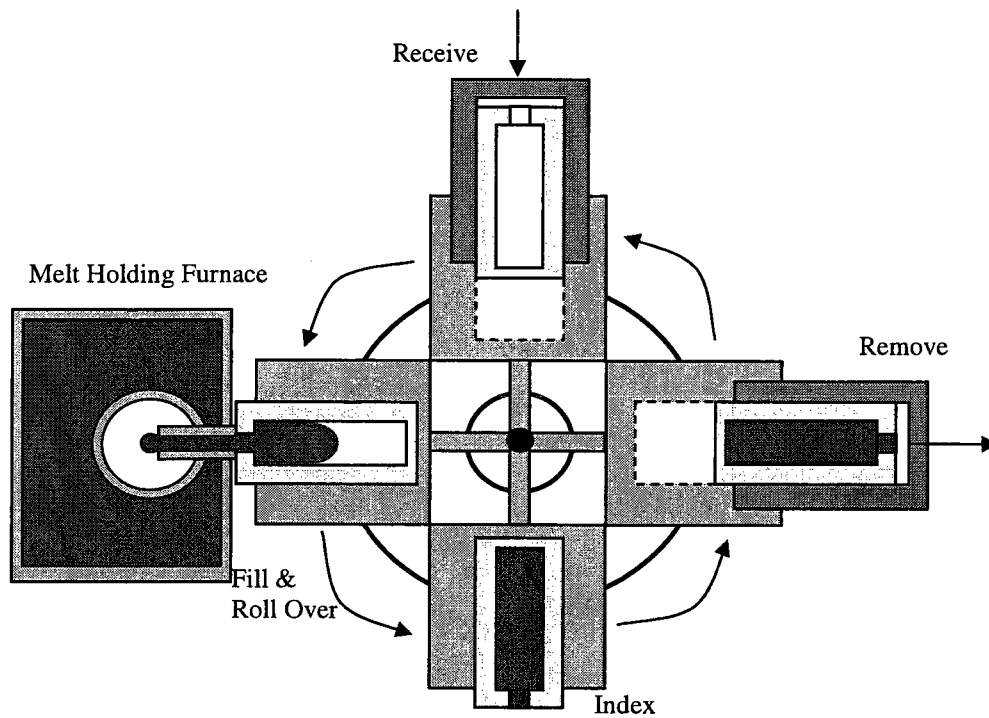


Figure 1.10. WAP casting pump carousel system.

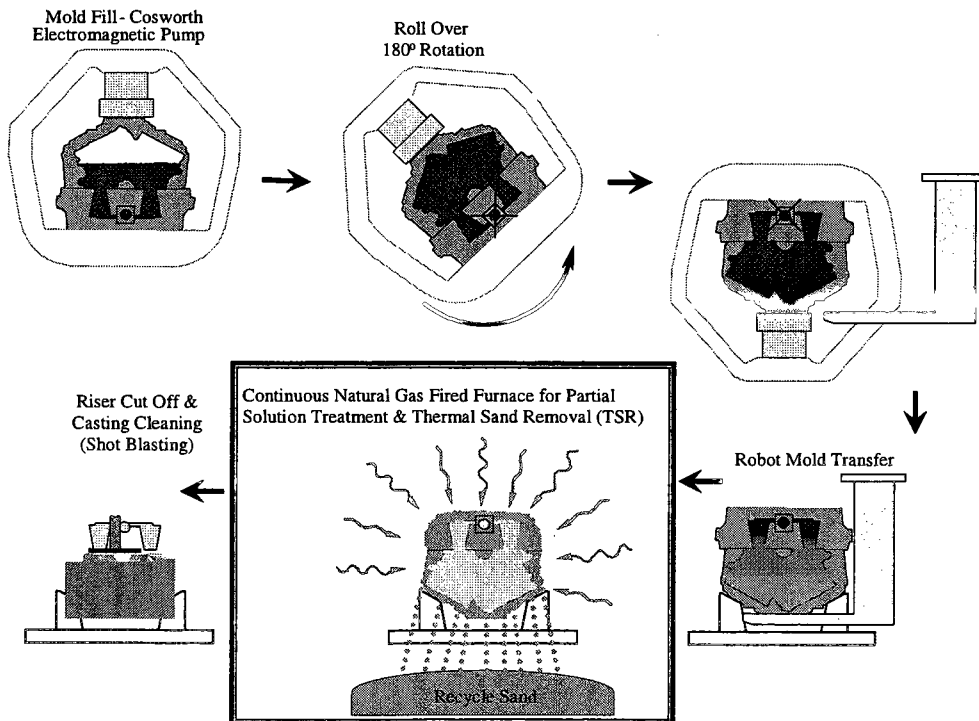


Figure 1.11. Mold rollover, TSR, and partial solution treatment.

### 1.2.7 Casting Process Quality Assurance

The task of QA is to regulate the quality of the raw materials, assemblies, products and components as well as management of production and inspection processes. The goal is to ensure that the product fulfills or exceeds customer expectations. There are several critical to quality inspections performed at WAP at different processing stages as described in Figure 1.13 **Figure 1.12**, which include:

- Ingot – Received from approved suppliers
  - Chemical composition analysis
- Melt- In process at melt holding furnaces
  - Chemical composition analysis
  - Hydrogen content analysis
  - Solidification characteristics analysis
- Sand – Zircon Sand
  - Grain size distribution analysis for new and used sand
- Cylinder Liners
  - Grain size distribution analysis for new and used shot blast media
- Casting – Engine block inner bulkhead sections
  - Hardness analysis before artificial aging treatment
  - Hardness analysis after artificial aging treatment
  - Porosity analysis near surface exposed after rough machining
  - Porosity analysis (gas and shrinkage)

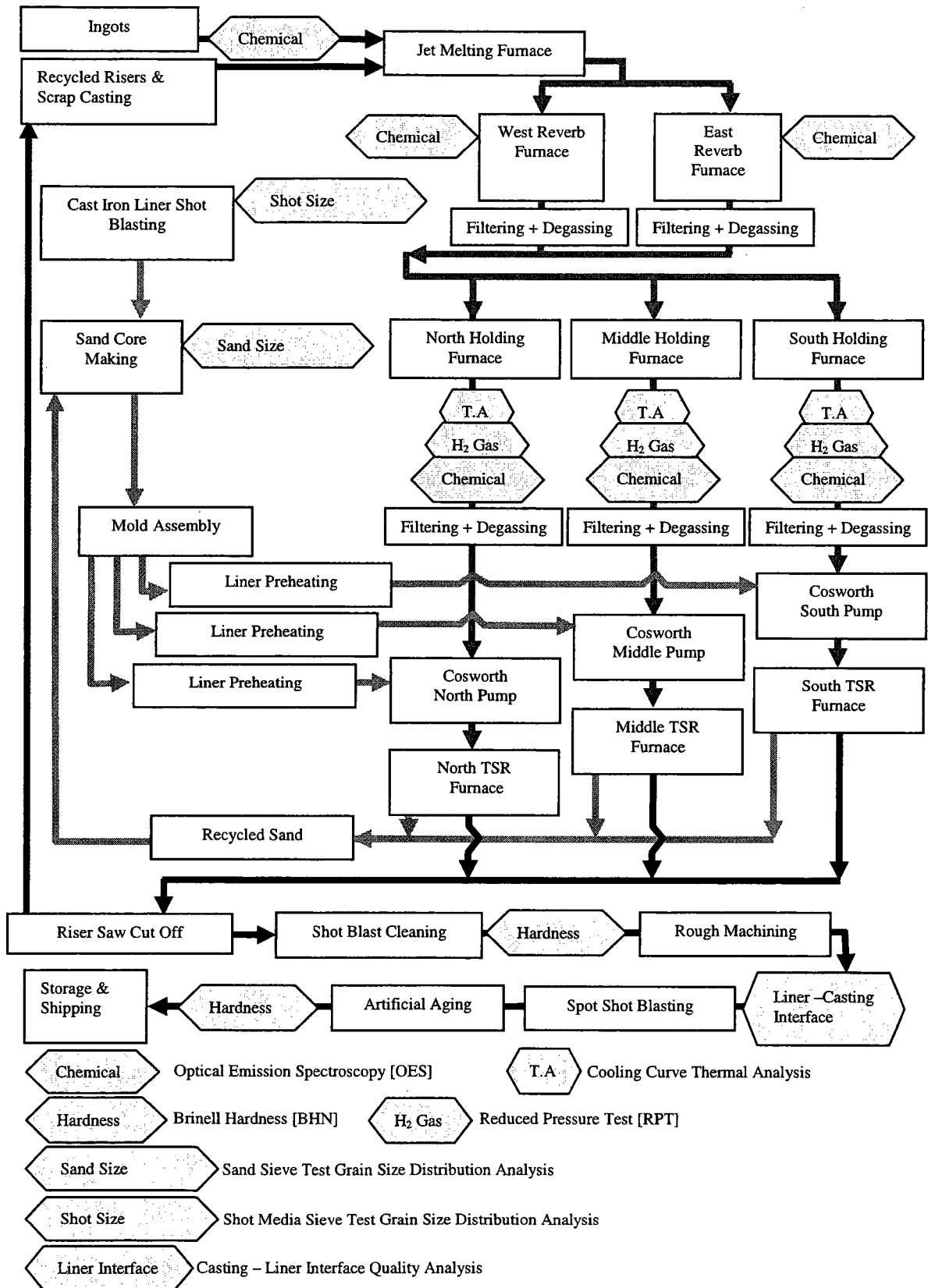


Figure 1.12. WAP quality inspection tests and process operations.

### 1.3 Research Objectives

The major objectives of this thesis were to develop QC analysis software programs and testing equipment for processing Al Alloy(s) melt. The following is a list of the tasks required to achieve the major objectives:

1. To develop software for statistical analysis of the chemical composition for multi-component Al Alloy(s). The software should also predict as cast material properties for 3XX Al Alloy(s) using the  $Si_{EQ}$  technique, which was developed by the IRC.
2. To develop software for cooling curve analysis of 3XX Al Alloy(s). The software must automatically detect characteristic points on the cooling curve and on the corresponding first derivative curve. The latent heat and fraction solid must be calculated using the baseline techniques developed by the IRC.
3. To develop a testing device for collecting melt furnace samples and perform online cooling curve analysis. The device must overcome the limitations of the traditional melt sampling techniques that use a steel ladle and a sand test cup.

## 2 REVIEW OF THE LITERATURE

### 2.1 Ten Rules for Good Casting

Casting is the process used to produce objects by pouring molten material into a cavity called a mold, which is the negative of the object, and allowing them to cool and solidify. The ten rules for producing good quality castings are outlined by Dr. John Campbell which are discussed in this section (Campbell, 2004).

Rule one is to provide a good quality melt. Immediately prior to casting, the melt shall be prepared and treated, if necessary, using the best current practices. The aim is to provide a melt at the correct temperature, correct chemistry, low residual levels of dissolved gas, and insoluble inclusions. Inclusions like oxide films may be introduced into the melt by poor handling techniques such as pouring the melt from furnaces and ladles. The recommendation is to reduce the melt drop distance below 100 mm and preferably below 50 mm where melt pouring is a must. The melt must be degassed as the solubility of the dissolved hydrogen in the melt abruptly decreases as shown in Figure 2.1 (Campbell, 2004), and may encourage the formation of porosity. Filtering of the melt oxides is required to avoid harmful effects on the casting mechanical properties as shown in Figure 2.2 (Campbell, 2004). Holding the melt for several hours may improve quality by allowing the suspended oxides to either sink to the bottom or float to the surface for skimming.

Rule two is to avoid liquid metal front damage. The velocity of the liquid metal front or the meniscus should be less than 0.5 m/s. It is difficult to control melt velocity in a traditional gravity casting without causing turbulence and melt splashing as shown in Figure 2.3 (Campbell, 2004). The damaging effect of high melt velocity is shown in Figure 2.4 (Campbell, 2004) as oxide film and air are entrapped in the bulk of the melt. This maximum melt velocity may be raised only in sections thinner than the critical sessile height to avoid droplet formation and splashing.

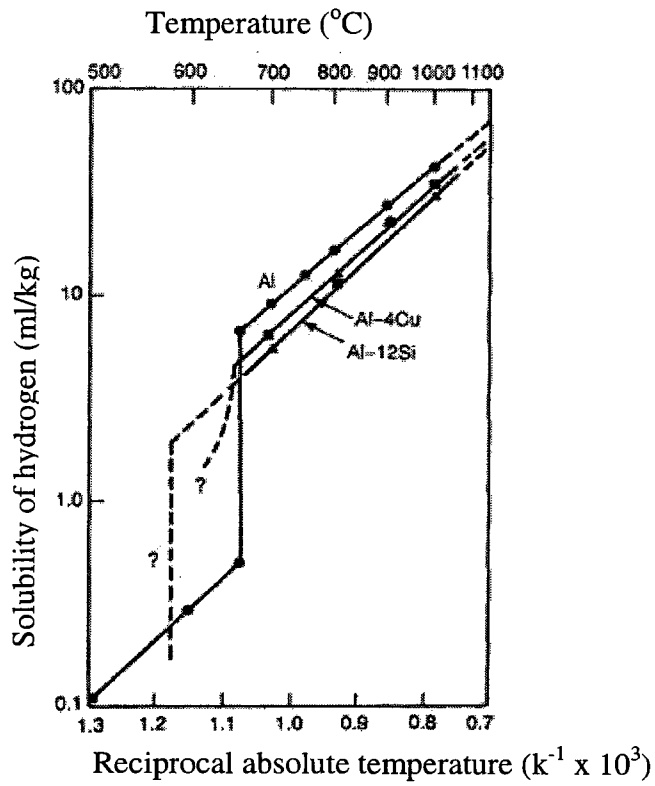


Figure 2.1. Hydrogen solubility in Al (Campbell, 2004).

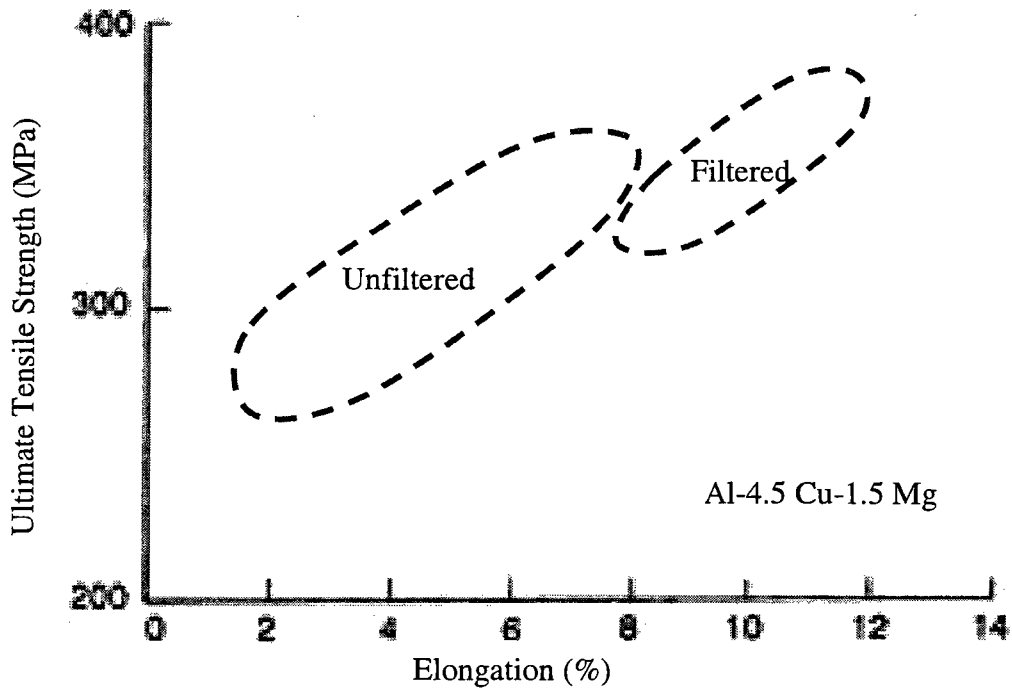


Figure 2.2. Effect of melt filtering on al alloy(s) mechanical properties (Campbell, 2004).



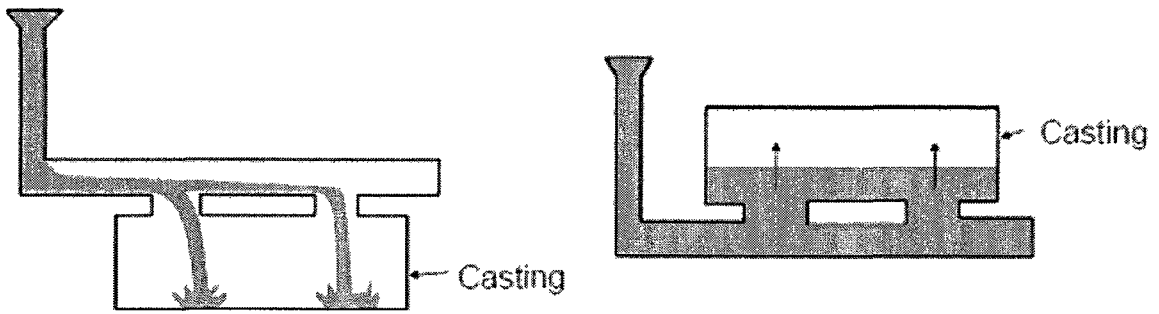


Figure 2.3. Turbulence avoided using bottom gating instead of top gating (Campbell, 2004).

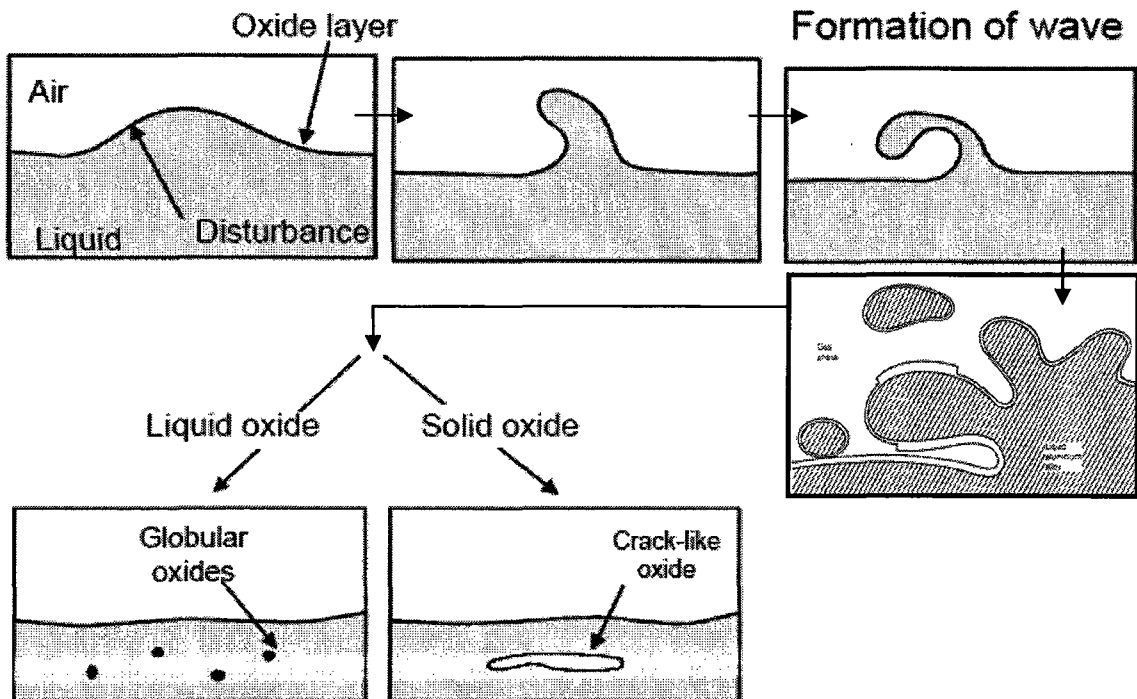


Figure 2.4. Excessive melt velocity results in folded oxides in the casting (Campbell, 2004).

Rule three is to avoid liquid front stop. The liquid metal front should not go too slowly, or more exactly, not stop at any time. The advancing melt meniscus must be kept "alive" or moving and free from thick oxide film that gets entrapped in the casting. The meniscus must experience continuous uninterrupted upward advances without extensive horizontal sections or waterfall effects as shown in Figure 2.5 (Campbell, 2004). The concept is to allow oxide formation on the melt front to break up and slide off to form a casting skin. If the melt front stops for a long time it may freeze creating a "cold lap" that acts as a crack in the casting. The mold gates should be placed at a very low point in the casting to avoid the "waterfall" condition. Horizontal surfaces in castings should be avoided by casting design, or by tilting the mold, or by filling at a sufficient speed.

Rule four is to avoid bubble damage. No air bubbles should be entrained in the casting runner system that eventually pass through the melt into the mold. The result of this defect is a mixture of oxide bubble trails, together with residual bubbles in the casting as shown in Figure 2.6 (Campbell, 2004). This is by far the most common source of porosity defect in castings, and is commonly mistaken for shrinkage porosity as bubbles trails are often irregularly shaped. The fill system should be designed to reduce bubble formation.

Rule five is to avoid core gas blow out. Gases from cores should not be allowed to pass through the melt in the mold. Core blows cause a rather different type of defect than the entrained air bubbles leading to huge defects, filling whole areas at the top of the castings. Even a small blow from a core can leave a bubble trail that can create a leak defect as shown in Figure 2.7 (Campbell, 2004). This is avoided by using cores with low gas content and proper mold ventilation.

Rule six is to avoid shrinkage damage. Avoid using uphill feeders because of an unreliable pressure gradient. Gravity aided downhill feeding should be used by positioning risers well above the top of the casting. This could be avoided by using a reliable computer modeling package to properly design the riser feeding system. The simulation software could be used to identify distinct feeding areas that must be served by risers as shown in Figure 2.8 (Cast Solutions, 2006). The software is then used to determine the size of the risers that would be sufficient to eliminate formation of the internal shrinkage porosity in the casting as shown in Figure 2.9 (Cast Solutions, 2006).

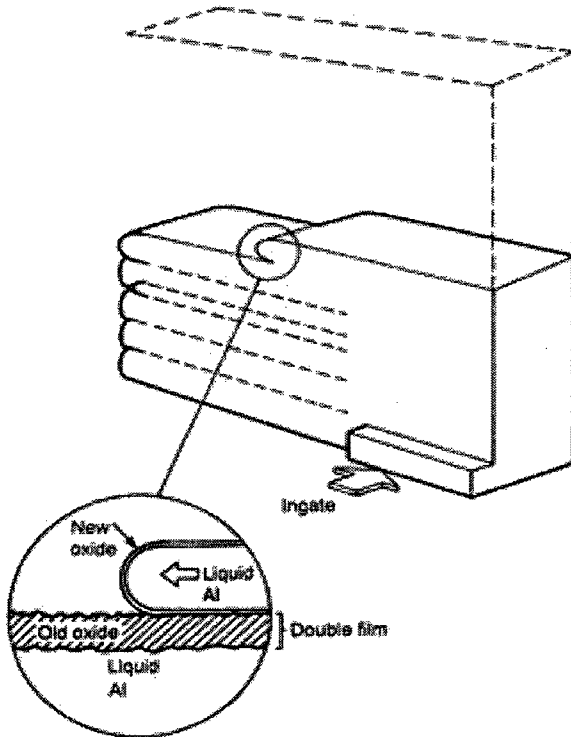


Figure 2.5. Slow moving melt results in undesired horizontal flow (Campbell, 2004).

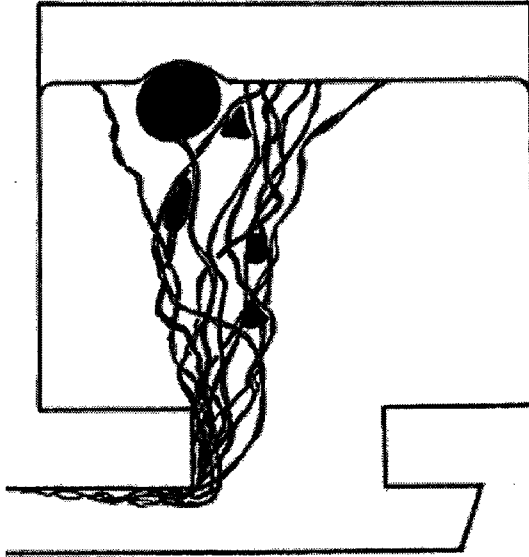


Figure 2.6. Bubble damage caused by a badly designed fill system (Campbell, 2004).

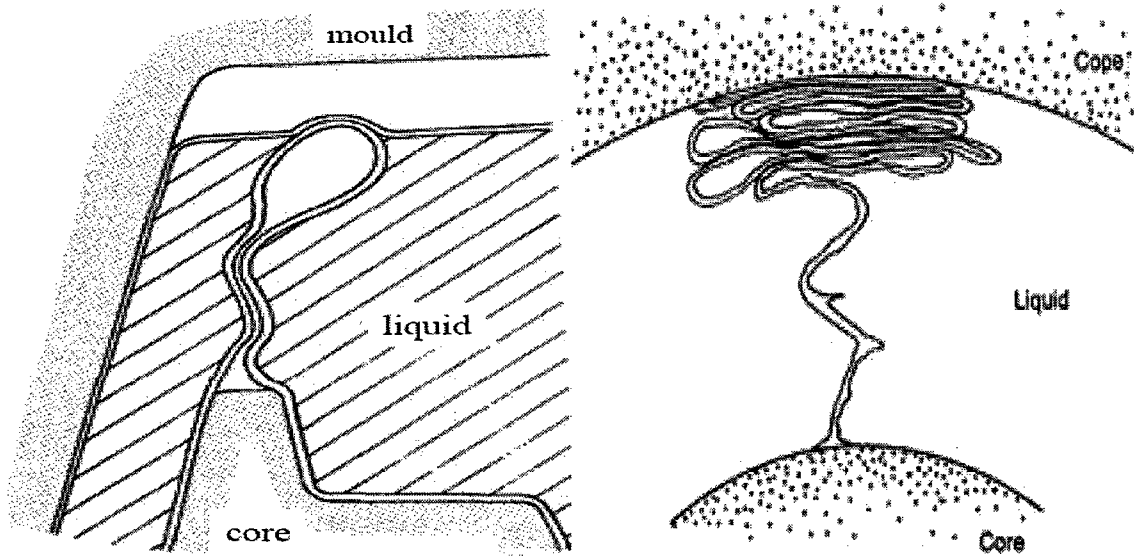


Figure 2.7. Bubble damage caused by core out gassing (Campbell, 2004).

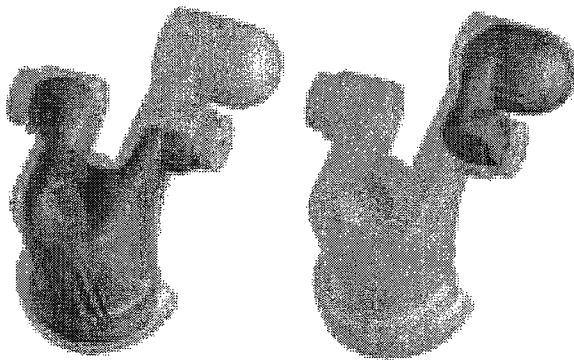


Figure 2.8. Software used to identify distinct feeding areas (Cast Solutions, 2006).

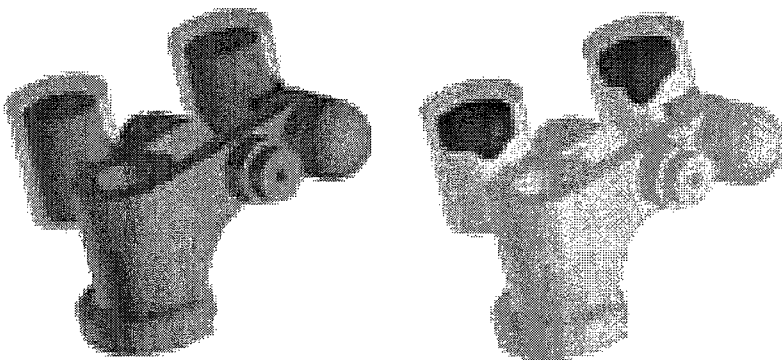


Figure 2.9. Software used to determine the proper size of risers (Cast Solutions, 2006).

Rule seven is to avoid convection damage. The casting may freeze within several minutes allowing for a sufficient time for convection currents of the hot and cold melts to occur and start re-melting the casting. Problems due to convection loops are most encountered in investment castings as shown in Figure 2.10 (Campbell, 2004). This may be eliminated by careful horizontal transfer as in tilt casting or counter-gravity filling followed by immediate mold roll-over. In traditional stationary molds this is achieved by using oversized gravity feeders placed on top of the casting as shown in Figure 2.11 (Campbell, 2004). Thin casting sections freeze quickly before convection becomes significant. Thick casting sections freeze over a long time period allowing the convection sufficient time to evenly redistribute the temperature.

Rule eight is to avoid segregation. The segregation of alloying elements in the casting may result in significant differences in material properties. Most alloys segregate to a small extent causing no noticeable problems. However, some alloys segregate excessively, to the point where parts of the casting will be well outside the chemical specifications. Parts of the casting that cools quickly may easily rise above the maximum specification limit. Parts of the casting that cools slowly fail to reach the minimum specification limit. Segregation may occur at abrupt thickness section changes that also represent critical stress concentration regions as shown in Figure 2.12 (Campbell, 2004).

Rule nine is to avoid Residual Stress. Severe quench using water should definitely be avoided during heat treatment of Al Alloy(s) castings. The water quench may effectively reduce the total strength of the castings by half and may cause a major failure while in service. The desired quench could be achieved using a polymer or air, which only causes less than a 10% loss of strength or ductility as shown in Figure 2.13 (Campbell, 2004).

Rule ten is to properly select locating points on the casting. Datum and pick-up points need to be agreed upon prior to machining to avoid unnecessary scrap after the casting has been produced. This agreement has to be put in place before ordering parts. Once the pick-up points have been set, the tool makers, foundry, and machinists have to work from the same datum points. The incorporation of lugs that simultaneously provide clamping points is helpful. The more expensive option is to use a Computerized Measurement Machine (CMM) to acquire several casting measurements.

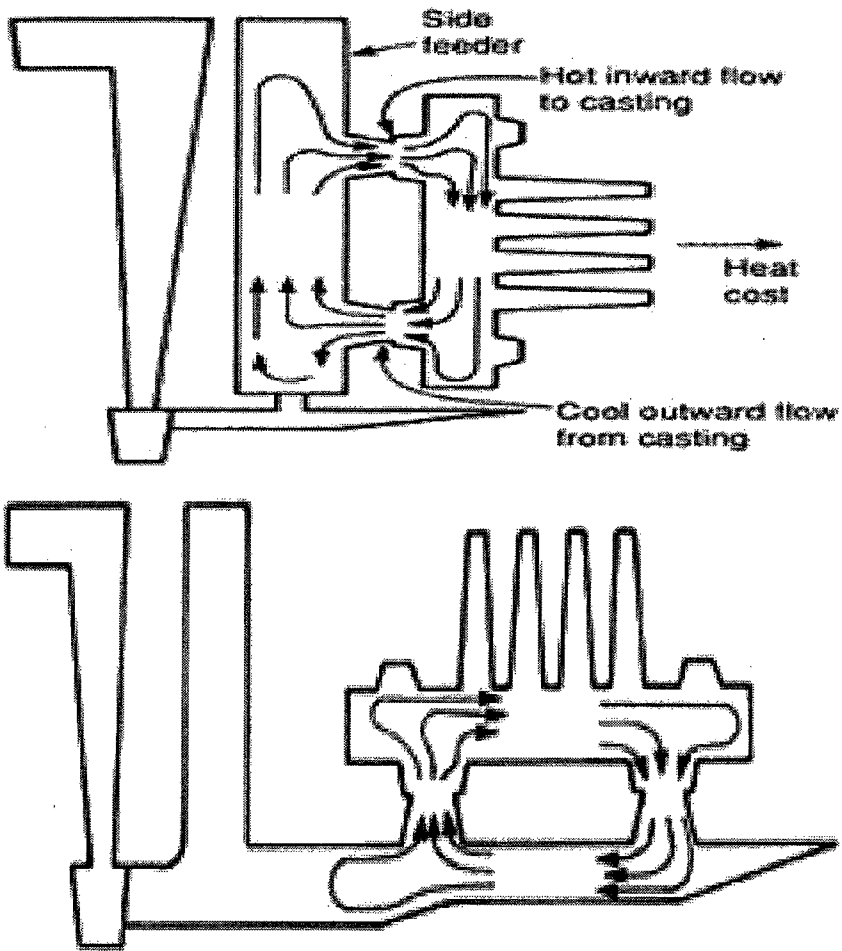


Figure 2.10. Convection loops re-melt casting during solidification (Campbell, 2004).

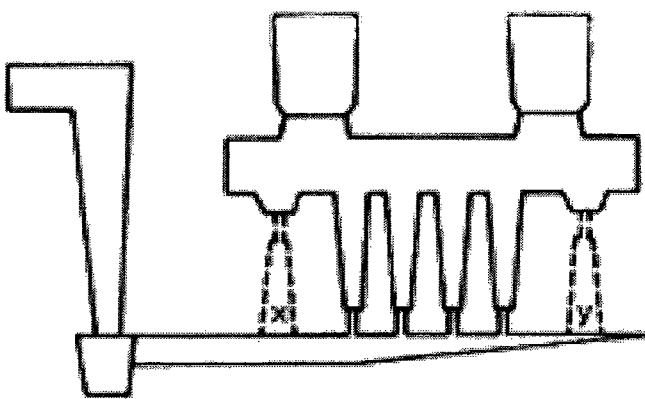


Figure 2.11. Convection loops eliminated by oversized risers (Campbell, 2004).

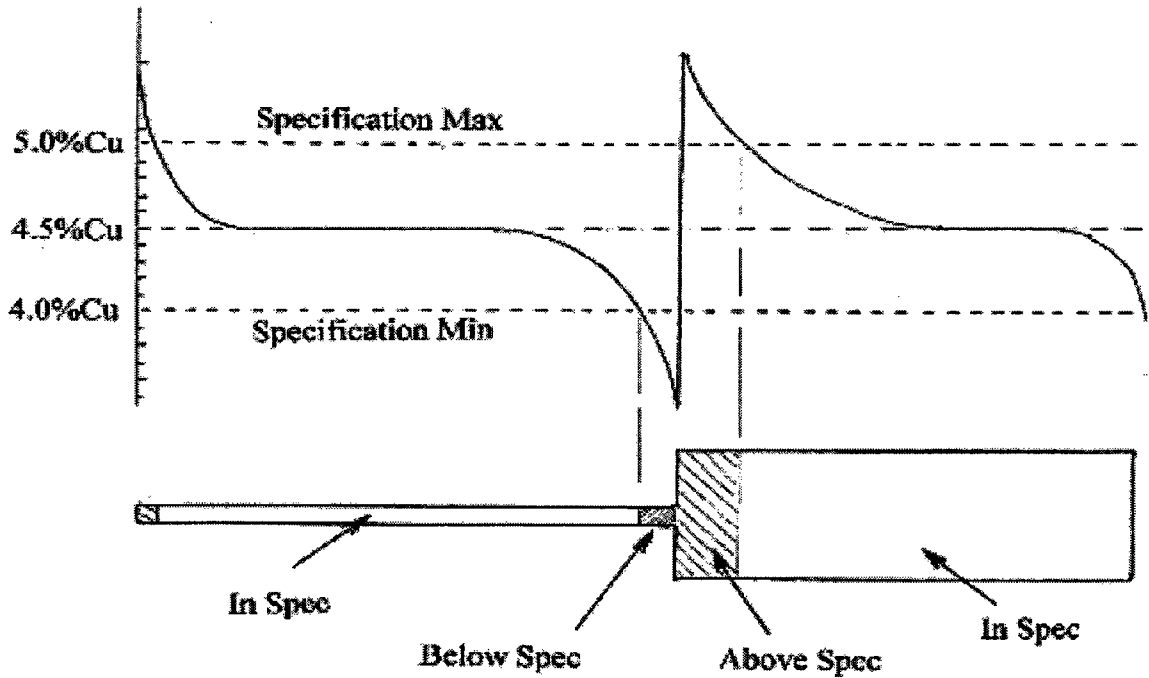
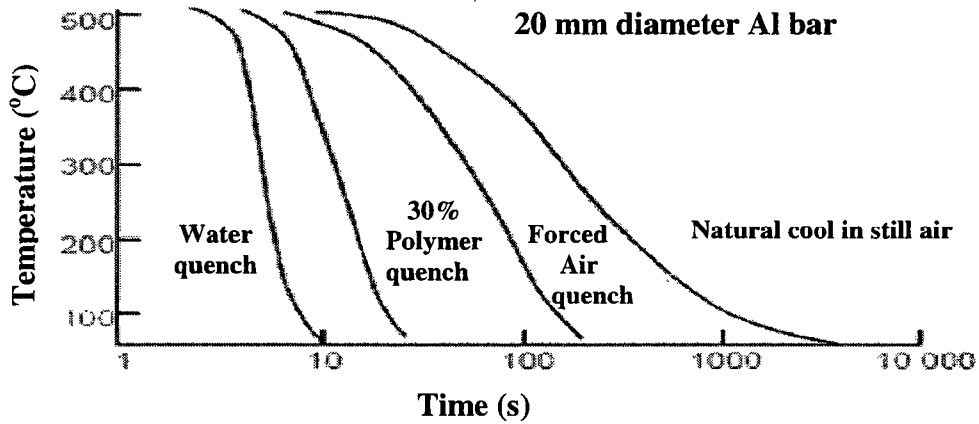


Figure 2.12. Segregation in different areas due to a slow or fast cooling rate (Campbell, 2004).



Quench Medium	Elongation %	
	Mean $\pm$ 2.5 $\sigma$	Minimum
Hot Water (70°C)	4.73 $\pm$ 2.72	2.01
Cold Water	6.47 $\pm$ 1.67	4.80
Water-Glycol Mixture	5.81 $\pm$ 0.96	4.85

Figure 2.13. Effect of cooling rate from the solution treatment temperature on the ductility of the as cast Al bar (Campbell, 2004).

## 2.2 Hypoeutectic Aluminum Silicon Alloys

Al-Si alloys are mainly used to produce castings, although some sheet or wire is made for welding and brazing, and some of the piston alloys are extruded for forging stock. The copper free alloys are used for low to medium strength castings with good corrosion resistance; the copper bearing for medium to high strength castings, where corrosion resistance is not critical. Because of their excellent castability, it is possible to produce reliable castings, even in complex shapes, in which the minimum mechanical properties obtained in poorly fed sections are higher than in castings made from higher strength but lower castability alloys. Automotive parts like engine blocks, cylinder heads, and pistons are commonly cast using Al-Si alloys like 319 (Al-Si-Cu) and 356 (Al-Si-Mg).

### 2.2.1 W319 Aluminum Alloy

This alloy is "heat-treatable" and generally used for castings that could be significantly strengthened through precipitation heat treatment. It has excellent casting characteristics and good mechanical properties. In the last decade the use of Al Alloy(s) for engine block castings increased from 13% to 50% in passenger cars and from 5% to 20% in light trucks (Sehitoglu, 2005). The W319 Al Alloy is considered as a commercial grade of the 319 Al Alloy with a higher Si content. This alloy provides excellent torque loading ability, a close mechanical flatness tolerance, close machined micro finishes, and excellent natural age hardenability. There are several codes that refer to the specific heat treatment designed for different purposes as described in Table 2.1 (Matweb, 2005). Material properties of the most common heat treated Al Alloy(s) are compared in Table 2.2 (Matweb, 2005), Table 2.3 (Matweb, 2005), Table 2.4 (Matweb, 2005). These properties could be affected by the presence of important alloying and impurity elements. The solidification process of this alloy starts with the formation of a dendritic  $\alpha$  aluminum network followed by precipitation of an Aluminum-Silicon eutectic phase, then Iron-Manganese phases, and finally Copper rich phases see Figure 2.14 (Kasprzak, et al., 2001). The amount of each phase depends strongly on the composition and solidification conditions.



### 2.2.2 Key Alloying and Impurity Elements

Silicon is added as one of the major alloying elements in Al Alloy(s). It improves melt fluidity in the mold during casting. The addition of Silicon is important to readily and easily fill the thinnest sections of the mold. The improved castability helps to minimize metal shrinkage during solidification. In a solidified alloy, Silicon tends to increase the strength with improvements in wear resistance at moderate-to-high levels. However increasing Silicon without modification causes a decrease in ductility as the natural morphology of unmodified eutectic Aluminum Silicon is acicular or plate like. Generally, chemical modification by addition of Na or Sr is used to refine the brittle plate like Aluminum Silicon eutectic into a more ductile fine fibrous morphology as shown in Figure 2.15 (Guthy, 2002). Thermal modification could be used to fragment and spheroidize the Silicon through a heat treatment driven by the solid state diffusion process.

Copper is added to form Copper rich phases that show higher hardness and strength even at elevated temperatures. However, Copper may decrease corrosion resistance (Key to Metals, 2006). Precipitation heat treatment is used to develop maximum hardness and strength. Depending on service conditions the peak aged state may not be optimum due to dimensional stability. Often castings are over aged to provide a compromise between strength and dimensional stability. The IRC has introduced over aging of the W319 engine block cast at WAP for the same reasons mentioned (Cáceres, et al., 1999). Heat treatment with over aging beyond peak strength stabilizes the precipitation hardened alloy against thermal growth. Rich eutectic phases may take several forms depending on alloy composition, solidification conditions, and heat treatment. The most common Copper rich phases in the W319 Al Alloy are listed below and shown in Figure 2.16 (Djurdjevic, et al., 2001).

- “Blocky” shape  $\text{Al}_2\text{Cu}$
- “Eutectic” Al-Cu-Si
- “Fine Eutectic”  $\text{Al}_5\text{Mg}_8\text{Cu}_2\text{Si}_6$

Iron is an unwanted element in Al Alloy(s) as it has significantly limited solid solubility below  $655^\circ\text{C}$  that leads to a decrease in feeding during solidification. This causes a drastic reduction in ductility and toughness through the formation of brittle

intermetallic phases that act as severe stress risers. Alloys produced from recycled materials have more iron than primary alloy. The Iron phases formed in Al Alloy(s) are largely dependent on local solidification rates and melt holding temperatures. The most common Iron phases are  $\beta$ -Al<sub>5</sub>FeSi, and  $\alpha$ -Al<sub>15</sub>Fe<sub>3</sub>Si<sub>2</sub> as shown in Figure 2.17 (Mei, et al. 2003). The morphology of the  $\alpha$ -phase is described as “Chinese script”, which is multi-armed or semi-symmetrical in shape. This is less harmful to ductility and stable during heat treatment. The morphology of the  $\beta$ -phase is described as thin plates. This is undesirable because it is known to reduce casting ductility and increase shrinkage porosity by blocking feed paths during solidification. Addition of transition elements such as Manganese promotes formation of the less harmful  $\alpha$ -Chinese script phase.

Manganese increases strength either in solid solution or as a finely precipitated intermetallic phase. It has no adverse effect on corrosion resistance. The solid solubility of Manganese is very limited in Aluminum. The addition of Manganese significantly increases strength without decreasing ductility. This refinement is possible through the heat treating process that forms Manganese rich precipitates such as Mg<sub>2</sub>Si or Al<sub>2</sub>CuMg.

Magnesium is the major alloying element in the 5XXX series of Al Alloy(s). Its maximum solid solubility in Aluminum is 17.4%, but below 5.5% in wrought alloy. The addition of Magnesium markedly increases the strength of Aluminum without unduly decreasing the ductility while offering good corrosion resistance and weldability (Key to Metals, 2006).

Nickel is added to an Al-Si alloys to improve hardness and strength at elevated temperatures and to reduce the coefficient of expansion. The solid solubility of nickel in Al does not exceed 0.04% (Key to Metals, 2006). If Nickel is over the solid solubility limit, it is present as an insoluble intermetallic, usually in combination with iron.

Tin is a metallic element considered as an impurity element that has restricted solid solution solubility in Al and forms soft low melting temperatures phases. Even at low levels, it determines heat treatment response after the age hardening process. A recently presented invention study related to the W319 Al Alloy indicated that the addition of Tin in trace amounts increased the heat treatment response. The study found that even trace amounts of Tin, up to 0.1 wt.% affect thermal growth kinetics and heat treatment response (Key to Metals, 2006).

Table 2.1. Heat treatment codes (Matweb, 2005).

Code	Thermal Processing Condition
F	As Fabricated - No special control has been performed to the heat treatment or strain hardening after the shaping process such as casting, hot working, or cold working.
W	Solution Heat Treated - This is seldom encountered because it is an unstable temper that applies only to alloys that spontaneously age at ambient temperature after heat treatment.
T	Solution Heat Treated - Applies to products which are thermally treated, with or without additional strain-hardening, to produce stable tempers.
T1	Cooled from an elevated temperature shaping process and naturally aged to a substantially stable condition.
T2	Cooled from an elevated temperature shaping process, cold worked, and naturally aged to a substantially stable condition.
T3	Solution heat treated, cold worked, and naturally aged to a substantially stable condition.
T4	Solution heat treated, and naturally aged to a substantially stable condition.
T5	Cooled from an elevated temperature shaping process then artificially aged.
T6	Solution heat treated then artificially aged.
T7	Solution heat treated then overaged/stabilized.
T8	Solution heat treated, cold worked, and then artificially aged.
T9	Solution heat treated, artificially aged, and then cold worked.
T10	Cooled from an elevated temperature shaping process, cold worked, then artificially aged.

Table 2.2. Mechanical properties of common Al alloys (Matweb, 2005).

Alloy	Heat Treatment	Minimum Ultimate Tensile Strength (MPa)	Minimum Yield Strength (MPa)	Minimum Shear Strength (MPa)	Minimum Elongation %
201	T7	414	345	290	3 Min
319	F	159	90	150	1.5 Min
319	T6	214	138	200	1.5 Min
W319*	T7	200	170	152	.05 Min
356	T7	214	200	165	2 Min
390	T6	275	275	166	1 Max
390	T7	250	250	152	1 Max

\* Limits based on Ford Specification WSE-M2A151-A2.

Table 2.3. Chemical specification limits for common Al alloys (Matweb, 2005).

Alloy		Si	Cu	Fe	Mg	Mn	Ni	Ti	Zn	Ag	Sn	Pb	Other, Each	Other, Total
201	Min	-	4	-	0.15	0.2	-	0.15	-	0.4	-	-	-	-
	Max	0.1	5.2	0.15	0.55	0.5	-	0.35	-	1	-	-	0.05	0.1
319	Min	5.5	3	-	-	-	-	-	-	-	-	-	-	.5
	Max	6.5	4	1	.1	.5	.35	.25	1	-	-	-	-	-
W319*	Min	6.5	3	-	.2	-	-	-	-	-	-	-	-	-
	Max	8	4	.4	.35	.3	.1	.25	.25	-	.1	.1	.05	.5
356	Min	6.5	-	-	0.2	-	-	-	-	-	-	-	-	-
	Max	7.5	0.25	0.6	0.45	0.35	0.25	-	0.35	-	-	-	0.05	0.15
390	Min	16	4	-	.45	-	-	-	-	-	-	-	-	-
	Max	18	5	.5	.65	.1	-	.2	.1	-	-	-	.1	.2

\* Per Ford Specification WSE-M2A151-A2.

Table 2.4. Relative Characteristics of Common Al Alloys (Matweb, 2005).

*1 Alloy	Fluidity *2	Hot Cracking Resistance *3	Pressure Tightness	Corrosion Resistance *4	Shrinkage Tendency *5	Machinability	Weldability *6
201	3	4	3	4	4	1	2
319	2	2	2	3	2	3	2
W319	2	2	2	3	2	3	2
356	1	1	1	2	1	3	2
390	3	3	3	2	3	4	2

1. Rating: 5 best /1 poorest.
2. Ability of melt to flow and fill thin sections.
3. Ability to withstand stress from contraction while cooling through hot short or brittle temperature range.
4. Composite rating based on ease of cutting, chip resistance, quality of finish, and tool life based on T6 temper.
5. Decrease in volume accompanying freezing and measurement of compensating feed metal required in the form of risers.
6. Based on ability to be fusion welded with a filler rod of the same alloy.

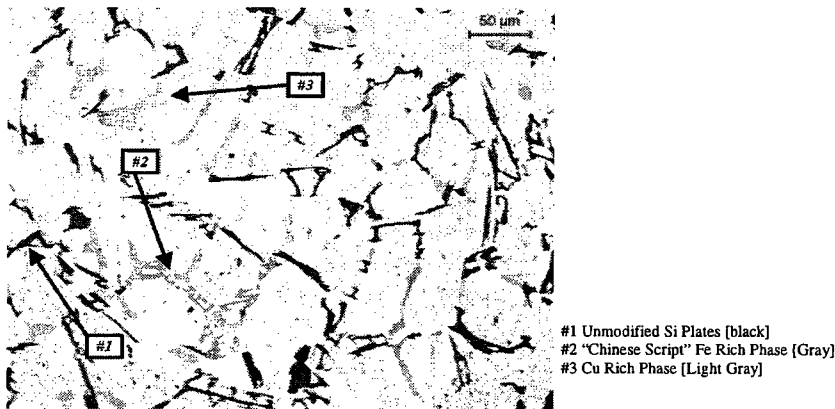


Figure 2.14. Micrographs of typical as-cast W319 Al sample (Kasprzak, et al., 2001).

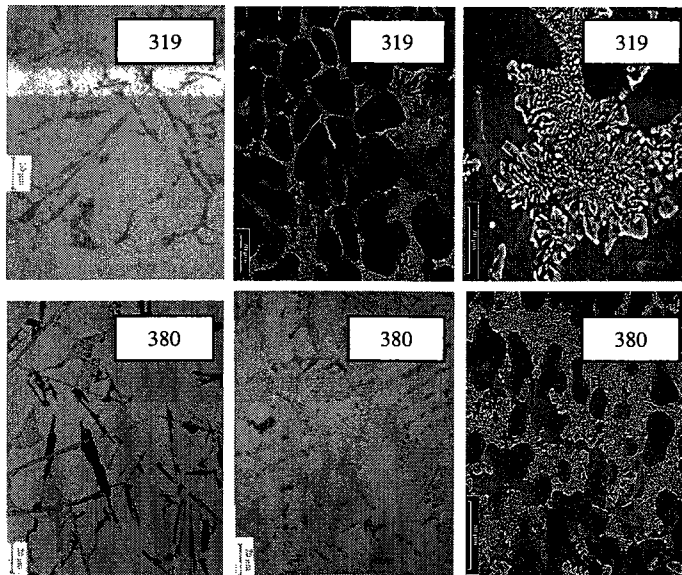


Figure 2.15. Modified and unmodified Silicon in 319 and 380 Al alloys (Guthy, 2002).

### 2.2.3 Silicon Equivalency Algorithm

The  $Si_{EQ}$  algorithm is an analytical approach developed by the IRC for the foundry industry. The concept of  $Si_{EQ}$  is based on equilibrium phase diagrams similar to Carbon Equivalency for ferrous alloys (Djurdjevic, et al., 2003). The major alloying element is Silicon instead of Carbon where the matrix is Aluminum instead of Iron. The  $Si_{EQ}$  for a specific element can be calculated using a combination of the corresponding element Al, and Al-Si phase diagrams. For example, the binary phase diagram of Al-Cu indicates that at 4%wt. Cu, the Liquidus temperature is 640°C. The binary phase diagram of Al-Si indicates that the Liquidus temperature 640°C occurs at 7wt% Si. Therefore the 4wt% of Cu can be translated into 7wt% Si using the  $Si_{EQ}$  method. The relationship between the concentration of any given element  $X_i$  and corresponding  $Si_{EQ}$  can be expressed in the form of a second degree polynomial equation. The  $Si_{EQ}$  for a multi component hypoeutectic Al-Si alloy is the sum of all individual  $Si_{EQ}$  calculated for each element as defined in Table 2.5 (Djurdjevic, et al., 2003). Valid correlations were established by IRC between the  $Si_{EQ}$  and solidification characteristics along with as cast mechanical properties; see Table 2.6 (Djurdjevic, et al., 1998).

### 2.2.4 Grain Refinement

Careful control of the microstructure is a major requirement in the production of high quality castings. The most effective way to provide a fine and uniform as-cast grain structure is to add grain refiners that act as artificial nucleating agents in the melt to control crystal formation during solidification. A large dendritic grain structure generally is undesirable as smaller grain size usually results in significant improvement in strength, ductility, castability, porosity size distribution, and machinability. Chemical additions using master alloys provide a particularly convenient method to introduce nucleation agents. This type of grain refinement is based on constitutional under-cooling where many small solid particles precipitate at high temperatures and act as nucleation and growth sites. The most common grain refiners include Al-Ti or Al-Ti-B master alloy. The addition of Boron in the master alloy improves the effectiveness of  $TiAl_3$  particles as a grain refiner in Al-Si alloy. The grain refiner master alloy could be either added to the melt directly or introduced in-mold prior to casting.

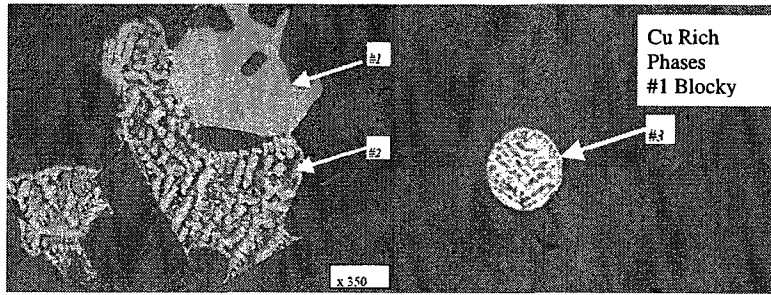


Figure 2.16. Micrographs of Copper rich phases in a W319 sample (Djurđević, et al., 2001).

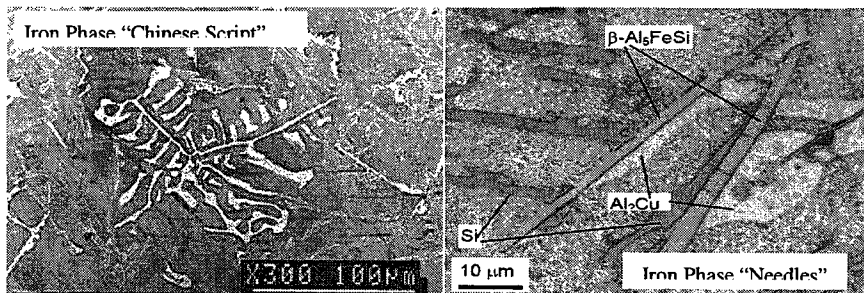


Figure 2.17. Micrographs of Iron phases in a W319 sample (Djurđević, et al., 2001).

Table 2.5. Algorithm to calculate  $S_{iEQ}$  in multi component hypoeutectic Al alloys (Djurđević, et al., 2003).

Definition	Equation	
$S_{iEQ}$ for Individual Element	$S_{iEQ}^{X_i} = b_0 \cdot X_i + c_0 \cdot X_i^2$	
$S_{iEQ}$ for Multicomponent Alloy	$S_{iEQ} = S_i + \sum S_{iEQ}^{X_i}$	
Al- $X_i$ Alloy (wt. %)	$b_0$	$c_0$
Al-Cu	0.529	-0.0004
Al-Mg	0.0258	-0.0088
Al-Mn	0.8221	-0.0349
Al-Fe	0.6495	0.0003
Al-Zn	0.1227	-0.0002
Al-Sn	0.7849	-0.0313
Al-Bi	0.9076	-0.0092
Al-Pb	0.859	0.02976
Al-Sb	0.8255	-0.0327
Al-Ni	0.5644	0.0285
Al-Sr	0.7854	-0.0157
Al-Ti	-0.8159	0.00993
Al-B	0.00075	7.5 E-05

Table 2.6. 3XX Al Alloy Solidification Characteristics and As Cast Mechanical Properties Predicted Using  $Si_{EQ}$  (Djurdjevic, et al., 1998).

Predicted Parameter	Prediction Equation
$\alpha$ -Al Dendrite Nucleation Temperature, $T_{LIQ}$ [Deg $^{\circ}$ C]	$= 660.452-6.11 Si_{EQ}-0.057 Si_{EQ}^2$
$\alpha$ Al dendrite Coherency Point Temperature [Deg $^{\circ}$ C]	$= 668.83-8.2756*X$
Fraction Solid Al-Si Eutectic Nucleation	$= \frac{Al\_Primary\_Vol\_Frac}{[Al\_Primary\_Vol\_Frac+Al\_Secondary\_Vol\_Frac+ Eutectic\_Si\_Vol\_Frac]}$  Where Primary-Al = $[11.874-Si_{EQ}]/[11.874-1.543]*100$ Eutectic = $[Si_{EQ}-1.5437]/[11.874-1.5437]*100$ Secondary-Al = $[98.9633- Si_{EQ}]/[98.9633-1.5437]*Eutectic$ Eutectic_Si = $[Si_{EQ}-1.5437]/[98.9633-1.5437]*Eutectic$ Al_Total = Primary_Al+Secondary_Al Al_Primary_Vol-Frac = Primary_Al/2.7 Al_Secondary_Vol-Frac = Secondary_Al/2.7 Eutectic_Si_Vol_Frac = Eutectic_Si/2.33
Al-Si Eutectic Nucleation Temperature [Deg $^{\circ}$ C]	$= 660.452-[6.11 Si_{EQ}+11.57 Si_{EQ}^2]*[12.3/ Si_{EQ}]$
Al-Cu Rich Eutectic Nucleation Temperature [Deg $^{\circ}$ C]	$= T_{LIQ}-[6.11 Si_{EQ}+11.57 Si_{EQ}^2]*[12.3/ Si_{EQ}]$
Grain Size [AFS GS #]	$= 83.484+324.5*X$
Secondary Dendrite Arm Spacing [ $\mu$ m]	$= 120.54-4.62*Si-10.16*Cu+0.56*Si*Cu$
As Cast Ultimate Tensile Strength [MPa]	$= -545.27+157.83*X-7.12*X^2$
As Cast Yield Strength [MPa]	$= -216.73+73.54*X-3.52*X^2$
Where X	$= Si+[[0.35*Cu-0.027*Cu^2]+$ $[0.6495*Fe+0.0003*Fe^2]+$ $[0.0258*Mg-0.0088*Mg^2]+$ $[0.8221*Mn-0.0349*Mn^2]+$ $[0.1227*Zn-0.0002*Zn^2]]$

### 2.3 Porosity

Porosity in Al castings is detrimental to mechanical properties, especially ductility, fracture toughness, fatigue life, surface finish, and corrosion resistance. The type of porosity in casting could be either shrinkage porosity or gas porosity or combination of both, see Figure 2.18 (Triveño, et al., 2003), and Figure 2.19 (Triveño, et al., 2003). Porosity results in a significant reduction of mechanical properties in Al Alloy(s) castings as shown in Figure 2.20 (Monroe, 2004). Castings have limited ductility, so small amounts of porosity can have a large effect on strength.

Gas porosity is attributed to the presence of Hydrogen gas as it is the only gas that is appreciably soluble in Al Alloy(s) at high temperatures. A common possible source of hydrogen gas is water vapor in the atmosphere, which also produces Al oxides at the exposed liquid surface. The critical level of Hydrogen dissolved in the melt has been reported to be 0.1 ml/100 g Al (Du). The formation of Hydrogen gas bubbles contributes to the considerable decrease in solubility between the liquid and solid state as shown in Figure 2.21 (Monroe, 2004). Shrinkage porosity is attributed to shrinkage of liquid metal during mushy zone solidification as it lacks interdendritic feeding. Most metals shrink by a range of 3.5 to 8.5% during transformation from liquid to solid. In addition, the remaining liquid metal contracts at a far greater rate than the solidified metal. The combined effect of volumetric shrinkage and the difference in contraction rate results in substantial hydrostatic tensile stresses. Ultimately voids form in the liquid metal as it struggles to maintain coherency under increasing stresses that exceed interface surface tension. The presence of a nucleus helps in the formation of pores to relieve stress and return to a previous stable status. The affected area of porosity grows due to an increase of hydrostatic tension caused by shrinkage of the areas around the pore, and shrinkage of the areas far away from the pore (Monroe, 2004). Combined gas shrinkage porosity is the most common case encountered in Al Alloy(s) castings. Gas evolution and shrinkage occurs simultaneously in the same volume of liquid metal. As a result, an interaction between the two phenomena can be expected. Both the gas and shrinkage pressure aid in the nucleation and growth of the pore as the pressure pushes from the inside and the shrinkage pressure pulls from the outside (Monroe, 2004).



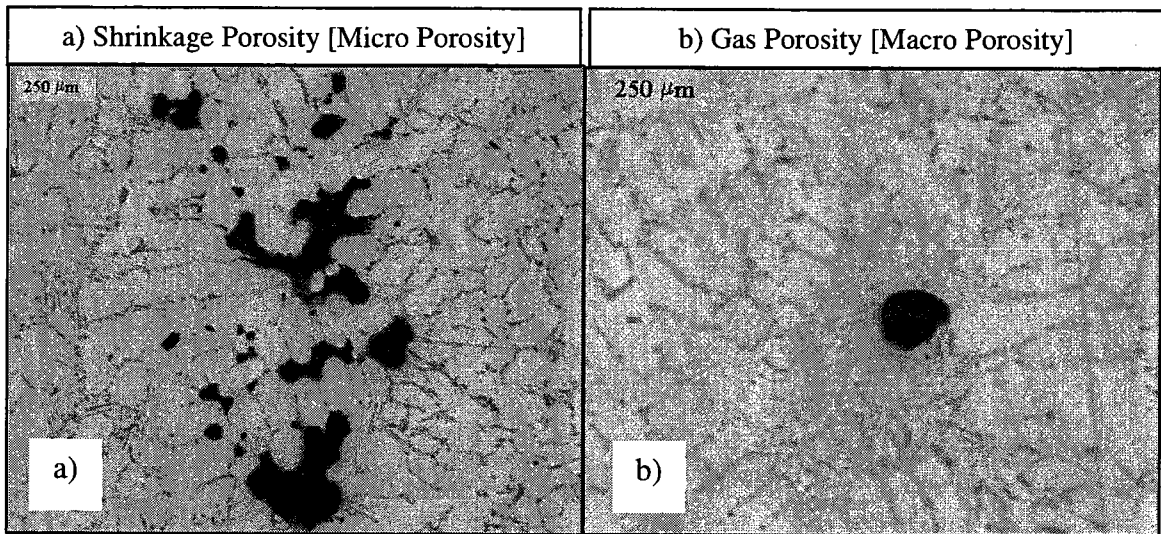


Figure 2.18. Micrographs of various types of porosity in the w319 Al alloy sample (Triveño, et al., 2003).

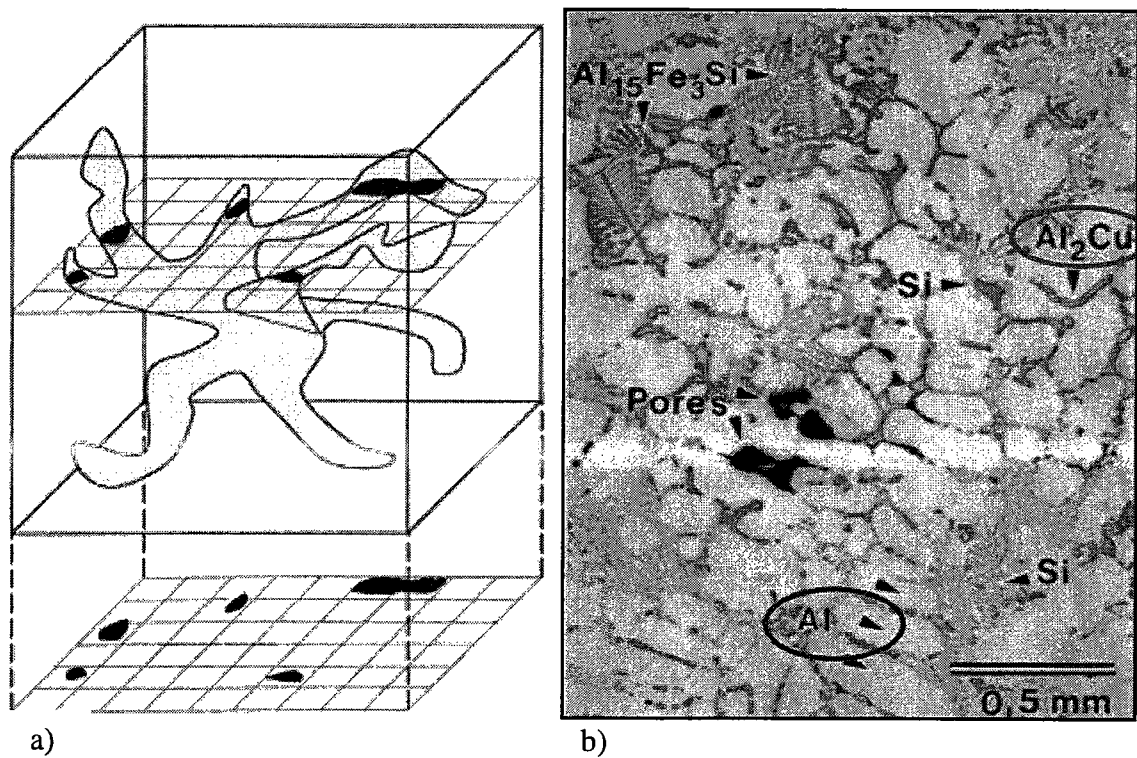


Figure 2.19. a) Schematic of a shrinkage pore in 3D and  
b) Corresponding 2D section (Triveño, et al., 2003).

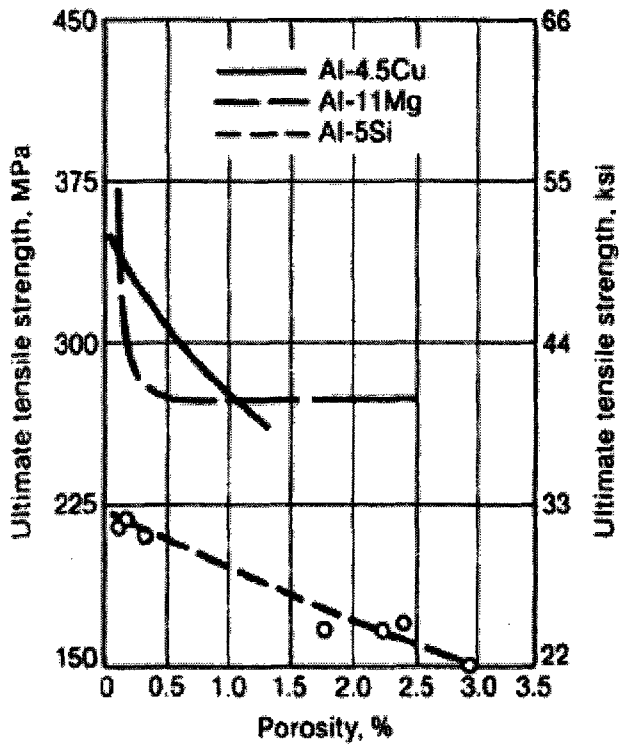


Figure 2.20. Effect of porosity on Al alloys ultimate tensile strength (Monroe, 2004).

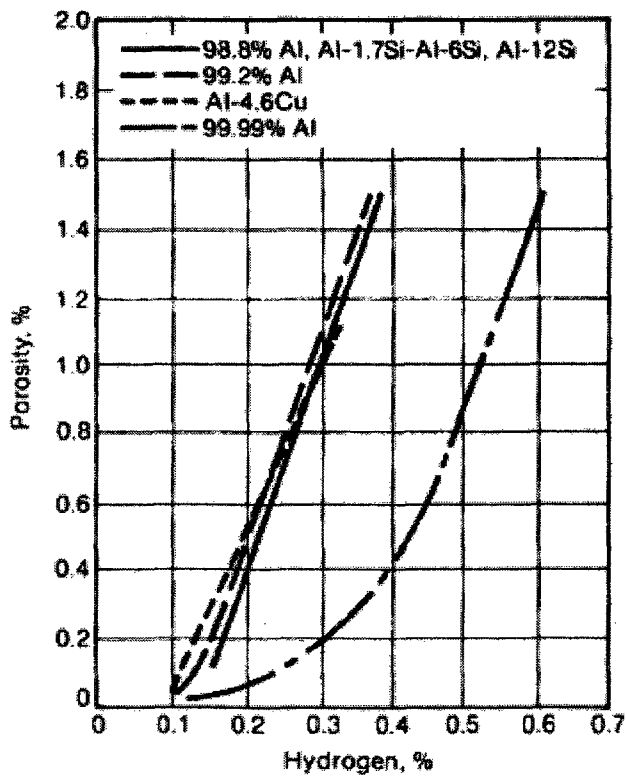


Figure 2.21. Effect of dissolved hydrogen on casting porosity (Monroe, 2004).

## 2.3 Heat Treatment

The term “heat treating” refers to specific operations employed to achieve specific properties such as an increase strength and hardness or dimensional stability. Precipitation heat treatment starts with solution treatment followed by age hardening. The T6 heat treatment produces higher strengths because of greater amounts of fine  $Mg_2Si$  and  $CuAl_2$  precipitates formed during aging. However, the T7 heat treatment exhibits higher ductility and minimum internal stresses. The castings at WAP go through T7 heat treatment starting with a partial Solution Treatment at  $500^\circ C$  for six hours, and then Artificial Aging at  $260^\circ C$  for four hours. The T7 heat treatment results in an over aged castings, which is aimed at improving dimensional stability, and mechanical properties. The heat treatment steps are described below and are shown in Figure 2.22.

1. Solution heat treatment: Heat and hold at an elevated temperature at about  $500^\circ C$  until a sufficient amount of soluble Cu rich phases are dissolved into the Al matrix.
2. Quench: Air quench to room temperature to achieve coherency stress strengthening by development of a SSSS. The SSSS matrix contains clusters of Cu atoms “G-P zones” surrounded by strong strain and stress fields, see Figure 2.23 (Roberts, 2006).
3. Age Hardening: Age hardening at room temperatures for days and then Artificial Age at an elevated temperature below melting for several hours. This results in precipitation of Cu rich phases that form fine, closely spaced, precipitates  $\theta''$ . The Yield Strength (YS) is noticeably improved as the finely distributed precipitates with complicated “intermetallic” crystal structure must be “cut” by dislocations; see Figure 2.24 (Roberts, 2006).
4. Over Age: Continue to hold at the previous elevated temperature as the last step to achieve a balance between improved dimensional stability and strength. Further precipitates form  $\theta'$  and finally  $\theta$  by continuing to hold at an elevated temperatures for a longer time. The material strength is decreased as widely spaced larger precipitates could be “bypassed” by dislocations; see Figure 2.24 (Roberts, 2006).

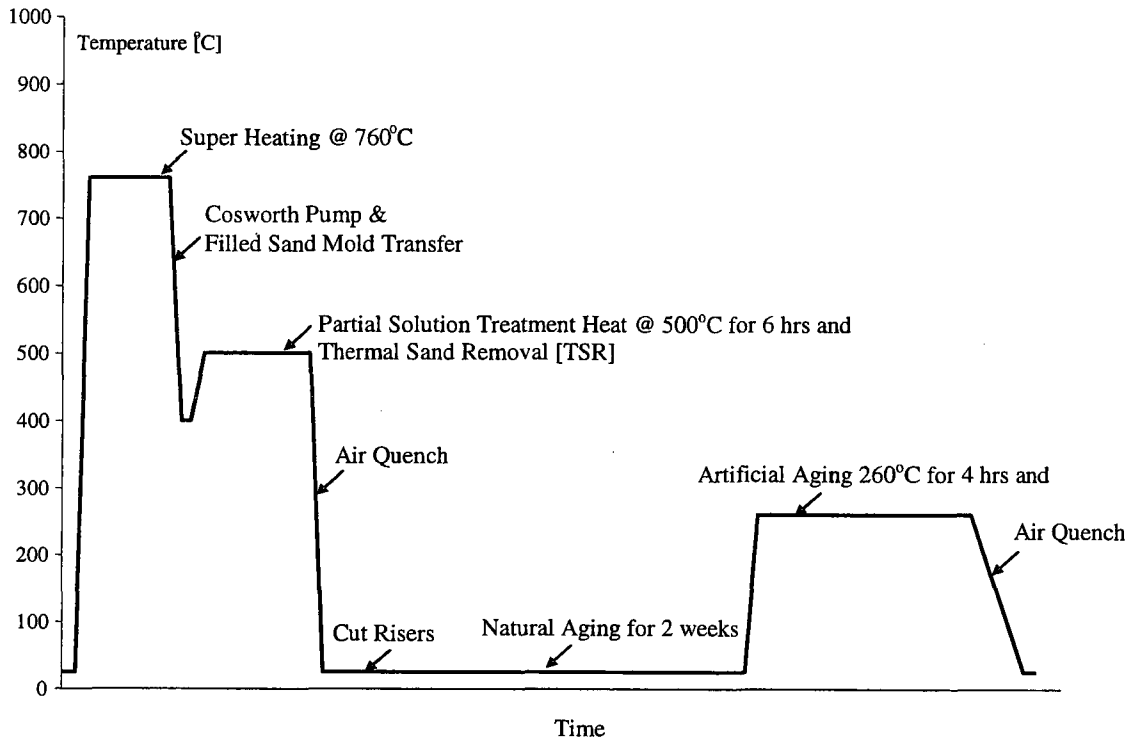


Figure 2.22. WAP Melt Thermal Treatment and Cast Component Heat Treatment T7 Temperature Time Schedule.

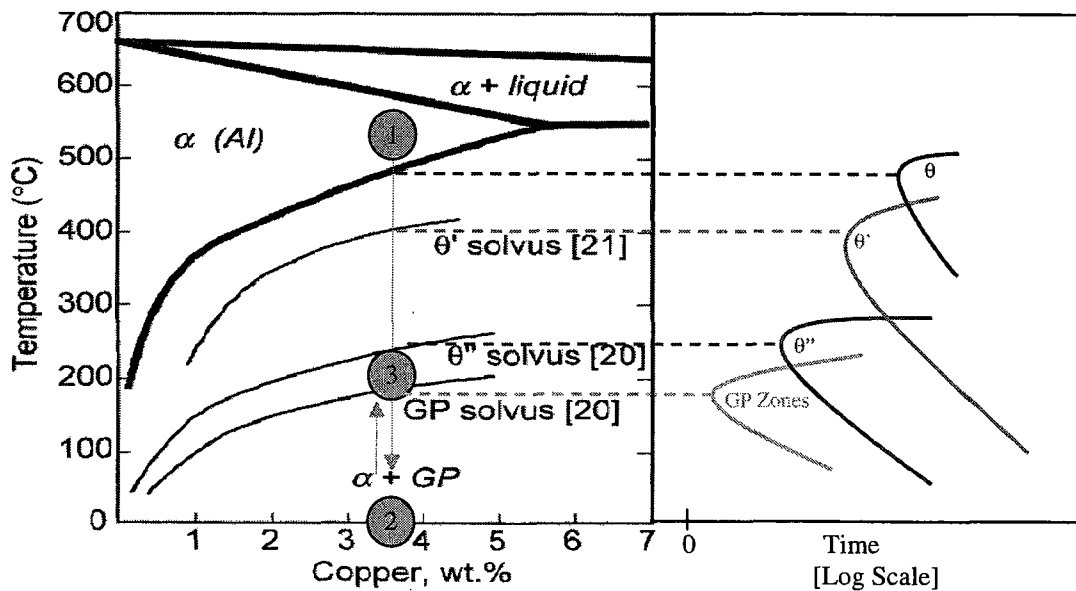


Figure 2.23. Phase Diagram and TTT Diagram for Aluminum Copper Alloy (Roberts, 2006).

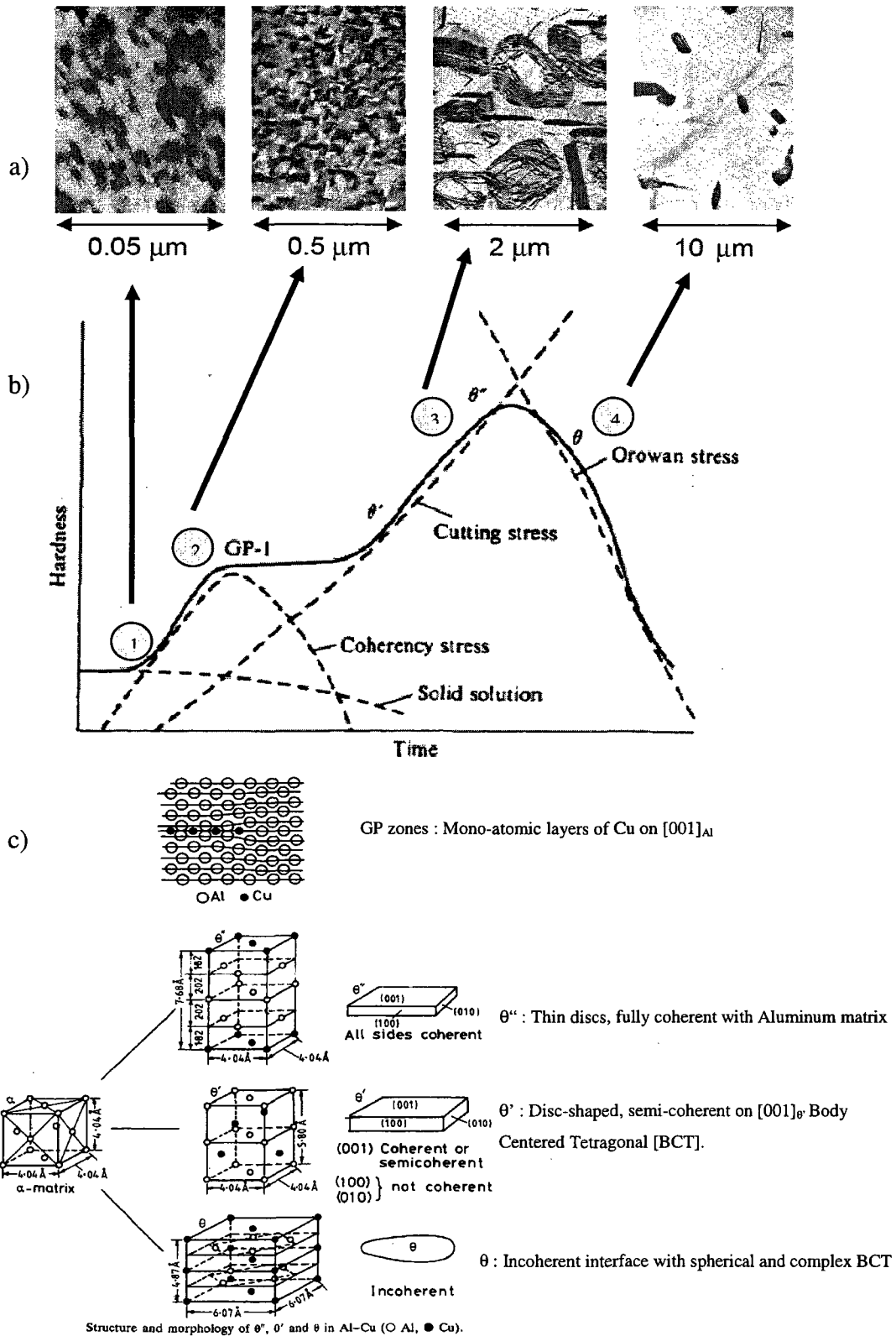


Figure 2.24. Effect of Artificial Aging on Hardness of Al-Cu Alloy (b), and schematic diagram of Al-Cu precipitates (a) and (c) (Roberts, 2006).

## 2.4 Cooling Curve Analysis

Thermal Analysis using cooling curves of a solidifying metal sample is the study of latent heat released during phase formation of the alloy. The liberation of latent heat affects the cooling rate, which allows the formation of each phase to be detected by a change in the slope of the cooling curve. Small volume phases are difficult to detect on the original curve and for this purpose the 1<sup>st</sup> derivative of the cooling curve is calculated. Each Al Alloy has a characteristic cooling curve in which metallurgical reactions are manifested by features such as inflection points and slope changes. The recorded cooling curve, along with its calculated time derivatives can yield useful information about the characteristics of the solidification process. These characteristic points could be related to alloy composition through phase diagrams as shown in Figure 2.25 (Sparkman, et. al., 1994). It is a common foundry practice to use this method to quantify the degree of grain refinement and the Silicon Modification Level (SiML). The algorithm developed by the IRC could be directly applied for cooling curve post processing (Sparkman, et. al., 1994).

The temperature signal should be recorded using a proper Data Acquisition System. One of the major limiting factors in the sensitivity of the temperature measurements is the analog to digital conversion electronics. The converter can only measure to a given accuracy that is determined by its internal electronics. If the signal is recorded using a 12 bit Analog-Digital converter it has an inherent sensitivity of 0.4995 degrees Celsius over a 1400-degree range. This could be improved by using a more sensitive 16-bit converter with better than 0.03 degrees Celsius sensitivity. This sensitivity, like an increase in magnification reveals smaller features in the signal as shown in Figure 2.26 (Sparkman, et. al., 1994). An increase in sampling rate may also reveal shorter time features improve efficiency of the data filtering. Similar to most experimental data, the cooling curve may include noise in varying degrees. Noise can obscure important features like peaks or valleys.

## 2.5 Chemical Spectroscopy Analysis

Analysis and positive material identification of metals is necessary in nearly all industries involving metal production or processing. The most common and trusted method is Optical Emission Spectrometry (OES). The test surface is burned using a high energy spark created across an argon-filled gap between the sample and the electrode. The created emissions radiate from the excited sample surface with wave lengths characteristic of the elemental composition as shown in Figure 2.27 (ARL, 2006). The spectrum of radiation is separated into distinct element lines and the intensity of each line is measured. Finally, these are precisely converted into concentration values for each element present. The unmatched combination of accuracy, high speed, precision, stability and reliability have made it an indispensable tool for production and verification of quality metallurgical products. The chemical composition of the samples representing the in-coming and in-process alloy is determined using the OES method per the ASTM E1251 "Test Method for Analysis of Aluminum and Aluminum Alloy by Atomic Emission Spectrometry". The IRC has developed guidelines for performing OES analysis as a QC tool in the production foundry (Sokolowski, et al., 2001). The advantages of OES analysis over metallographic investigation allow for proper detection and correction steps to be carried out during production to avoid cost. Metal samples are typically ground to produce a flat uncontaminated surface for analysis. The small area on the sample test surface is vaporized by a spark discharge under an argon protective atmosphere. The atoms and ions contained in the atomic vapor are excited by a second spark to emit radiation. The optic disperses the emitted radiation into spectral components. Photomultipliers measure the most suitable line from the range of wavelength emitted by each element. Concentration of each element is determined internally using a stored set of calibration curves for the known composition. Computer software is used for easy calculation and display of results. The energies of the outer shell electrons on which OES is based can be substantially influenced by the surrounding atoms to which they are bonded in solid samples. As a result, these bonds need to be completely broken for OES spectra to appropriately reflect the energies of the elements present in the sample.

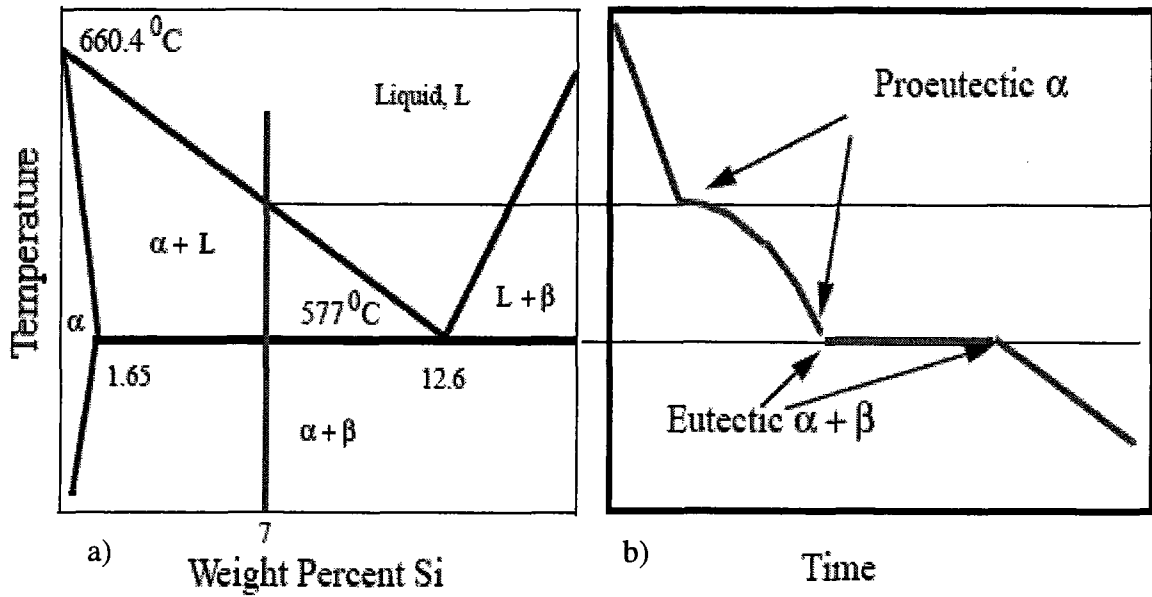


Figure 2.25. Phase diagram (a) correlation to the cooling curve (b) for Al-Si Alloys (Sparkman, et. al., 1994).

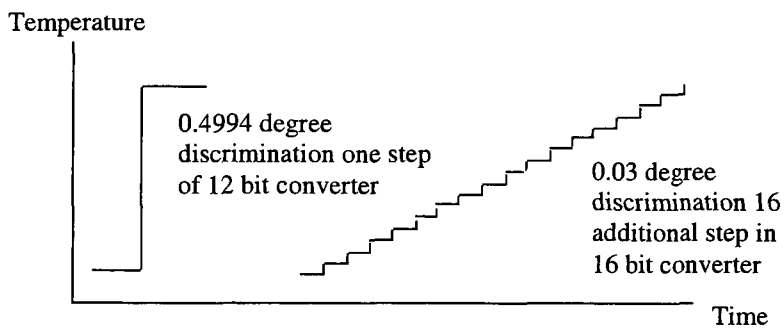


Figure 2.26. Increase of sensitivity using a 16 bit instead of a 12 bit AD converter (Sparkman, et. al., 1994).

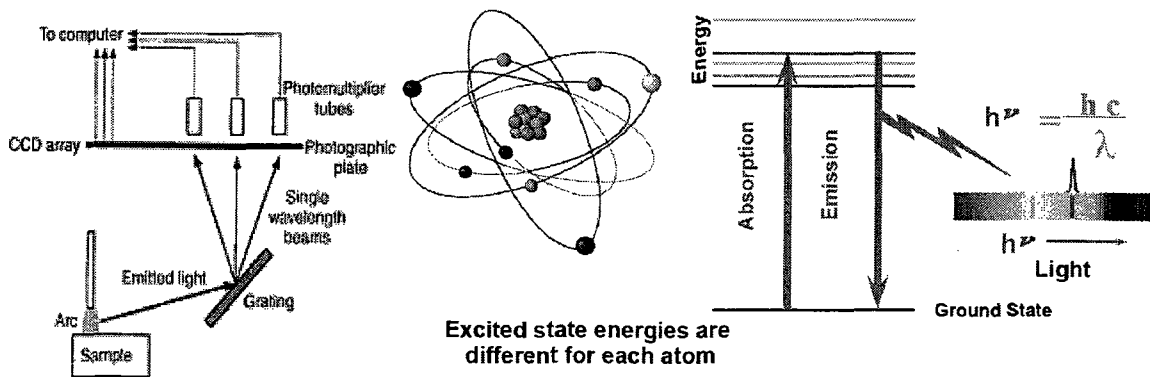


Figure 2.27. Spark emissions represent precise element concentrations (ARL, 2006).



## 2.6 Gas Comparative Analysis

One of the simplest and oldest methods for gas comparative analysis is the Straube-Pfeiffer Test commonly known as the Reduced Pressure Test (RPT). This test is comprised of a melt in a metal crucible the size of an eggcup placed under a low pressure vacuum at less than one tenth of one atmosphere pressure, see Figure 2.28. The reason for carrying out the test under reduced pressure is simply for the convenience of extension of the evolved gas volume by a factor of at least ten. The gas pores appear to be larger and easily visible after the sample is cut in half for visual evaluation, see Figure 2.29 (Campbell, 2004). The cut section could be qualitatively evaluated based on a visual standard. This test is interesting, as a high level of Hydrogen gas may still be retained in the supersaturated solution even if no bubbles are visible. The reason is that even at a high level of dissolved hydrogen, the gas may only precipitate if sufficient nuclei are present such as oxides with non-wetted interfaces. It should be noted that well wetted interfaces such as  $TiAl_3$ ,  $TiB_2$ , and Al solid particles are considered good nuclei for grain refining during solidification, but of no use as nuclei for forming pores. Therefore, the RPT is good for evaluating the combined effects of Hydrogen and the presence of non wetted nuclei in the melt. The RPT is really a "pore forming potential" test, in other words, a porosity test. Unfortunately the RPT test is misunderstood as a gas test, and unjustly criticized when the test fails to agree with other fundamental techniques for measurement of gas content.

## 2.7 Radiography Analysis

Internal porosity can be detected by using X-Ray analysis. This method becomes a destructive test for relatively large castings such as engine blocks and cylinder heads. The large casting is saw cut into discrete sections with a specified thickness around one inch. Each section of the casting is cleaned by sand blasting and then radiographed to be graded for the amount and distribution of porosity. The grading is done in accordance with ASTM E155. Each section is graded from 1 to 8 with grade 1 having the least and grade 8 having the most porosity.

## 2.8 Brinell Hardness Analysis

One of the oldest hardness test methods still being used today is the Brinell test, which was invented by Dr. J. Brinell in 1900 in Sweden (Instron, 2006). The Brinell test is frequently used to determine the hardness of forgings and castings that have a grain structure too coarse for smaller indenters used in Rockwell or Vickers testing. Therefore, Brinell tests are frequently done on large parts. By varying the test force and ball size, nearly all metals can be tested using a Brinell test. Brinell values are considered test force independent as long as the ratio of ball size to test force is the same.

The Brinell hardness test method consists of indenting the test material with a 10 mm diameter hardened steel ball subjected to a certain load. When testing soft metals such as Al Alloy(s), a load of 500 kg for 10 seconds is applied to avoid excessive indentation. The diameter of the indentation left in the test material is measured with a low powered microscope. The Brinell Hardness Number (BHN) is calculated by dividing the load applied by surface area of the indentation, as shown in Figure 2.30 (Instron, 2006). The indentation diameter is the average using two readings perpendicular to each other. The calculation of hardness is simplified by using a table relating mean diameter to the BHN. This test method makes the deepest impression compared to other methods, which averages the hardness reading over a wider volume of material. As the test is performed on a wider area, it can more accurately account for multiple grain structures and any material irregularities. This method is the best for achieving bulk or macro-hardness, particularly materials with heterogeneous structures. The Brinell hardness test measurement is considered valid if the diameter of the permanent impression is in the range of 2.5 to 4.75 mm. As a result, the 3000 kgf load yields a BHN between 160 and 600; the 1500 kgf load yields a BHN of 80 to 300; and the 500 kgf load yields a BHN of 26 to 100 (eFunda, 2006). According to the ASTM Standard E10-66, a steel ball may be used up to a BHN of 450, and carbide may be used up to a BHN of 630. It is recommended to avoid using the Brinell test on materials harder than a BHN of 630. These limits were set to avoid errors introduced by the deformation of the indenter itself.

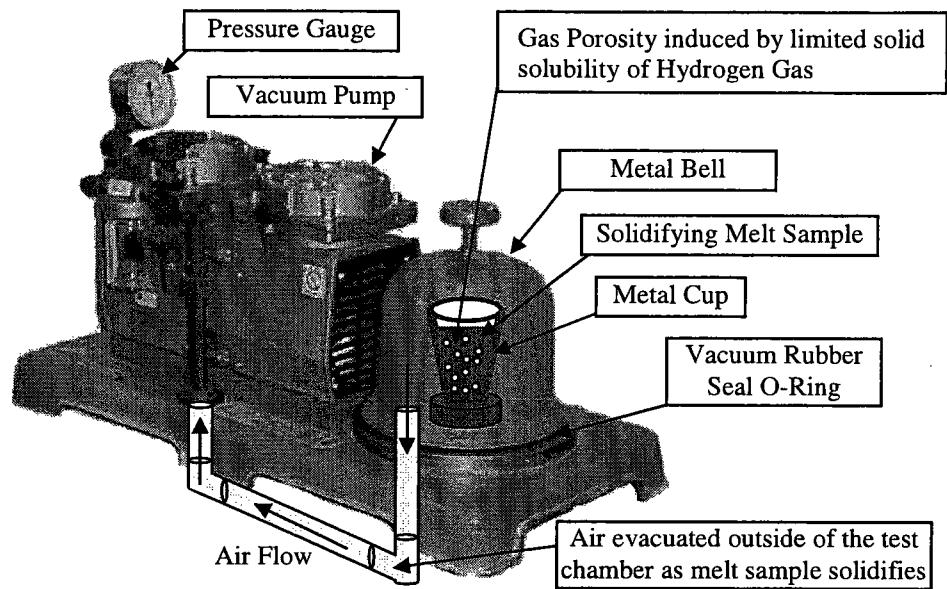


Figure 2.28. Reduced pressure test or Straube-Pfeiffer test used for hydrogen analysis.

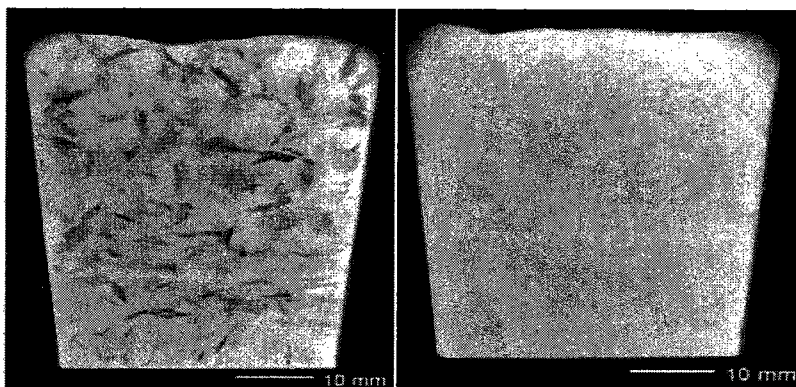


Figure 2.29. X-Ray radiographs of Al alloy solidified under 0.01 atm (left), and 1 atm (right) (Campbell, 2004).

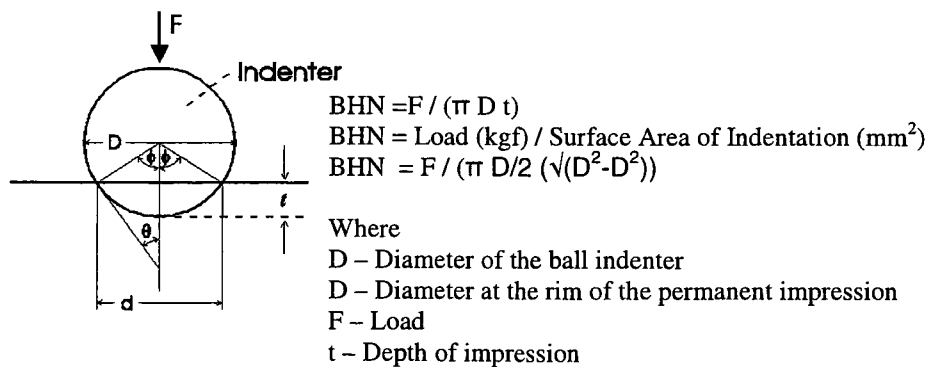


Figure 2.30. Calculation of BHN for the brinell hardness test (Instron, 2006).

## **2.9 Six Sigma DMAIC Method for Process Improvement**

Unlike other complex quality methods, Six Sigma relies only on tried and true methods that have been used for decades. These tools are applied within a simple performance improvement framework known as DMAIC, which is described in Figure 2.32 (i Six Sigma, 2006). This method is used to guide Six Sigma projects like process improvement. It may be necessary to apply DMAIC as an iterative approach. For instance, it may be noticed after performing data analysis that not enough data was gathered to isolate the root cause of the problem, and the measured step may be iterated. In addition, prior knowledge of the tools and techniques is necessary in determining which tools are useful in each phase. Only certain tools may be used for a correct and effective approach.

## **2.10 Statistical Quality Control**

Controlling a process usually means maintaining its output parameters to within certain specifications by providing a correct set of inputs. Statistical techniques provide a set of tools to detect whether the process being observed is “stable”. Statistical Process Control (SPC) charts may be employed to closely observe and predict significant deviations that may result in scrap or rejects. However, no matter how good or bad the process, SPC can only ensure that the product is being manufactured consistently as designed. Thus, SPC will not improve reliability of a poorly designed product or process. The choice of control chart for continuous data analysis is between the Individuals and Moving Range (XmR), and TUKEY as shown in Figure 2.33. The statistical probability for observed data to fall within XmR control limits is 99.3%, and 99% for TUKEY control limits. The most preferred is the TUKEY chart for cases where outlier data could radically shift the mean and standard deviation as shown in Figure 2.34 (i Six Sigma 2005). The TUKEY approach is more robust since no data distribution is assumed.

Keeping process inputs within defined specifications is not enough to ensure that production output will always be acceptable. Other factors not initially considered in the process design can come into play and degrade performance, even if the inputs follow the specifications. Therefore control limits should be established based on process

capabilities and fixed to control the process. It is an advantage to benchmark future production using fixed limits established under normal conditions. However, fixed control limits may become invalid after certain process changes. If the process improves, fixed limits must be recalculated to properly reflect an acceptable range as shown in Figure 2.35 (i Six Sigma 2005). Continuing to use wide limits may result in a lost opportunity to realize and maintain process improvement. If the process becomes worse due to material changes for example, the control limits may become too narrow. This results in false reporting of an out of control condition that reflects poorly on the process control methodology. It is best to avoid spending time addressing conditions that simply are part of a common process variation. Fixed limits should be evaluated regularly to minimize errors. Each limit could be evaluated separately by calculating the Performance Index (PI) as shown in Figure 2.32 (i Six Sigma 2005). In the ideal case the fixed control limit equals the calculated limit such that PI equals one. If PI is larger than one, the limits may be too wide, and if less than one, the limit may be too narrow.

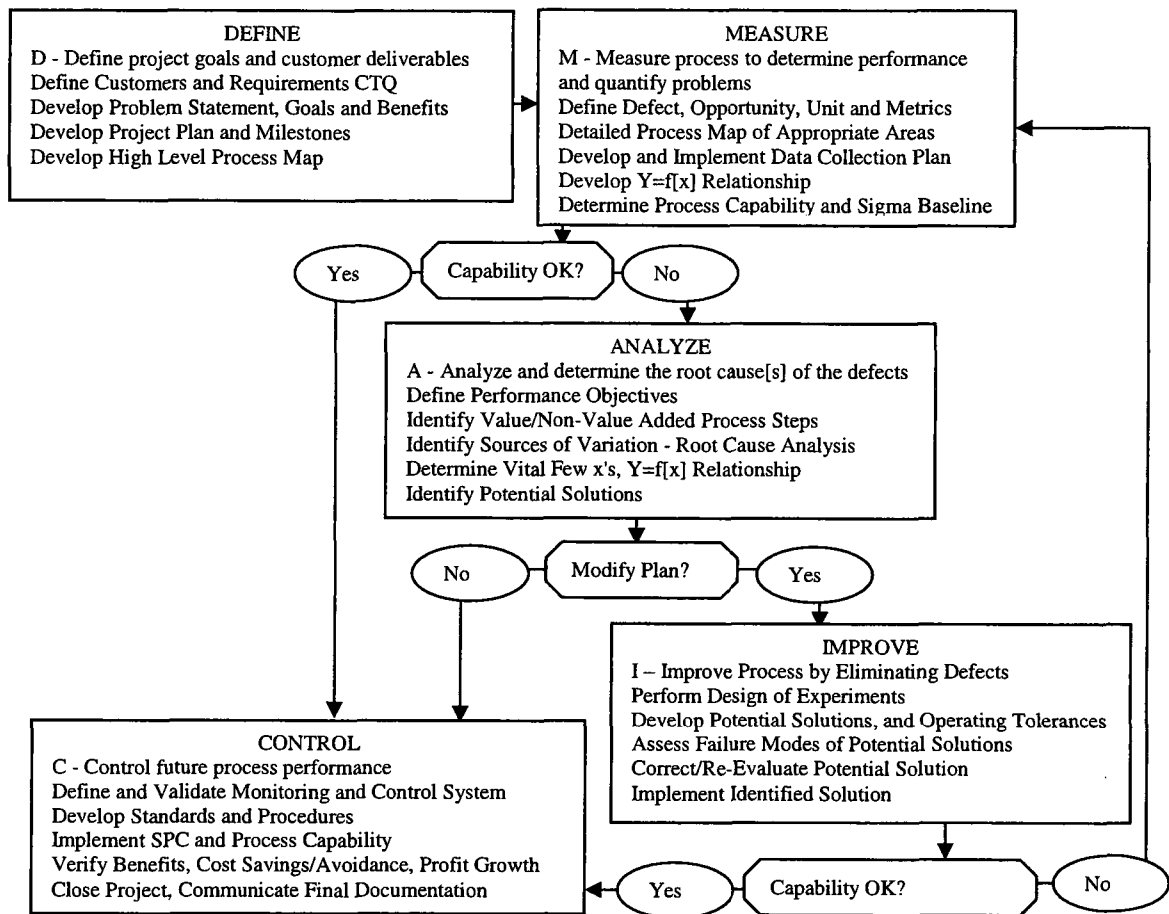


Figure 2.31. Define Measure Analyze Improve Control (DMAIC) road map (i Six Sigma, 2006).

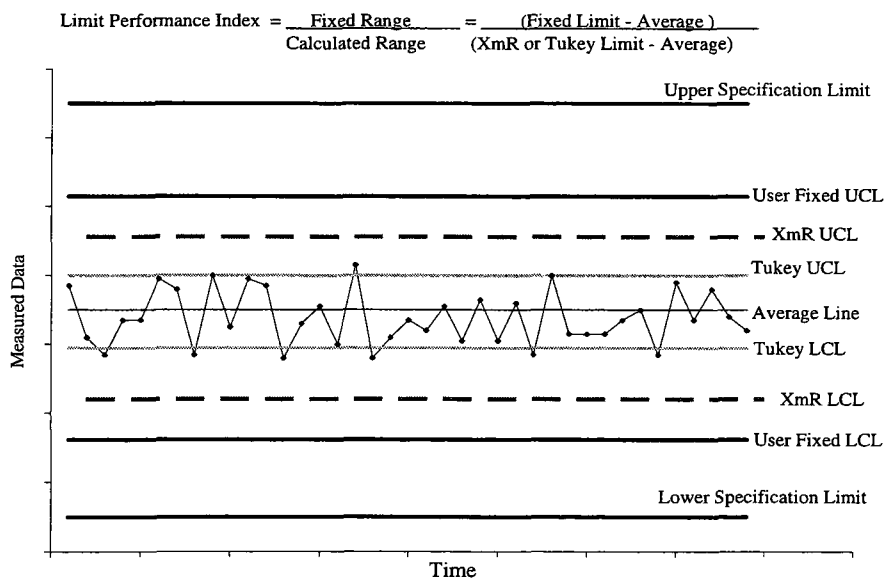


Figure 2.32. Control charts using individual moving average XmR and Tukey method.

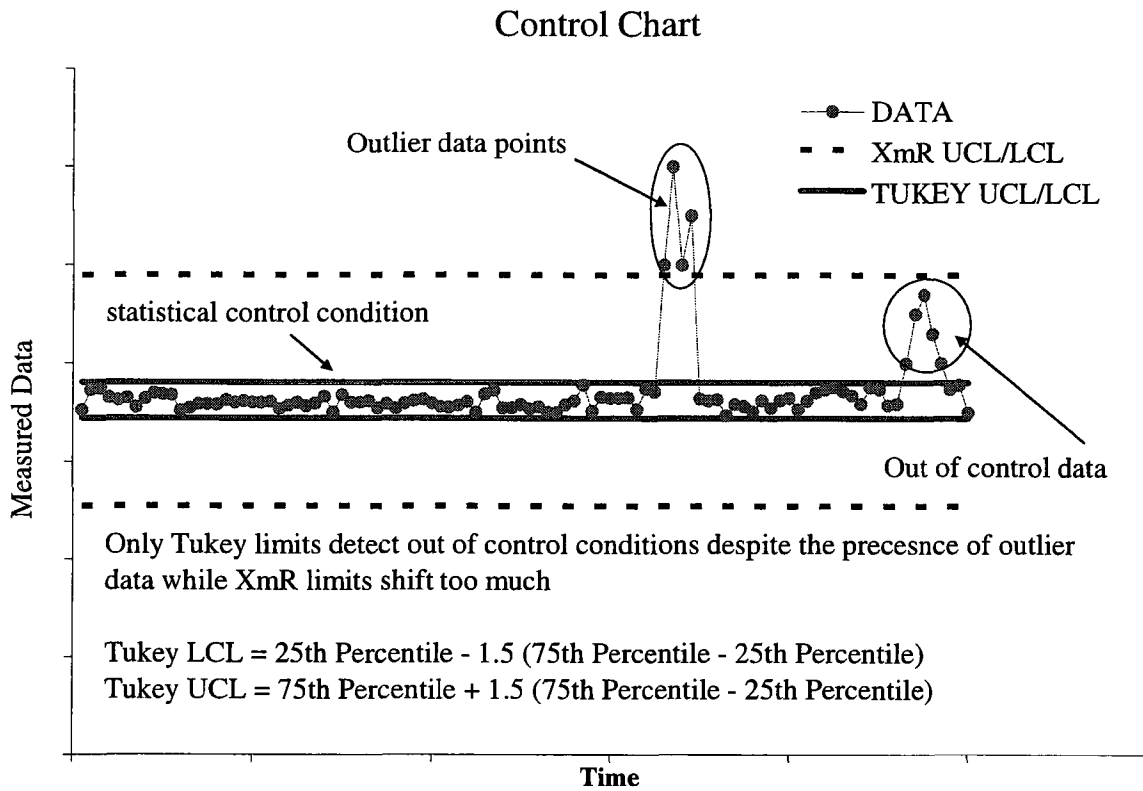


Figure 2.33. Advantage of using tukey control charts (i Six Sigma 2005).

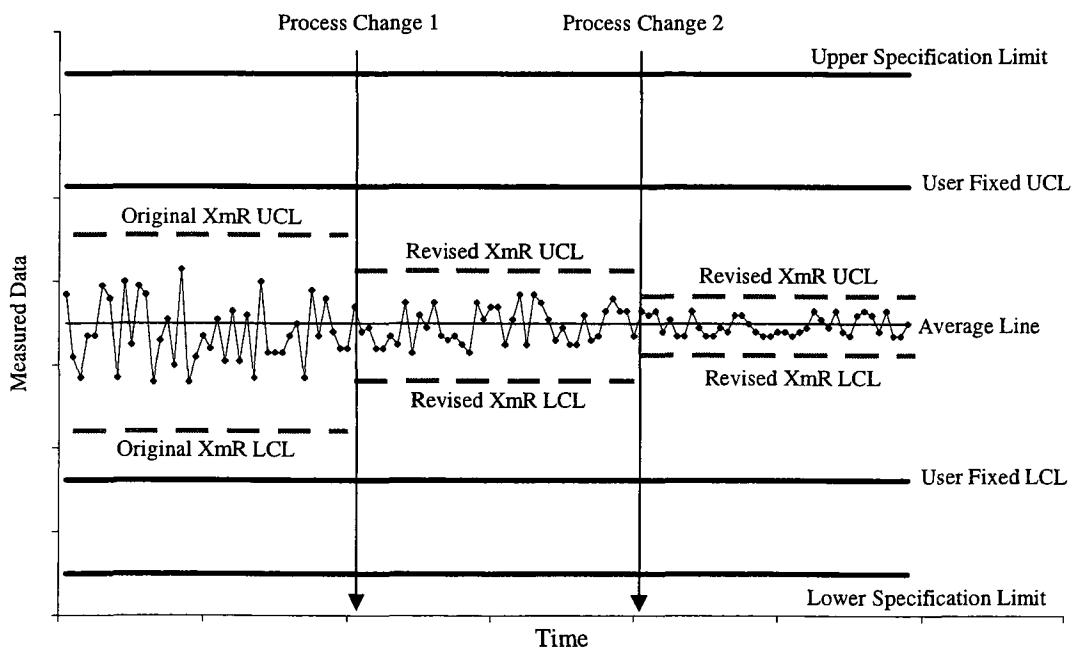


Figure 2.34. Danger of using fixed limits instead of statistically calculated limits (i Six Sigma 2005).

### 3 METHODOLOGY OF EXPERIMENTS

#### 3.1 Introduction

This chapter discusses the experimental setup and data collection plan used in this thesis. The experiments for this study were conducted using samples collected from different stages of the WAP production process. Statistical analysis of the in process W319 Al Alloy measured composition was used to calculate valid chemical control limits established under stable process conditions. The process was determined to be stable based on the results of the casting quality testing that focused on hardness and x-ray porosity data. Cooling curve experiments were conducted to establish control limits for the W319 Al Alloy solidification characteristics. The melt samples for cooling curve analysis were collected using Melt Sampling Device (MSD) that was redesigned and constructed during the course of this study. Heating and cooling curve experiments were conducted using Universal Metallurgical Simulator and Analyzer (UMSA) samples from ingots, melt, and castings as described in Figure 3.1 (Kasprzak, et al., 2002). The UMSA experiment was used to establish the start of the melting point control limit that is critical for the heat treatment process. The collected samples are summarized in Table 3.1.

#### 3.2 Chemical Analysis

The alloy composition used at WAP was measured using OES spark analysis performed per ASTM E1251. Samples for chemical analysis were collected every four hours during production from each melt furnace as shown in Figure 3.2. In addition a representative sample was shipped by the supplier along with each ingot heat batch. The spectrometer used at WAP was the ARL 3460 Metals Analyzer shown in Figure 3.3 (ARL, 2006). The OES test samples were cast using ASTM type B mold that conforms to the ASTM E176 shown in Figure 3.4 (ARL, 2006). This sample is approximately 64mm in diameter and 10 mm in thickness. The sample is mill machined on the riser side to prepare the surface for analysis. An average of at least three measurements on each sample were calculated and stored in a quality records database. The chemical analysis test can be performed along a band just inside the sample's circumference.



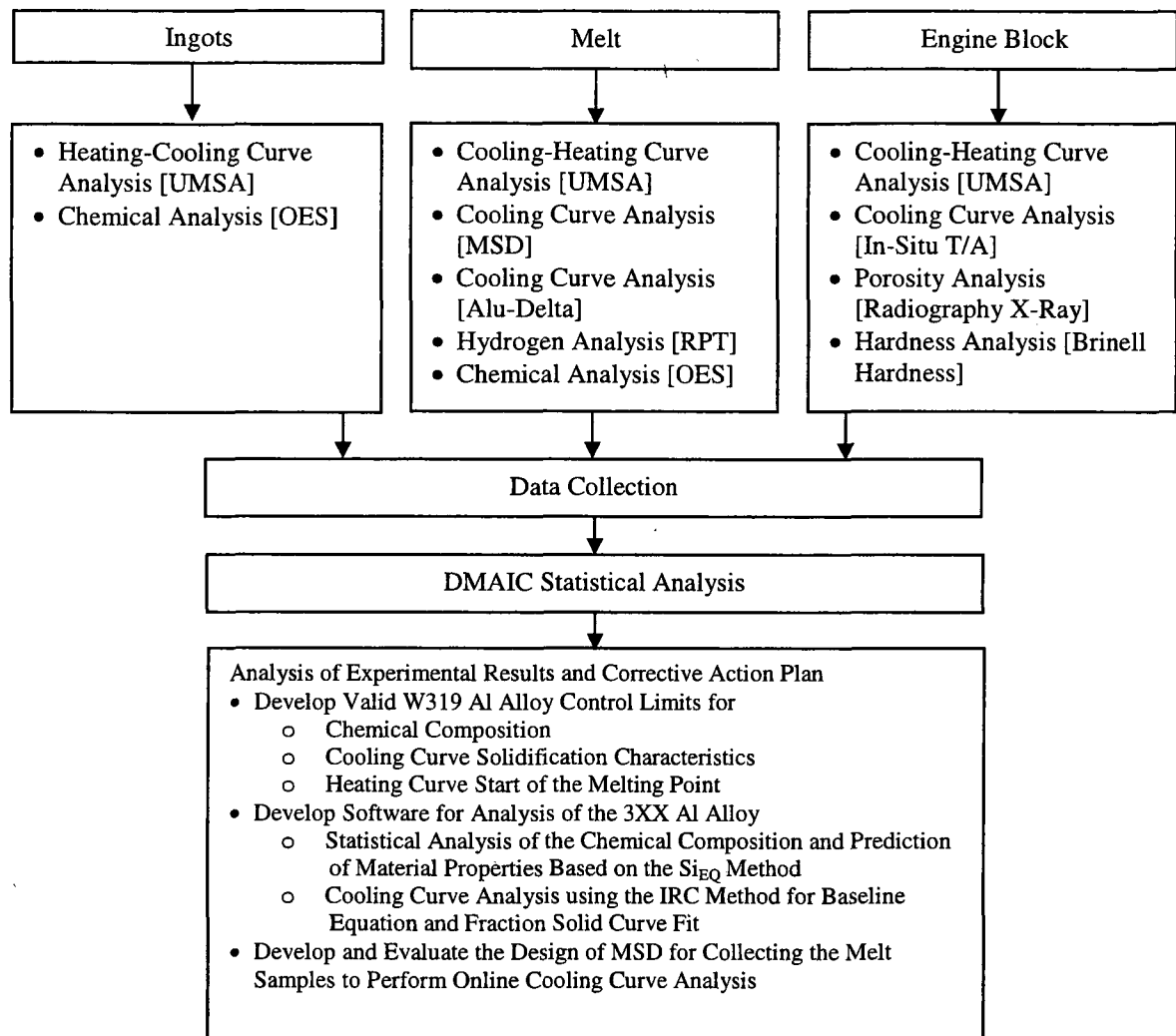


Figure 3.1. Design of experiments for WAP plant wide quality assessment.

Table 3.1. Summary of data collected from the WAP production process.

Sample Type	Sample Origin	Test Method	Analysis Type	Number. of Samples
Ingot	Ingots from Two Approved Suppliers	UMSA	Heating-Cooling Curves	6
		OES	Spark Chemical Analysis	300
Melt	Melt Holding Furnace after Filtering and Degassing	UMSA	Heating - Cooling Analysis	3
		MSD	Cooling Analysis	25
		OES	Spark Chemical Analysis	300
		RPT	Hydrogen Analysis	300
Casting	3.0L V6 Engine Block Inner Bulkhead Sections	UMSA	Heating - Cooling Curves	6
		Brinell	Macro Hardness Analysis	144
		X-Ray	Porosity Analysis	69

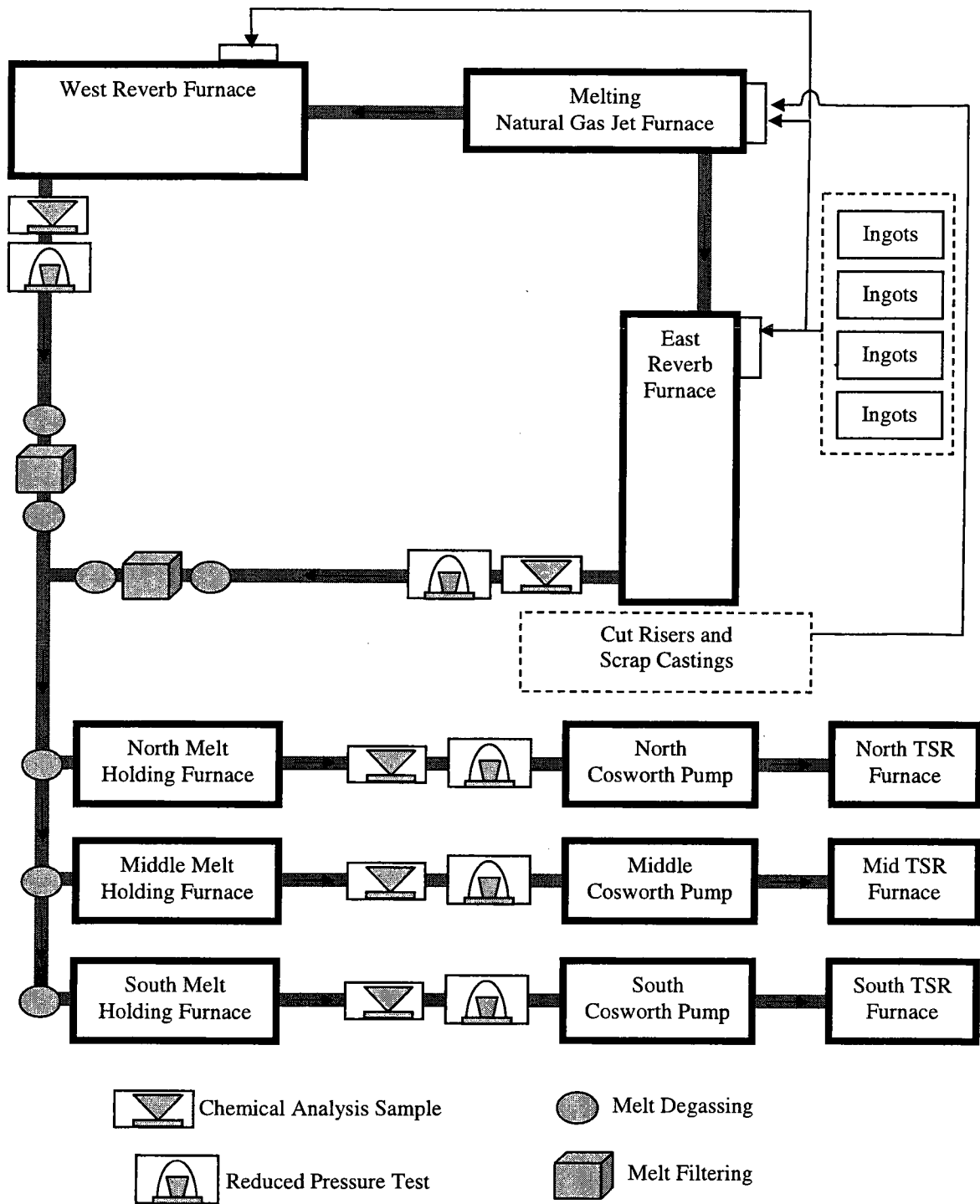


Figure 3.2. Sampling plan for OES analysis and Hydrogen analysis at WAP.

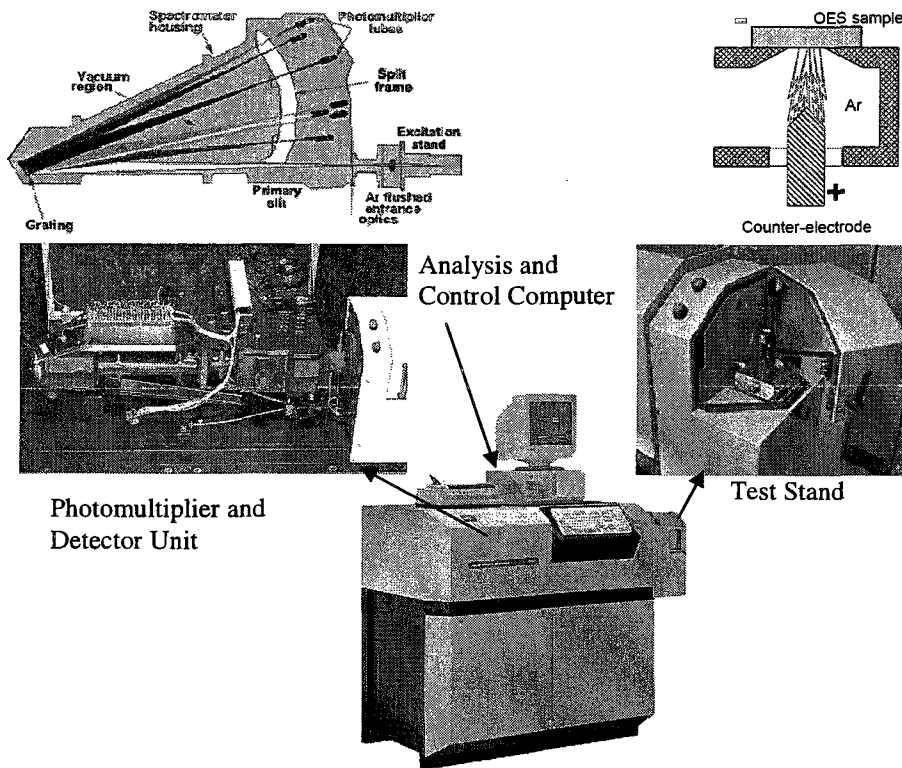


Figure 3.3. ARL 3460 Metal Analyzer Spectrometer for Metal Analysis (ARL, 2006).

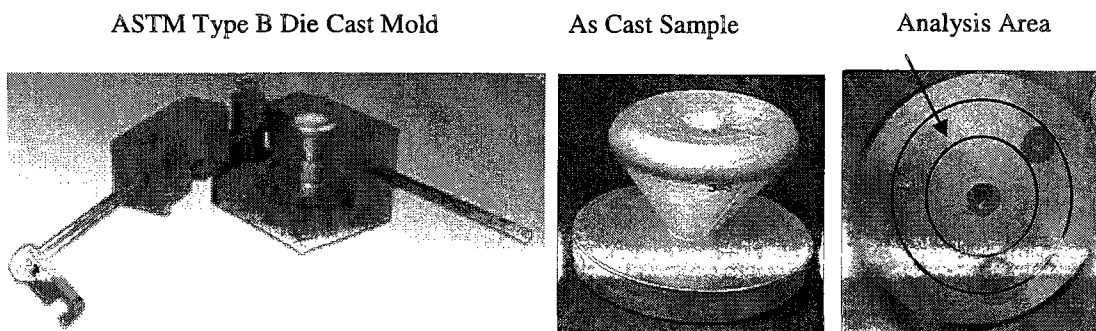


Figure 3.4. ASTM Type B Mold and OES Test Sample (ARL, 2006).

### **3.3 Dissolved Hydrogen Gas Analysis**

The RPT test was used to evaluate the tendency of the melt to form porosity as a result of dissolved hydrogen content and melt cleanliness. The melt samples for the RPT were collected every four hours during production from each melt furnace. Each RPT sample was rated from one to twelve with grade one having the least and grade twelve having the most porosity as shown in Figure 3.5 (WAP, 2004). The UCL used for rating the porosity of the RPT sample is four where up to three is still considered acceptable.

### **3.4 Radiography Analysis**

Radiography analysis was used at WAP to rate the level of internal casting porosity. This test was performed at the beginning of each day shift by randomly sampling two castings from each production line. The selected castings were saw cut into discrete sections of about one inch in thickness. Each section was rated from one to eight with grade one having the least and grade eight having the most porosity per ASTM standard E155. The WAP acceptable maximum limit for section porosity rating was grade level four where grade two was the most common under normal production conditions. The most critical radiography analysis measurements are performed on the inner bulkhead sections as shown in Figure 3.6.

### **3.5 Hardness Analysis**

Hardness analysis of the engine blocks cast at WAP was measured after partial solution heat treatment and after artificial aging heat treatment. The hardness was measured using a Brinell hardness test per ASTM E10 standard with a 10mm ball, 500kg load, and 15 seconds loading time. The WAP acceptable hardness measurements were between 85 to 115 BHN as defined in the customer specification. The most critical hardness test points are located on the bottom surface of the inner bulkhead sections as shown in Figure 3.7.

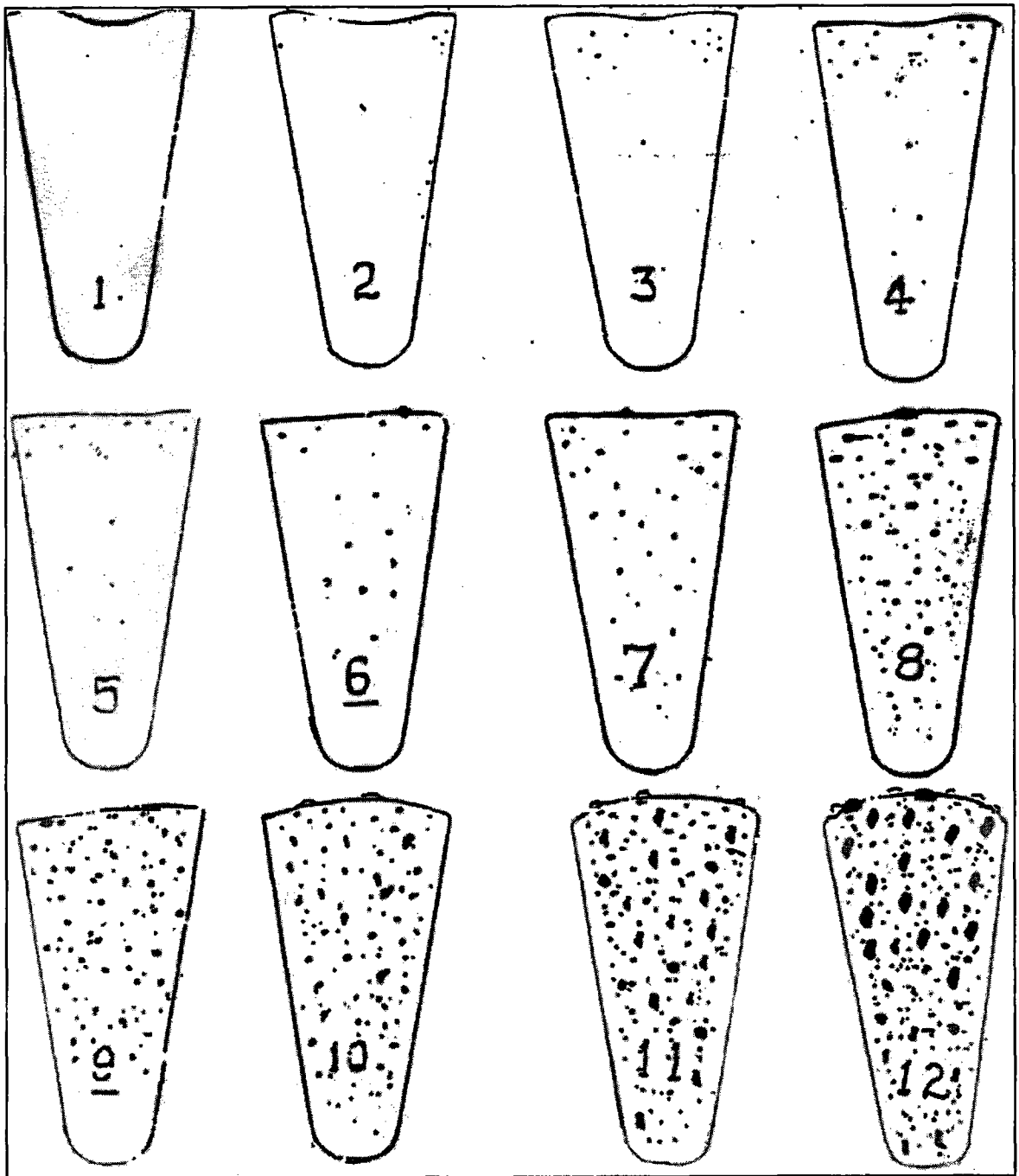


Figure 3.5. Visual Rating Standard for the Reduced Pressure Test (WAP, 2004).

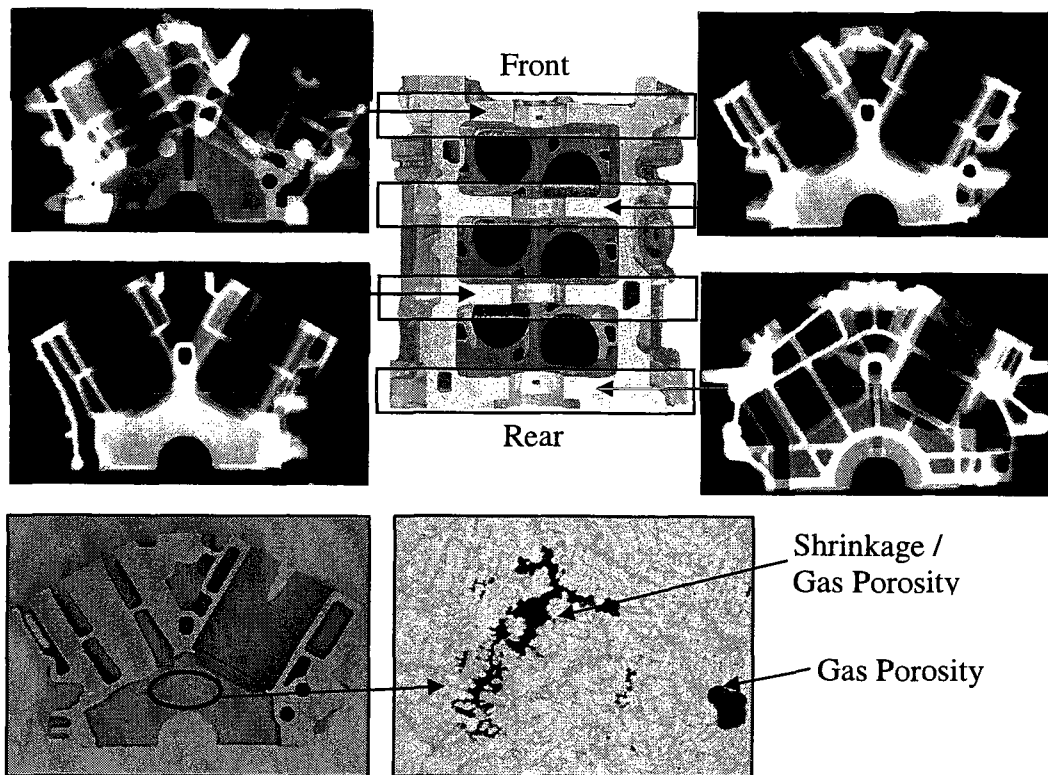


Figure 3.6. X-Radiography Porosity Analysis of Engine Block Bulkhead Sections.

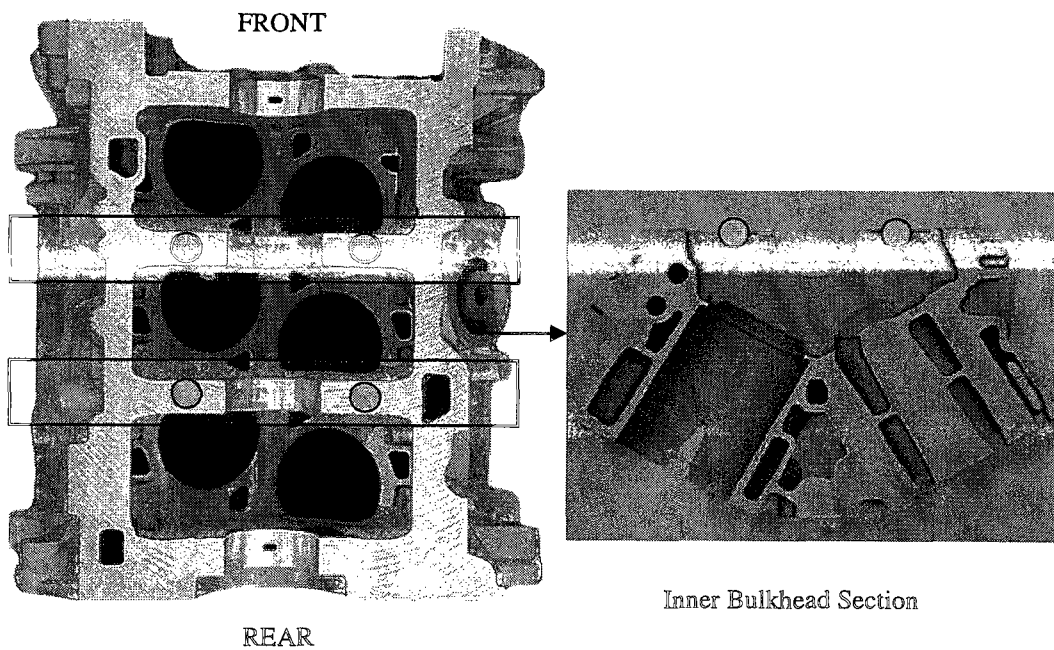


Figure 3.7. Hardness Brinell Analysis of Engine Block Bulkhead Sections.

### 3.6 Heating Curve Analysis

Heating curve analysis was performed to detect the start of the melting point for samples collected from the WAP production process. The start of the melting point was detected using the UMSA equipment. The UMSA sample was machined and placed inside a ceramic test cup that was then heated using an electrical heating coil. Temperature variations during heating and cooling were detected using a thin low mass thermocouple inserted in the center of the sample, as shown in Figure 3.8 (Kasprzak, et al., 2002). The start of melting could be detected by an abrupt change in the calculated first derivative of the recorded temperature signal as described in Figure 3.9. The advantage of using UMSA was the ability to conduct melting and solidification analysis on samples collected from different stages of the production process as shown in Figure 3.10 (Kasprzak, et al., 2002). The UMSA samples were machined out of the following:

- Ingots: sectioned ingots from two supplier sources released for use in production.
- Melt: bars die cast using a filtered and degassed melt from the middle of the holding furnace.
- Casting: Inner bulkhead sections cut from the 3.0L V6 engine block castings.

The UMSA test equipment could be used to perform metallurgical simulations of thermal processes at different heating and cooling rates.

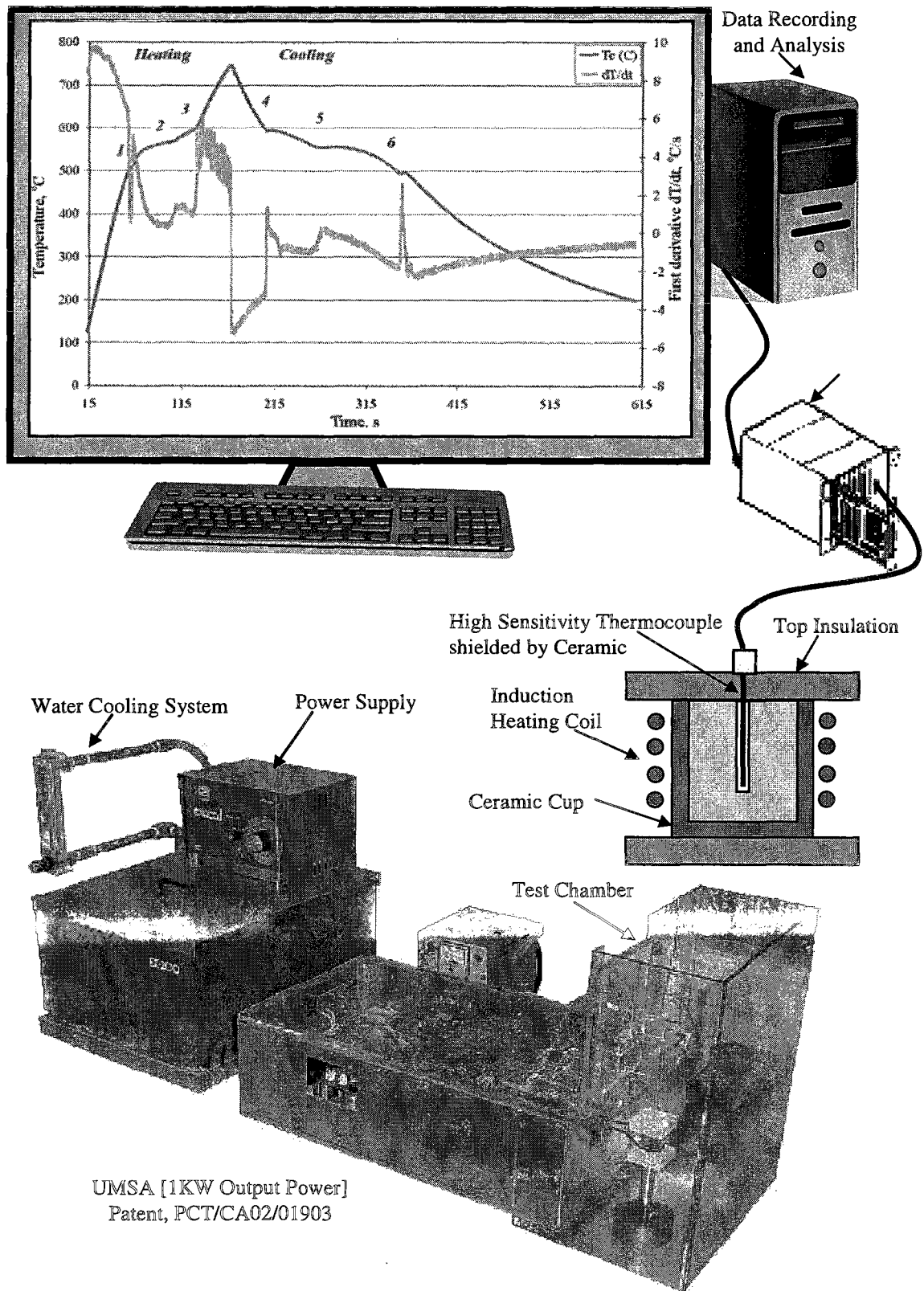


Figure 3.8. Heating and cooling curve analysis using UMSA (Kasprzak, et al. 2002).



The main metallurgical reactions that occur during heating are:

1. Start temperature for melting of Cu enriched phases
2. Start temperature for Al-Si eutectic dissolution
3. Start temperature for Al dendrite network dissolution

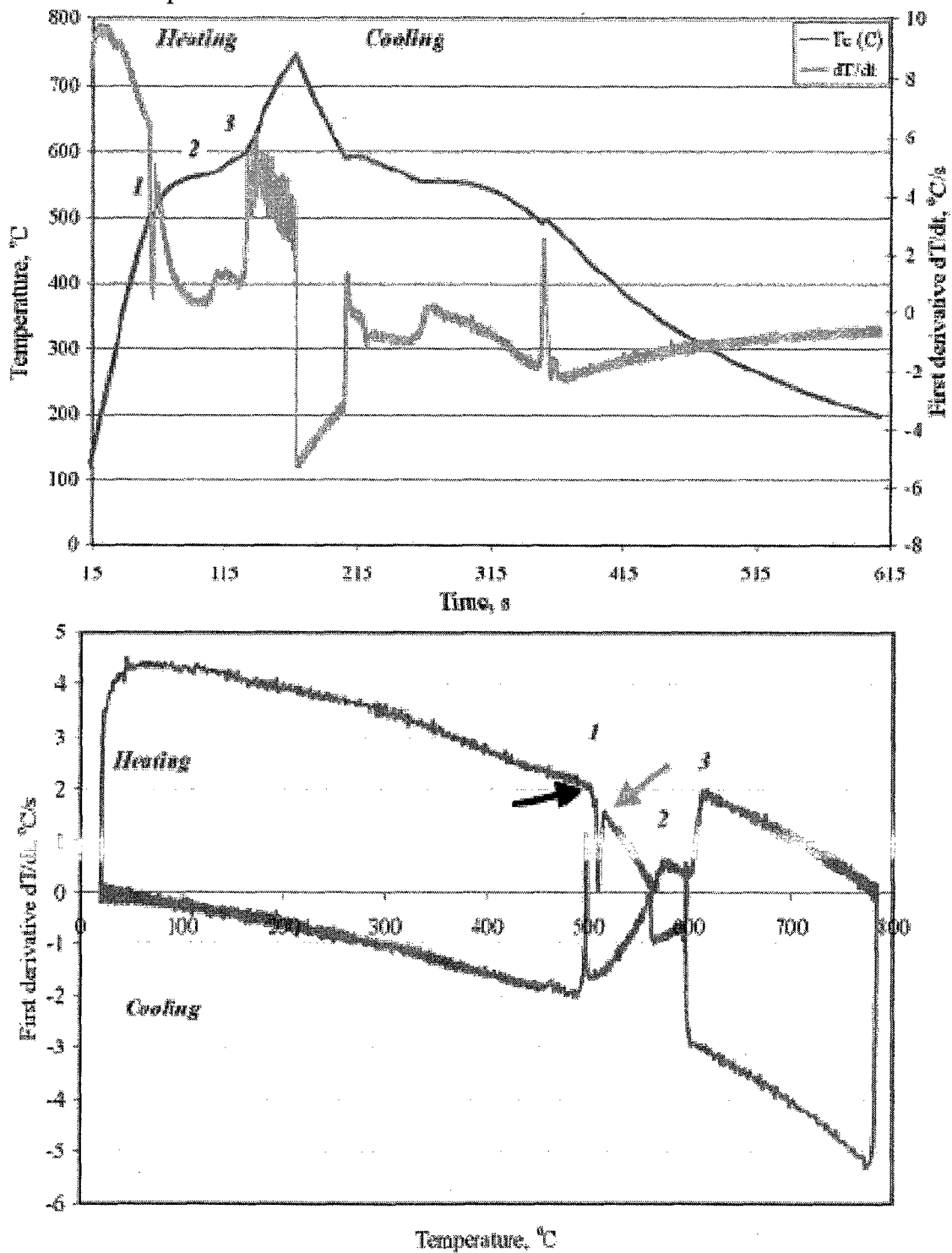


Figure 3.9. Heating / cooling curves and 1<sup>st</sup> derivative for the W319 Al alloy sample (Kasprzak, et al., 2002).

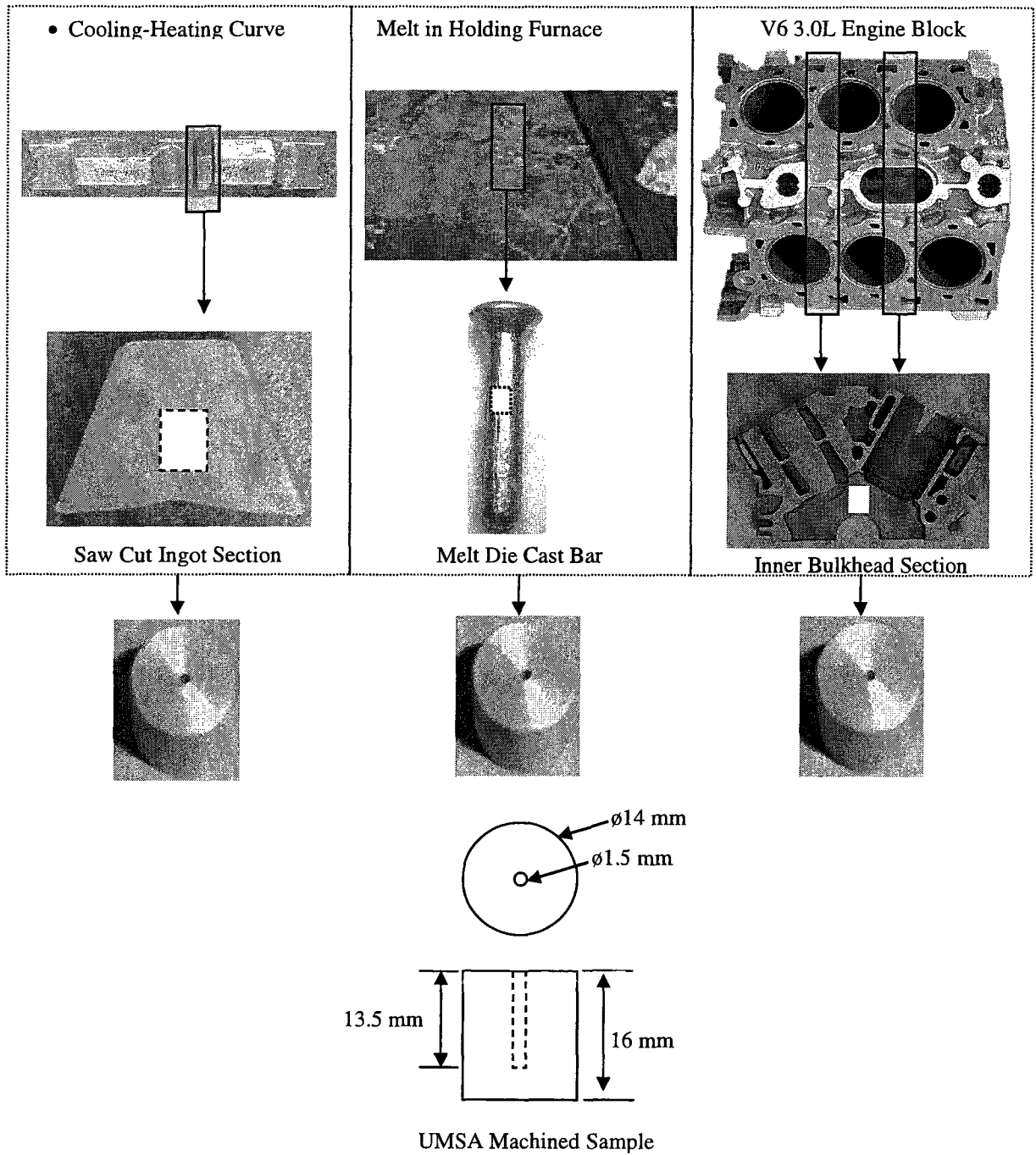


Figure 3.10. Description of UMMA Samples Extracted from Ingots, Melts, and Castings (Kasprzak, et al., 2002).

### 3.7 Cooling Curve Analysis

Cooling curve experiments were performed using the MSD that was constructed during the course of this study. The solidification characteristics for the W319 Al Alloy are listed in Table 3.2 and were detected through cooling curve analysis calculations and are described in Figure 3.11 and Figure 3.12. The melt samples were collected from the WAP Middle melt holding furnace. The design of the MSD shown in Figure 3.13 features a hollow test cup with a moving end cap. The advantage of the MSD design is the ability to collect the melt sample from a depth of up to six inches below the top surface without causing any harmful disturbance, see Figure 3.14. The cooling curve signal for each sample was recorded using the Aluminum Thermal Analysis Platform (AITAP) software developed by the IRC. The thin wall steel test cup was coated with a graphite-water based solution and preheated to 200<sup>0</sup>C for at least 10 minutes. The melt top surface was carefully skimmed before sampling to remove the top floating oxides. The bottom end cap was first submerged into the melt followed by a hollow test cup until both contact each other and form a two piece test cup with a sealed interface inside the melt. The two piece test cup was raised out of the melt together until it reached the top plate that held a thermocouple to measure the cooling curve of the solidifying melt sample. The key to prevent melt leakage during sampling was to use flexible ceramic insulation between the test cup and the end cap that would form a seal when the two pieces were pressed against each other. The National Instrument 16 MIO data acquisition equipment was used to record the temperature signal at a rate of five readings per second. The recorded cooling curves for samples collected with the MSD were compared to cooling curves recorded by the Alu-Delta test equipment. The Alu-Delta procedure used at WAP was used transfer the melt from the furnace to the sand test cup using a steel ladle as shown in Figure 3.15.

Table 3.2. Cooling curve characteristics for the W319 Al alloy ()

Symbol	Critical Temperature	Metallurgical Significance
$T_{\text{NUC}}^{\alpha\text{DEN}}$	$\alpha$ -Al Dendrite Nucleation	Beginning of Solidification as stable $\alpha$ -Al dendrites nucleate, where only mass feeding occurs.
$T_{\text{MIN}}^{\alpha\text{DEN}}$	$\alpha$ -Al Dendrite Under cooling	In the absence of grain refiners the molten Aluminum is under-cooled to a minimum temperature below the equilibrium solidification temperature. At this point the Latent heat generated during dendrite nucleation equals the sample heat loss. After this point the temperature rises until it reaches a steady state growth temperature.
$T_{\text{G}}^{\alpha\text{DEN}}$	$\alpha$ -Al Dendrite Growth Recalescence	The solid nuclei start to grow beyond a critical size and act as nucleation particles for new crystals slowing down the cooling rate of the metal. In the meantime the previously formed crystals start to grow. The solidifying melt reaches a steady state growth temperature as more latent heat is released by the nucleation of new $\alpha$ -Al crystals. After this point the temperature decrease resumes.
$T_{\text{COH}}^{\alpha\text{DEN}}$	Dendrite Coherency Point (DCP)	The dendrite structure starts to coarsen until neighbouring dendrites start to impinge upon one another and further growth occurs only by dendrite coarsening. At this point transition from mass feeding to interdendritic feeding occurs. This point is considered as an indicator of the feeding efficiency which marks the beginning of possible feeding problems resulting in shrinkage pore formation.
$T_{\text{E,NUC}}^{\text{Al-Si}}$	Al-Si Eutectic Nucleation	As the dendrites become coarser, Al is depleted out of the liquid in the solidification front until it reaches a eutectic composition. At this point the Al-Si eutectic starts to solidify in the interdendritic regions.
$T_{\text{E,MIN}}^{\text{Al-Si}}$	Al-Si Eutectic Minimum	The latent heat generation from co-precipitation of stable Al and Si equals the sample heat loss. After this point the temperature rises until reaching a steady state growth.
$T_{\text{E,G}}^{\text{Al-Si}}$	Al-Si Eutectic Growth	Considerable eutectic growth occurs indicated by a long plateau in temperature. As the Al-Si eutectic solidification proceeds and the fraction solid increases, feeding becomes more tortuous in the reduced interdendritic channels.
$T_{\text{E,NUC}}^{\text{Al-Cu}}$	Al-Cu Rich Eutectic Nucleation	Formation of the Al-Cu rich eutectic as the remaining liquid becomes enriched with Cu and Si. This point is critical to establish adequate solution treatment parameters.
$T_{\text{E,MIN}}^{\text{Al-Cu}}$	Al-Cu Rich Eutectic Minimum	The latent heat generation from precipitation of the Copper rich phases equals the sample heat loss. After this point the temperature rises until it reaches a steady state growth.
$T_{\text{E,G}}^{\text{Al-Cu}}$	Al-Cu Rich Eutectic Growth	The relatively small presence of Copper results in a small amount of latent heat released after reaching the steady state growth. The solidification of these phases is critical for formation of micro-porosity since the deposits of ternary liquid solidify when the rest of the bulk of the casting is already solid and the volumetric shrinkage in these deposits is difficult to feed.
$T_{\text{SOL}}$	Solidus	End of the solidification process.

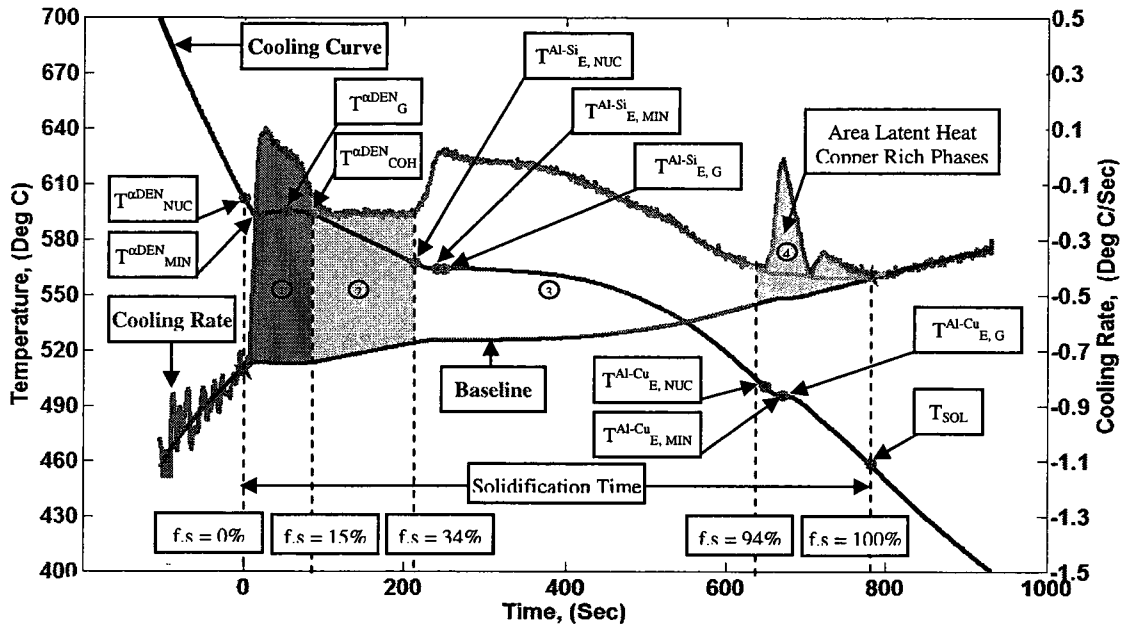


Figure 3.11. Cooling curve analysis temperature – time with baseline plot and temperature 1<sup>st</sup> derivative – time plot for the W319 Al alloy Sample from WAP.

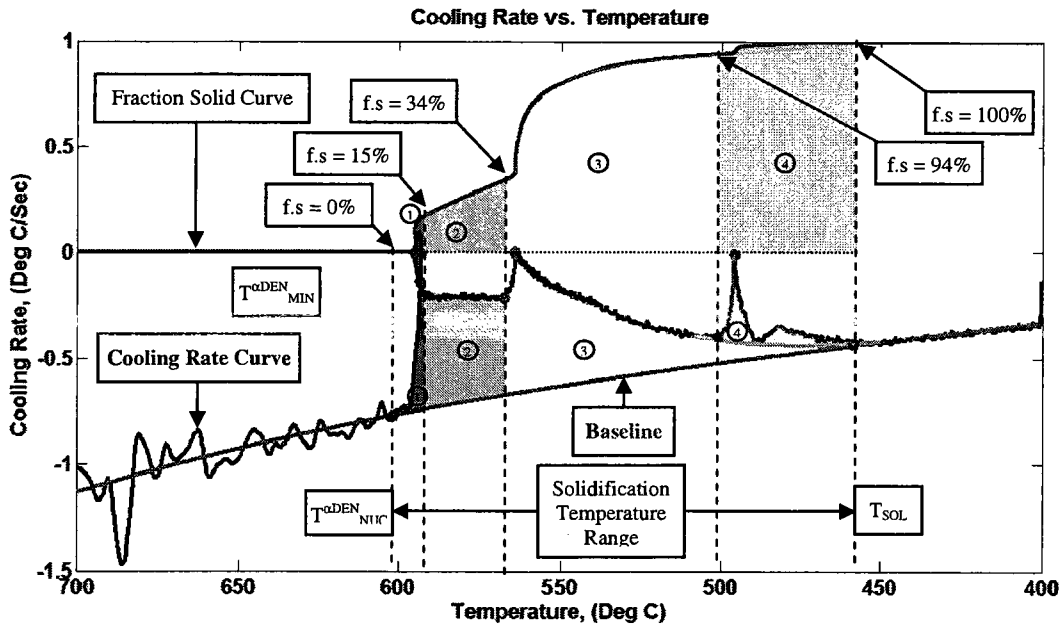


Figure 3.12. Cooling curve analysis - temperature 1<sup>st</sup> derivative - temperature with baseline plot and fraction solid – temperature plot for the W319 Al alloy Sample from WAP.

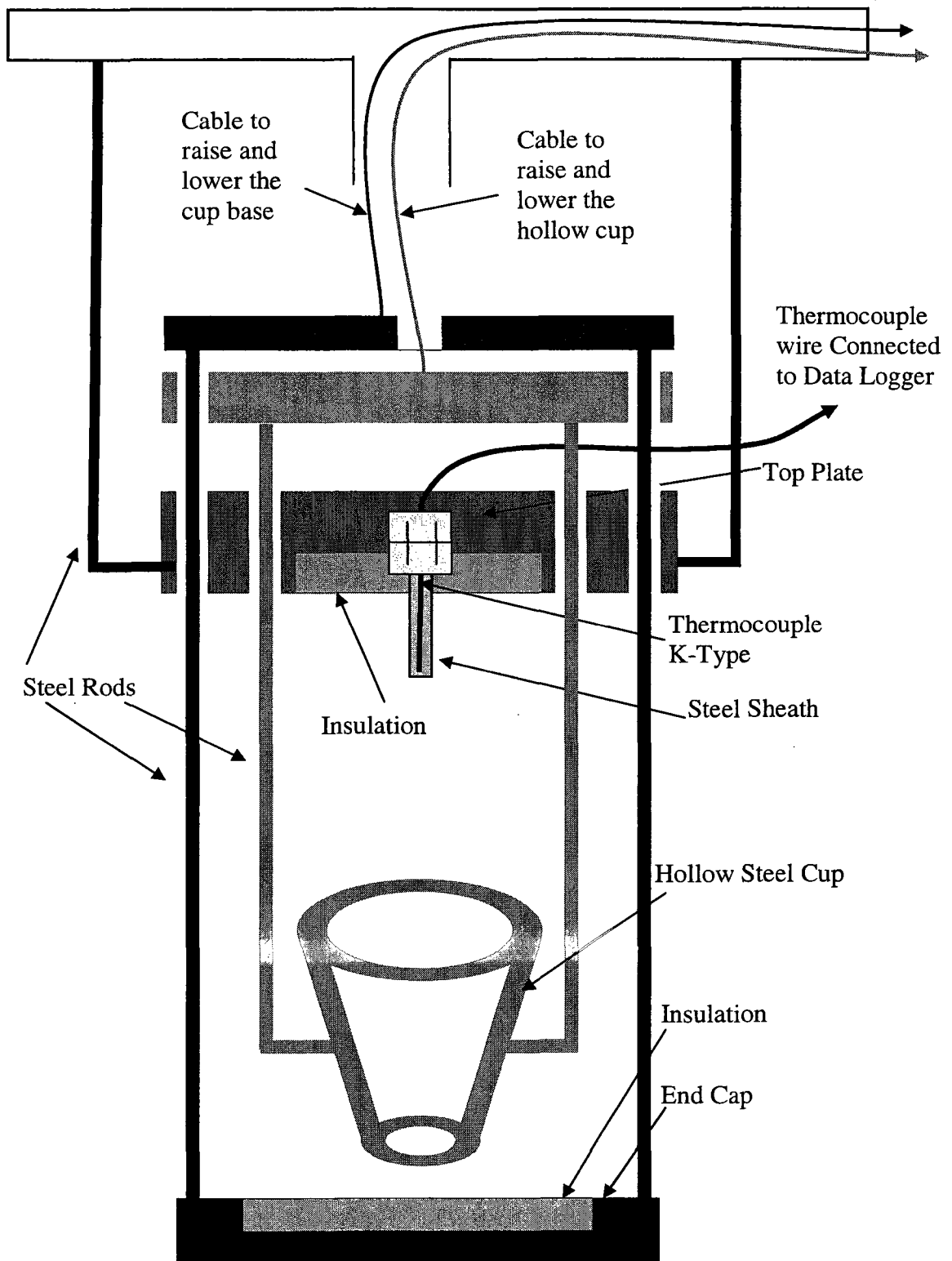
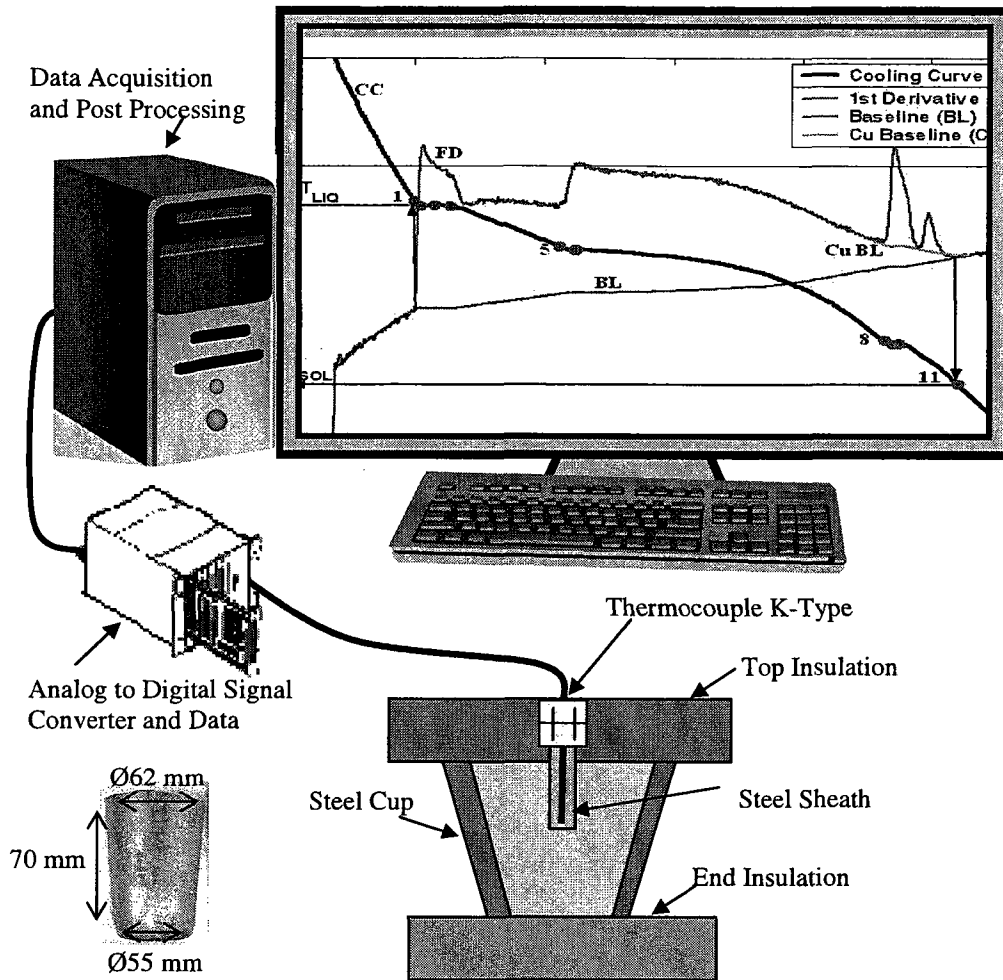


Figure 3.13. Schematic diagram of the MSD.



Step #1 Submerge End Cap	Step #2 Submerge Steel Test Cup	Step #3 Raise End Cap, and Filled Test Cup	Step #4 Start Recording Cooling Curve

Figure 3.14. Cooling curve analysis using the MSD.

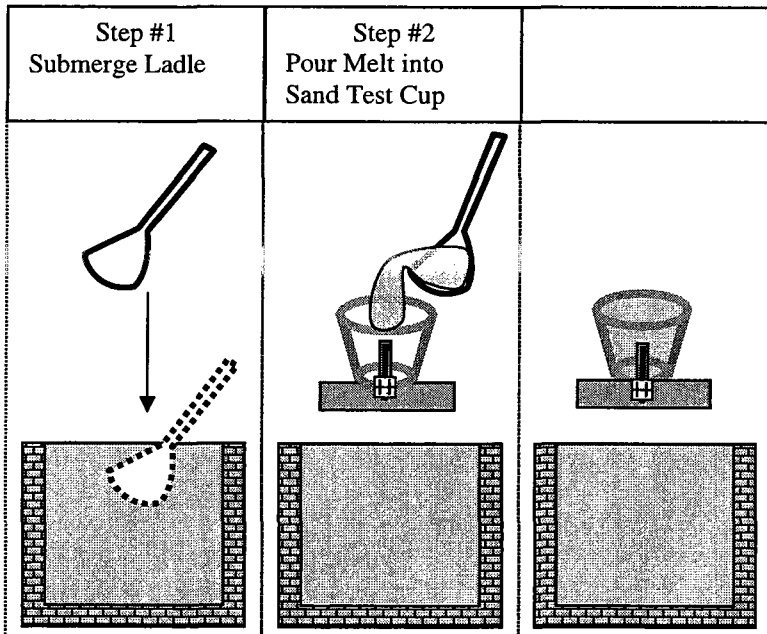
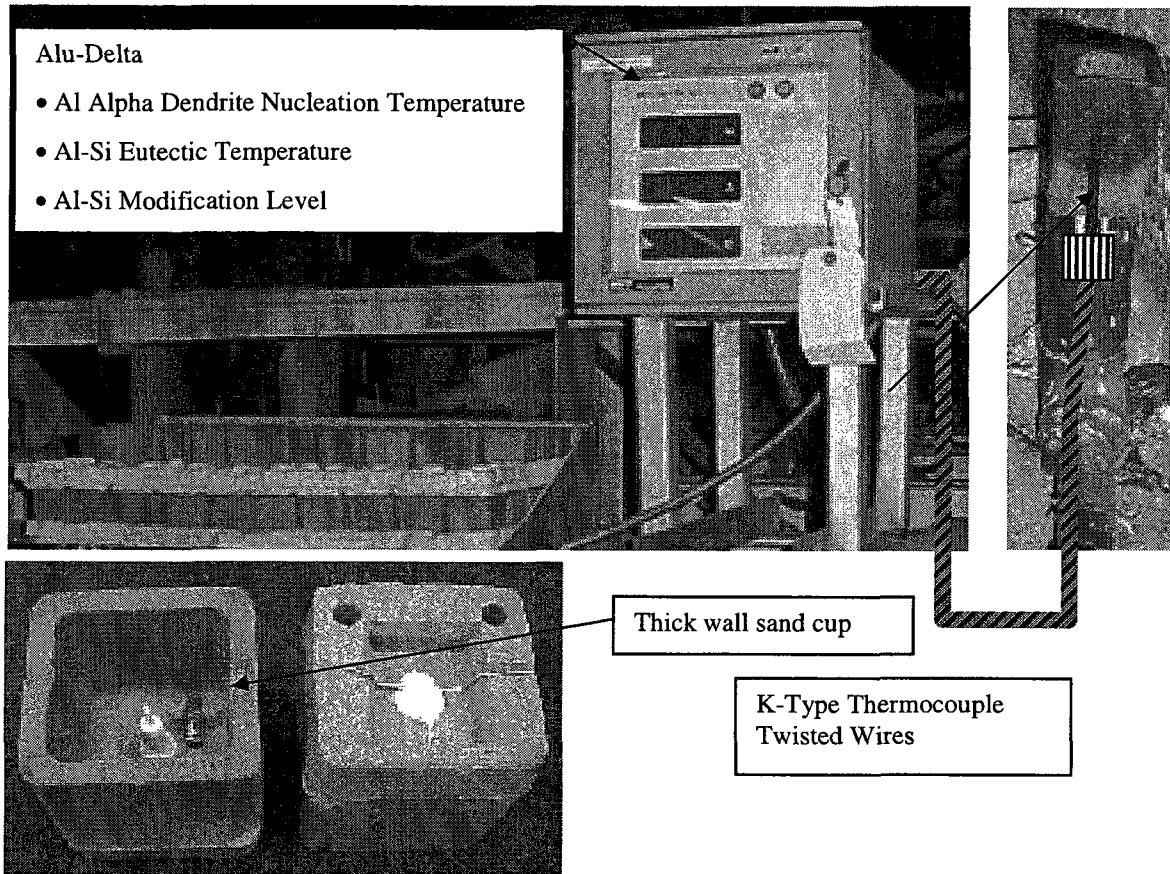


Figure 3.15. Sand cup used for cooling curve analysis with the Alu-Delta equipment.



## 4 RESULTS AND DISCUSSION

### 4.1 Recalculation of the W319 Al Alloy Control Limits

The fixed control limits used at WAP for the in process W319 Al Alloy were exclusively established based on Ford Material Specification WSE-M2A151-A2. In addition, there was no procedure enforced at WAP to regularly evaluate control limit performance. It is important to distinguish between process control limits and material specifications limits. The limits defined in the material specification must be wide enough to be used in more than one specific application. On the other hand, process control limits must be calculated statistically to reflect expected variations under stable conditions. As a rule the limit was considered too wide if PI was above 3.5, and too narrow if PI was below 1.0. The author proposed UCL and LCL that were recalculated such that the PI for each limit would be between an acceptable range of 1.2 and 2.8 as summarized in Table 4.1. The most alarming finding was that the fixed UCL for Tin was 17 times more than the Six Sigma limit, and 20 times more than the average measured value. The Tin content increased to more than twice the average measured value as shown in Figure 4.1. This increase in Tin content was identified as the only root cause for the hardness decrease in the bulkhead sections of the heat treated 3.0L V6 engine block casting as shown in Figure 4.2. The bulkhead hardness decreased to a level below the Six Sigma LCL and became dangerously too close to the LCL defined in the customer specification. The engine block casting hardness returned to normal levels only after using ingots with Tin content less than 100 ppm instead of 1000 ppm, which was implemented as a permanent corrective action. Statistical analysis using normal probability, histogram, and box plots shown in Figure 4.3, Figure 4.4, and Figure 4.5 indicate that any amount of Tin above 200ppm could be considered as suspect and out of normal distribution. The soft phases with a low melting point may form with the addition of Tin in Al Alloy(s) causing a decrease in hardness after heat treatment. The UMSA was used to perform heating curve analysis for the WAP samples collected from ingots, melts, and engine castings to measure the start of the melting point temperature as shown in Figure 4.6, and Figure 4.7. Summary of the heating curve analysis confirmed that an increase in Tin content noticeably lowers the start of the melting point temperature as

shown in Figure 4.8. High temperatures must be avoided during heat treatment of the casting to avoid localized melting that solidifies and forms weak grain boundary layer phases. It is suggested that the addition of Tin may suppress formation of the hardening particles during aging (Key to Metals, 2006). The Tin atoms may interact with vacancies more strongly than the solute atoms added specifically for strengthening such as Magnesium, Silicon, and Copper. The Tin atoms trap more quenched in vacancies. This results in a reduction of the number of free vacancies available as the potential solute atom carriers. This results in a diffusion delay of the solute atoms causing a suppression of precipitation during aging. However, it should be considered that the response may be different for each case depending on the type and concentration of precipitation formed during the aging processes. Special care must be taken when dealing with low melting point elements that are higher than historical levels. The high amount of low melting point element such as Tin introduced into the furnace as an ingot charge may not only melt but also vaporize. If the Tin vapor enters the porous refractory, it may condense especially in the lower temperature areas near the furnace walls and then solidify. When the furnace is next heated, the solid metal expands and cracks the refractory.

The wide control limits identified in this study were recalculated such that the PI would be in an acceptable range between 1.2 and 2.8 as shown in Table 4.2. The alloy composition used for the recalculation of the limits was measured under stable process conditions. The recalculated control limits reflect the chemical variations that still yield acceptable casting quality. The casting quality was based on two critical tests performed on the inner bulkhead sections as summarized in Table 4.3. The critical to quality bulkhead hardness after heat treatment was well within the historical range as shown in Figure 4.9. The critical quality bulkhead porosity based on radiography analysis was acceptable and never exceeded the maximum historical ratings as shown in Figure 4.10. Statistical analysis of the collected WAP quality test results ensured that the recalculated limits would be valid for further benchmarking.

The author proposed that the Silicon LCL to be 7.0 wt.% instead of a 6.5 wt.% since the Silicon content for the WAP never decreased below 7.18 wt. %. There is no assurance indicating that engine blocks cast with only 6.5 wt.% Silicon in the W319 Al Alloy would have acceptable levels of strength and wear. The author proposed that the

Iron LCL to be increased from 0.00 wt.% to 0.30 wt.% as this may actually be an advantage for improving strength. The Iron content at WAP was never below 0.31 wt.% and never caused any harmful effect on casting quality. The author proposed that the Manganese LCL to be increased from 0.00 wt.% to 0.2 wt.% to insure that a sufficient amount of Manganese is present and effective to reduce the effects of high amounts of iron. In fact Ford Material Specification WSE-M2A151-A2 requires the ratio of Mn to Fe to be maintained at a minimum of 1:2. The Manganese content at WAP was never below 0.2 wt. %. Titanium is considered as an impurity element in the W319 Al Alloy that may form stable particles. These Titanium particles are stable and may cause EM pump failure by clogging as reported previously at WAP during 2000. The author proposed that the Titanium UCL to be decreased from 0.25 wt.% to 0.14 wt.% to decrease the potentially harmful effects caused by the stable Titanium particles formed during melt processing. The Titanium content at WAP was never above 0.125 wt. %. The author proposed that the Nickel UCL to be decreased from 0.10 wt.% to 0.07 wt.% as the content of this element at WAP was never above 0.04 wt. %. Lastly the author proposed that the UCL for Lead, a soft element with low melting point, to be decreased from 0.10 wt.% to 0.06 wt.% to avoid potential harmful effects caused by soft low melting point lead rich phases formed during solidification and heat treatment. The Lead content at WAP was never above 0.05 wt. %. Increasing amounts of Lead are undesired as the formed low melting point phases reduce hardness especially after heat treatment, and increase grain boundary segregation during solidification.

Table 4.1. Evaluation Analysis of the WAP Chemical Control Limits.

Chemical Element	Statistical Analysis of WAP composition based on 2220 samples				Performance Evaluation of WAP Lower Control Limit			Performance Evaluation of WAP Upper Control Limit		
	Mean (wt. %)	Standard Deviation	Min (wt. %)	Max (wt. %)	LCL * (wt. %)	Performance Index	Limit Status	UCL * (wt. %)	Performance Index	Limit Status
Si	7.50	0.09	7.18	7.83	6.5	3.8	Too Low	8	1.9	OK
Cu	3.46	0.07	3.22	3.78	3	2.1	OK	4	2.5	OK
Fe	0.36	0.01	0.31	0.40	0	10.4	Too Low	0.4	1.3	OK
Mg	0.27	0.01	0.24	0.31	0.2	2.9	OK	0.35	2.9	OK
Mn	0.24	0.01	0.21	0.27	0	10.8	Too Low	0.3	2.5	OK
Zn	0.145	0.026	0.082	0.199	0	1.9	OK	0.250	1.4	OK
Ti	0.113	0.004	0.096	0.125	0	9.8	Too Low	0.250	11.9	Too High
Ni	0.026	0.006	0.013	0.044	0	1.5	OK	0.100	4.2	Too High
Cr	0.029	0.007	0.014	0.061	0	1.4	OK	0.100	3.3	OK
Pb	0.018	0.005	0.006	0.044	0	1.1	OK	0.100	5.2	Too High
Sn	0.005	0.002	0.002	0.016	0	0.9	OK	0.100	17.1	Too High

Limit needs to be changed \* Control limits based on Ford Material Specification WSE-M2A151-A2

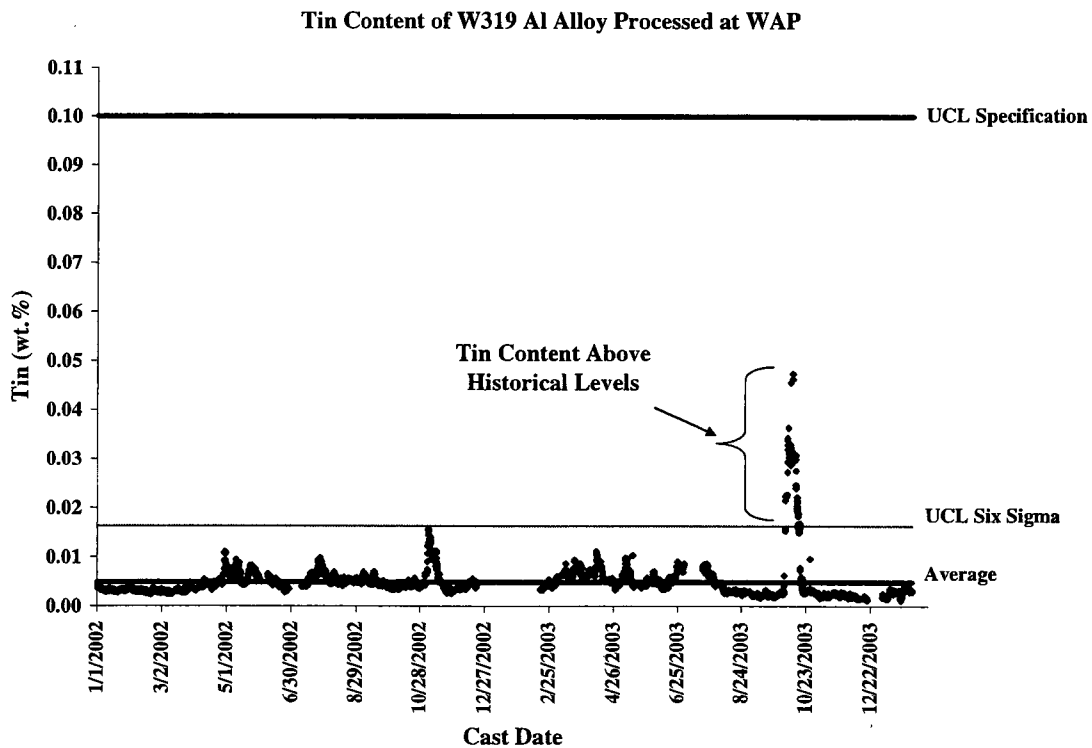


Figure 4.1. Run Chart for Tin in the W319 Al Alloy Processed at WAP.

WAP Block Brinell - 3.0L, Inner Bulkhead Hit Location 6

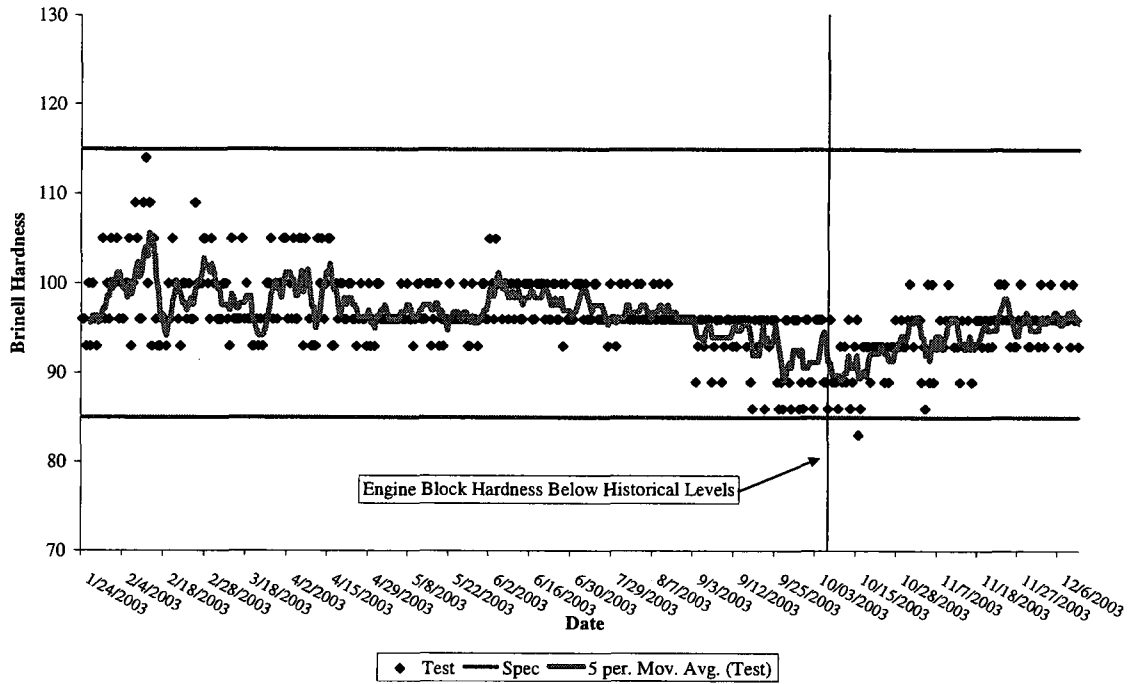


Figure 4.2 Hardness Analysis of the Engine Block Bulkheads Cast at WAP.

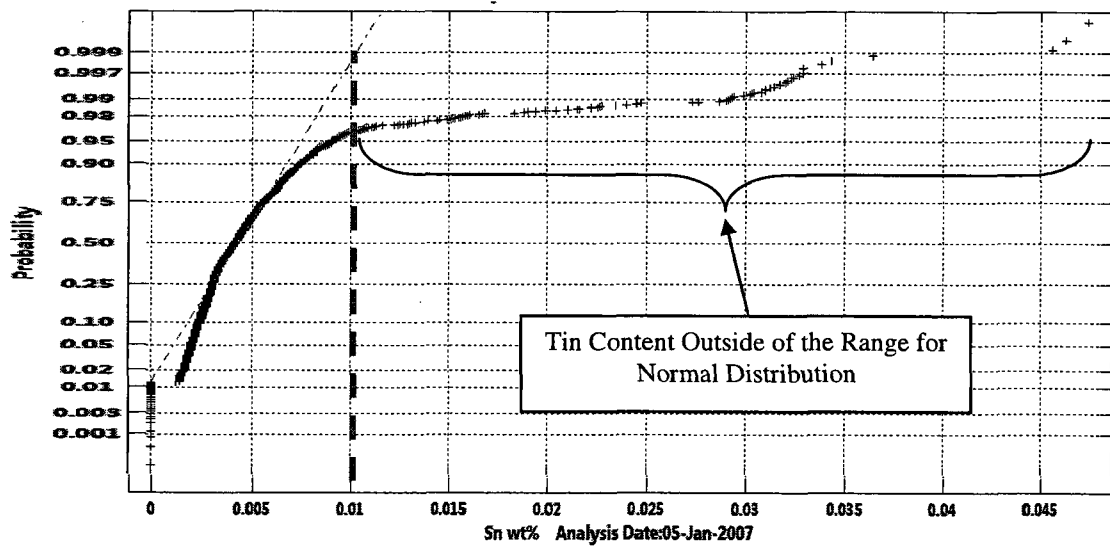


Figure 4.3. Normal Probability of Tin in the W319 Al Alloy Processed at WAP.

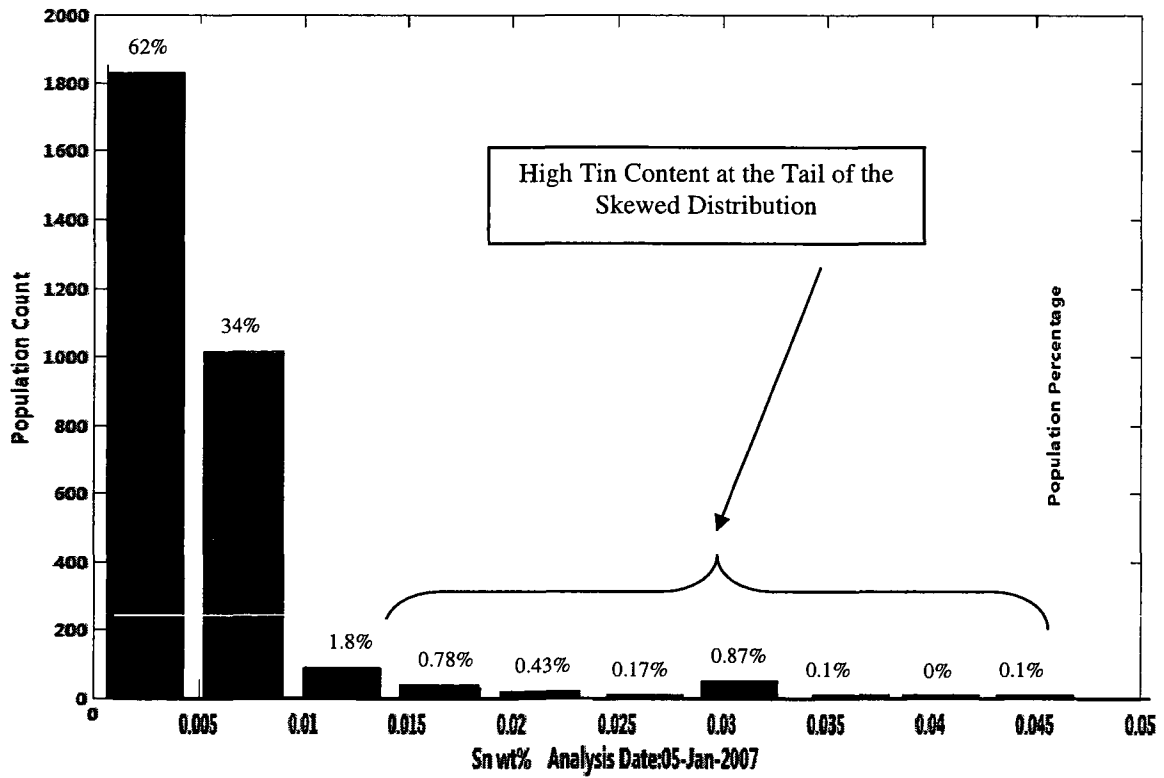


Figure 4.4. Histogram Plot of Tin in the W319 Al Alloy Processed at WAP.

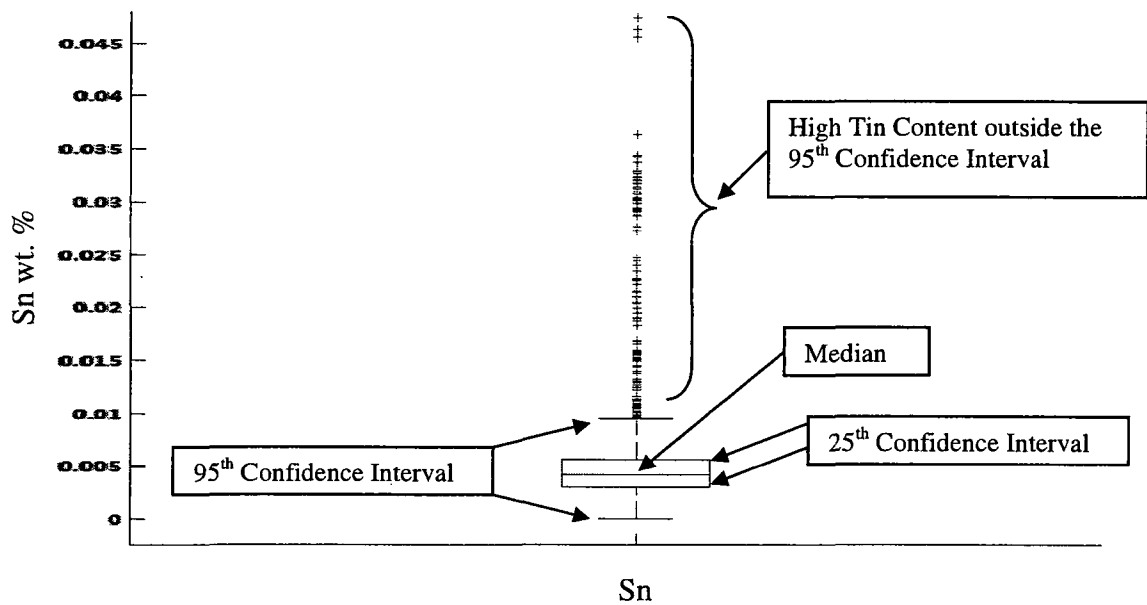


Figure 4.5. Box Plot of Tin in the W319 Al Alloy Processed at WAP.

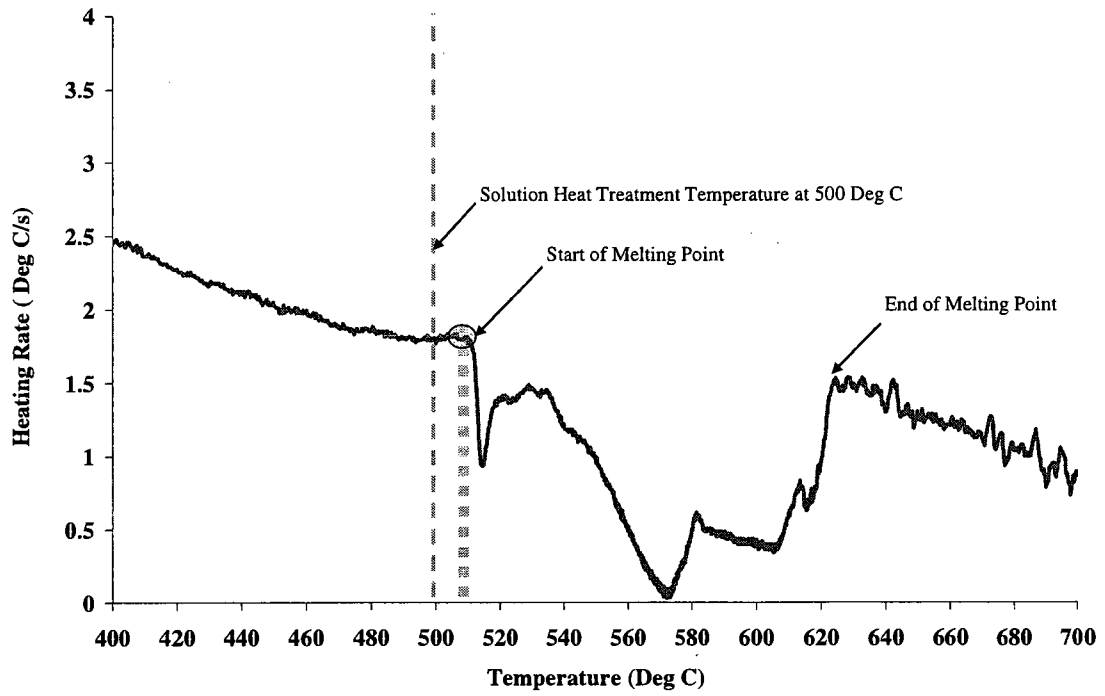


Figure 4.6. Heating Curve Analysis Featuring Temperature – Time Plot.

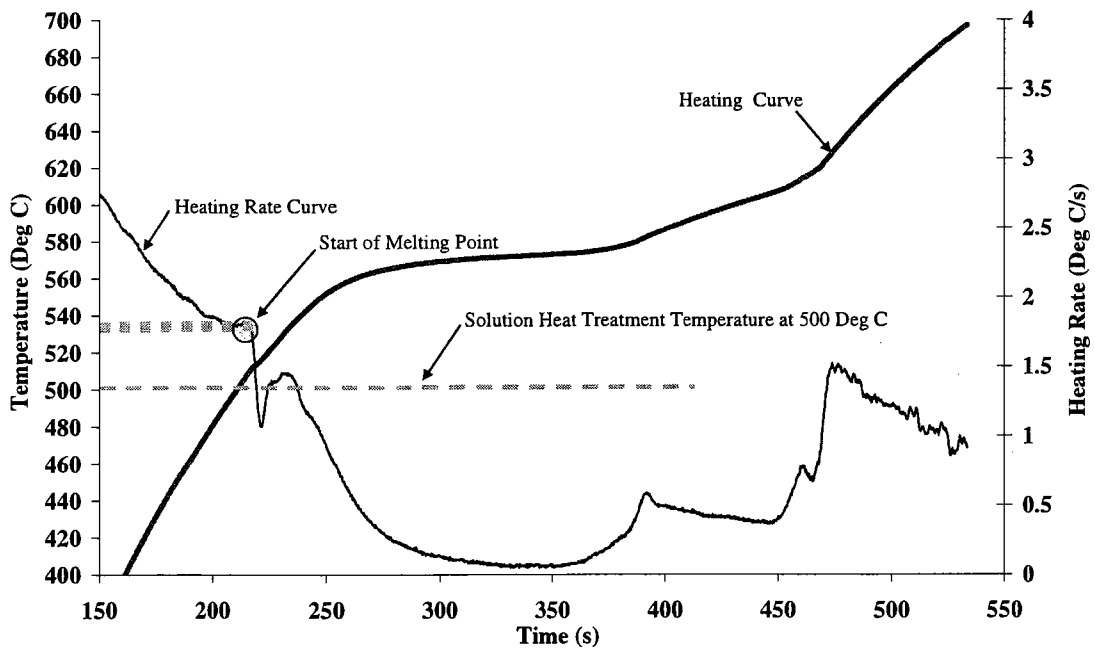


Figure 4.7. Heating curve analysis featuring temperature 1<sup>st</sup> derivative – temperature plot.

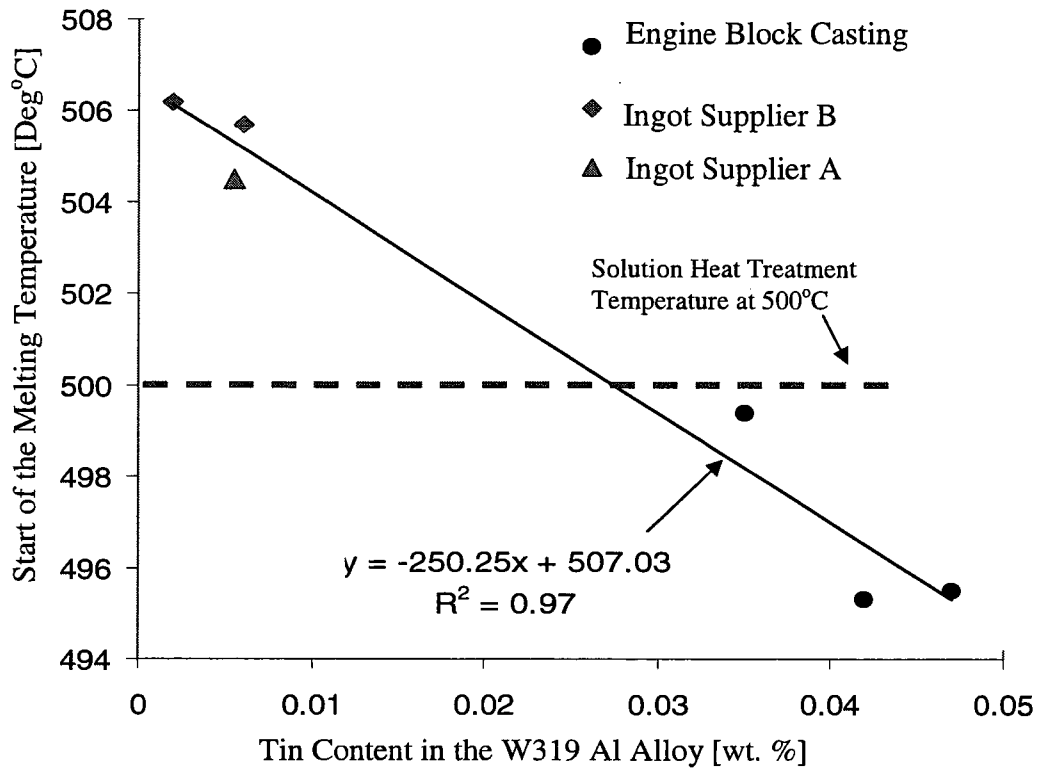


Figure 4.8. Effect of different levels of tin in W319 Al alloy on the start of melting temperature measured by UMSA heating curve analysis.



Table 4.2. Evaluation analysis of the proposed WAP chemical control limits.

Element	Statistical Analysis of WAP composition based on 340 samples				Performance Evaluation of Proposed WAP Lower Control Limit			Performance Evaluation of Proposed WAP Upper Control Limit		
	Mean (wt. %)	Standard Deviation	Min (wt. %)	Max (wt. %)	LCL (wt. %)	PI LCL	Performance LCL	UCL (wt. %)	PI UCL	Performance UCL
Si	7.51	0.09	7.23	7.77	7	1.9	OK	8	1.8	OK
Cu	3.49	0.07	3.31	3.74	3	2.3	OK	4	2.4	OK
Fe	0.36	0.01	0.32	0.39	0.3	2.1	OK	0.45	2.8	OK
Mg	0.28	0.01	0.25	0.31	0.2	2.7	OK	0.35	2.4	OK
Mn	0.25	0.01	0.23	0.27	0.2	2.4	OK	0.3	2.4	OK
Zn	0.125	0.017	0.082	0.174	0	2.4	OK	0.250	2.4	OK
Ti	0.111	0.003	0.102	0.119	0.09	2.0	OK	0.140	2.8	OK
Ni	0.028	0.006	0.017	0.042	0	1.7	OK	0.070	2.5	OK
Cr	0.037	0.012	0.021	0.060	0	1.0	OK	0.100	1.8	OK
Pb	0.020	0.005	0.010	0.038	0	1.3	OK	0.060	2.5	OK
Sn	0.006	0.002	0.003	0.011	0	1.2	OK	0.015	1.9	OK

Proposed limits to replace the original limit in Ford Material Specification WSE-M2A151-A2

Table 4.3. Statistical analysis of the WAP brinell hardness and porosity.

Parameter Critical to Quality Measured at WAP	Number of Samples	Mean	Median	Mode	Standard Deviation	Minimum	Maximum	Count	LCL Six Sigma	UCL Six Sigma	LCL Specification	UCL Specification	Status
Brinell Hardness of Inner Bulkhead Section After Heat Treatment (BHN)	288	97.38	96	96	3.03	89	105	288	88	106	85	115	OK
Porosity of Inner Bulkhead Section (Radiography Rating)	138	1.83	2	2	0.63	0	3	138	0.00	3.7	0	4	OK

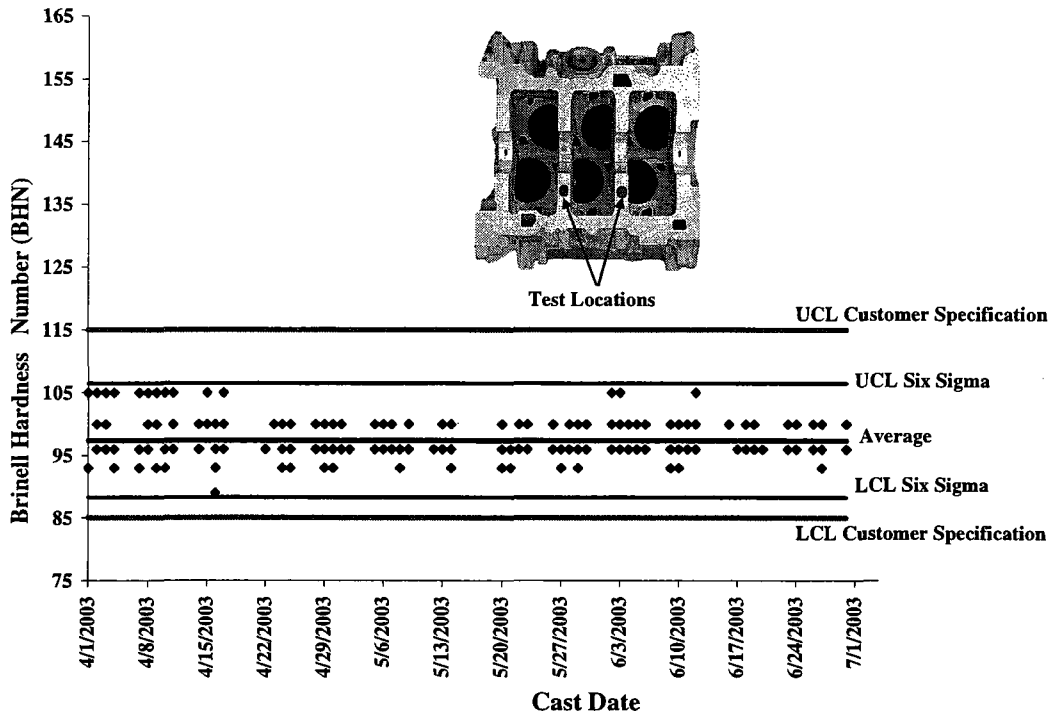


Figure 4.9. Run chart for brinell hardness of engine blocks cast at WAP.

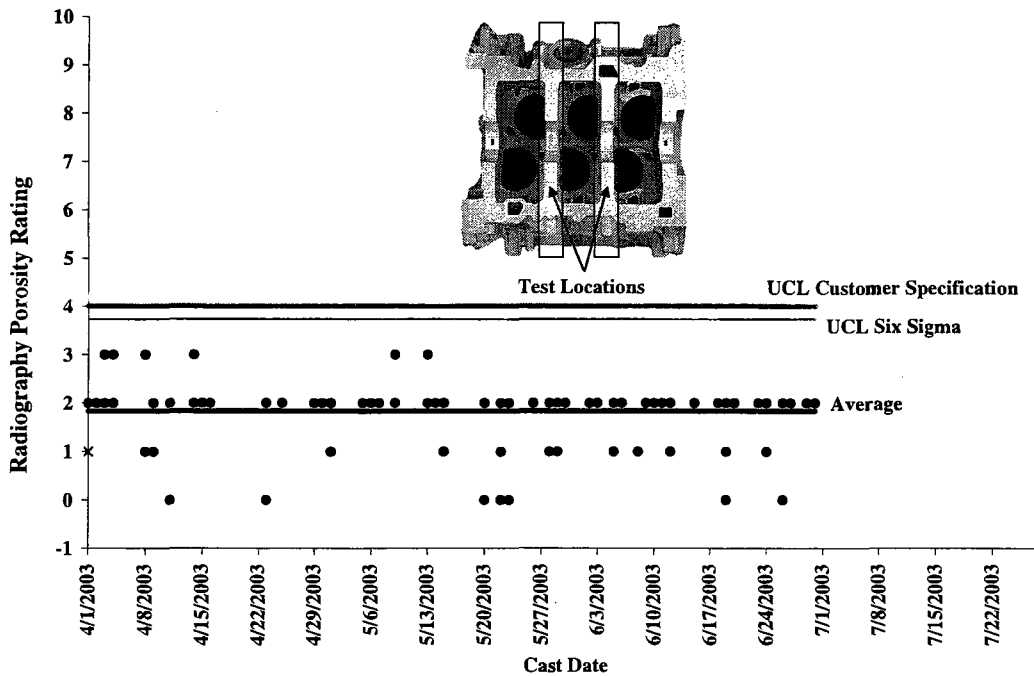


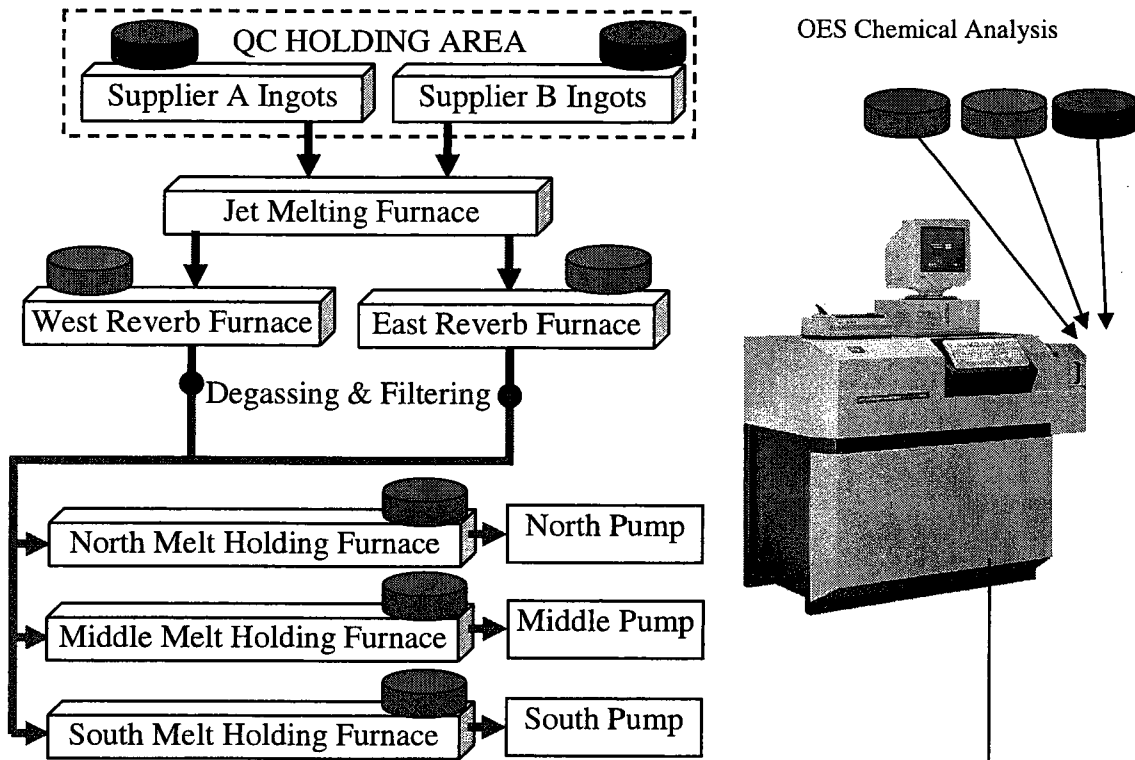
Figure 4.10. Run chart for porosity analysis of engine blocks cast at WAP.

## 4.2 Development of “Chemistry Viewer” Software for 3XX Al Alloy(s)

The chemical composition of cast components must be closely monitored and controlled during melt processing to meet customer product quality requirements. Statistical analysis of in process melt composition is critical to insure that the cast products meet customer material specifications. The original procedure used in the WAP Spectrometer lab requires the operator to print the measured composition data sheet for each sample and then manually enter the value for each element in an Excel file called “Melt Data.xls” as shown in Figure 4.11. This manual entry method for archiving alloy composition measurements consumes too much time and creates additional sources of error that should be avoided.

The author developed the stand alone “Chemistry Viewer” software to perform statistical analysis, and to predict as cast materials properties for the 3XX Al Alloy(s) composition based on the IRC methodology (Djurdjevic, et al., 2003). The alloy composition data is loaded for analysis using the “Refresh” button to browse and select the user defined data file that may contain multiple spectrometer test results as shown in Figure 4.12. The loaded spectrometer test results are segregated by the software based on the spectrometer analysis date, and on the sample source location. The manual for the “Chemistry Viewer” shown in Figure 4.13 explains the graphical user interface with examples for each built in function. The most unique feature of the “Chemistry Viewer” is the ability to predict critical solidification parameters and as cast mechanical properties using the  $Si_{EQ}$  algorithm, which was explained in Chapter Two. The  $Si_{EQ}$  algorithm can be used for hypoeutectic Al-Si alloy in an approach similar to the well known Carbon equivalency for Fe-C alloy. Statistical analysis tools built into the “Chemistry Viewer” software include the following:

- Run chart with Tukey limits, user defined control limits, and descriptive statistical summary, see example in Figure 4.14.
- Histogram plot, see example in Figure 4.16
- Box and Whisker Plot, see example in Figure 4.17.
- Normal Probability Plot, see example in Figure 4.18.
- Running Variance Plot, see example in Figure 4.18.



Printed test results are normally entered for future analysis of the alloy's chemical composition.

Element	Average	Enter dry sample weight	Enter weight of displaced water	Relative Density	Relative Density Test	Alu Delta	Alu Delta Modification	Alu Delta	Alu Delta	File Name
Si %	7.6983			2.7442	Theoretical Density					nov 02 1 142N2230
Cu %	5.4309									
Fe %	2.924									
Mn %	2.570									
Zn %	4.920									
Ti %	0.000									
Al %	0.000									
Mg %	0.000									
Ni %	0.000									
Pb %	0.000									
Cr %	0.000									
U %	0.000									
Bi %	0.000									
Sn %	0.000									
Cd %	0.000									
V %	0.000									
Total	99.9997									

Figure 4.11. 2003 WAP Original OES Chemical Analysis Procedure.

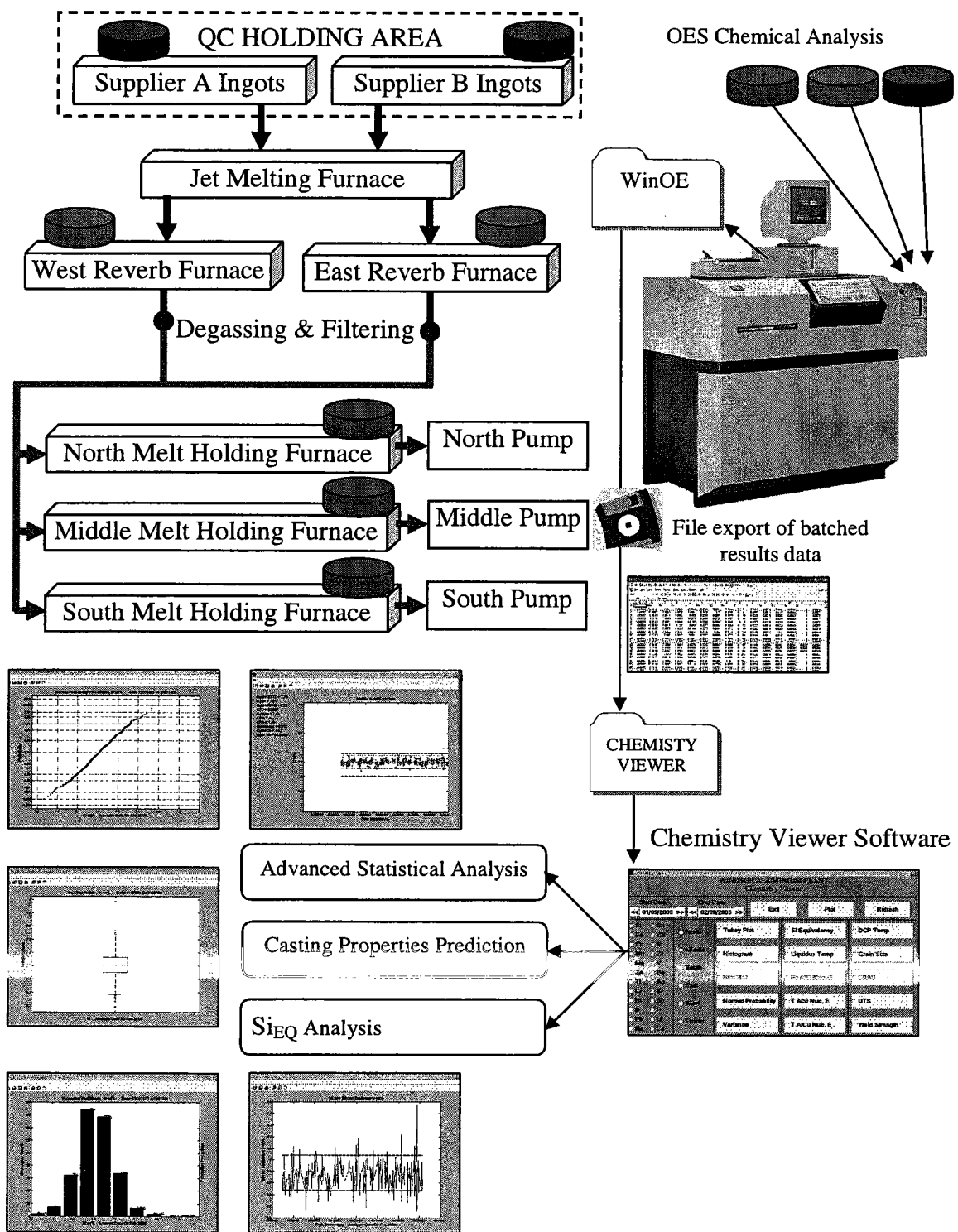


Figure 4.12. Proposed New Chemical Analysis Procedure for the in Process W319 Al Alloy.

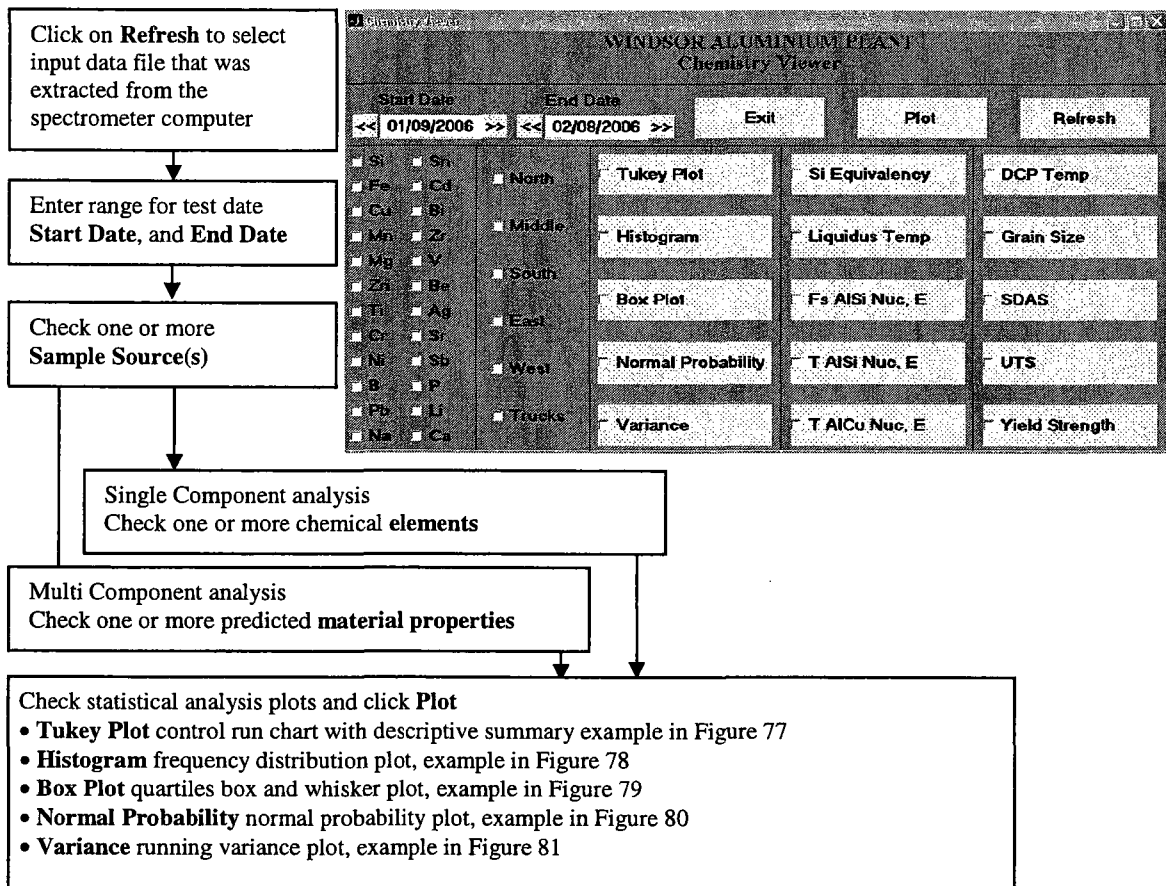


Figure 4.13. Screen Shot of the Control Window in the “Chemistry Viewer” Software.

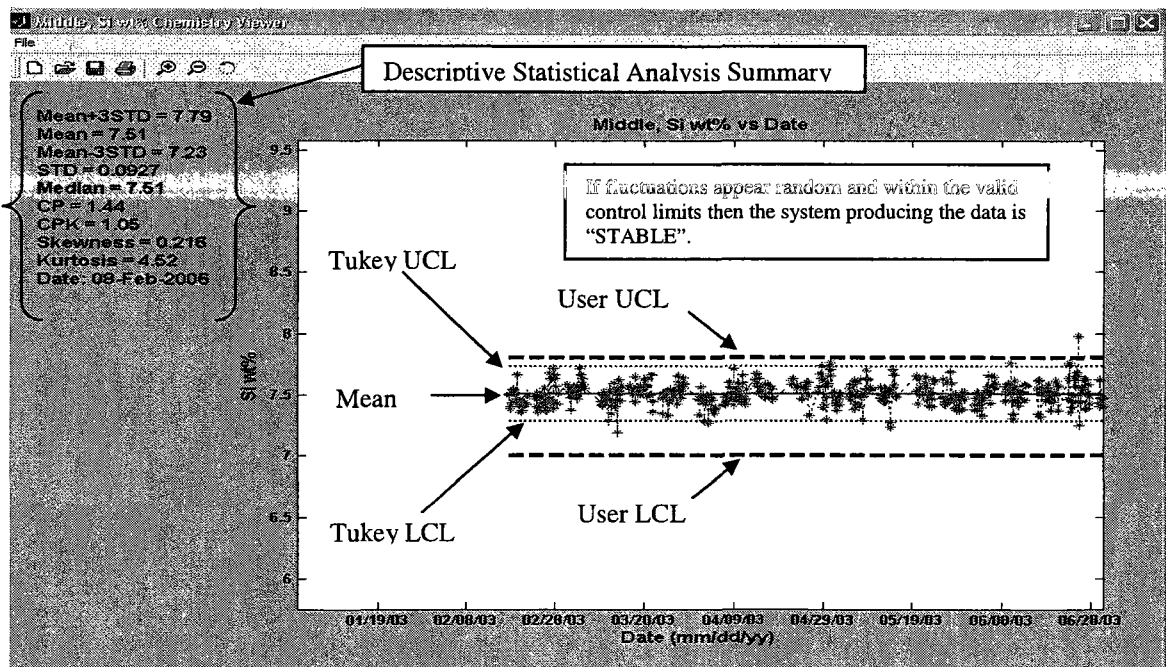


Figure 4.14. “Chemistry Viewer” Example of the Tukey Control Chart.

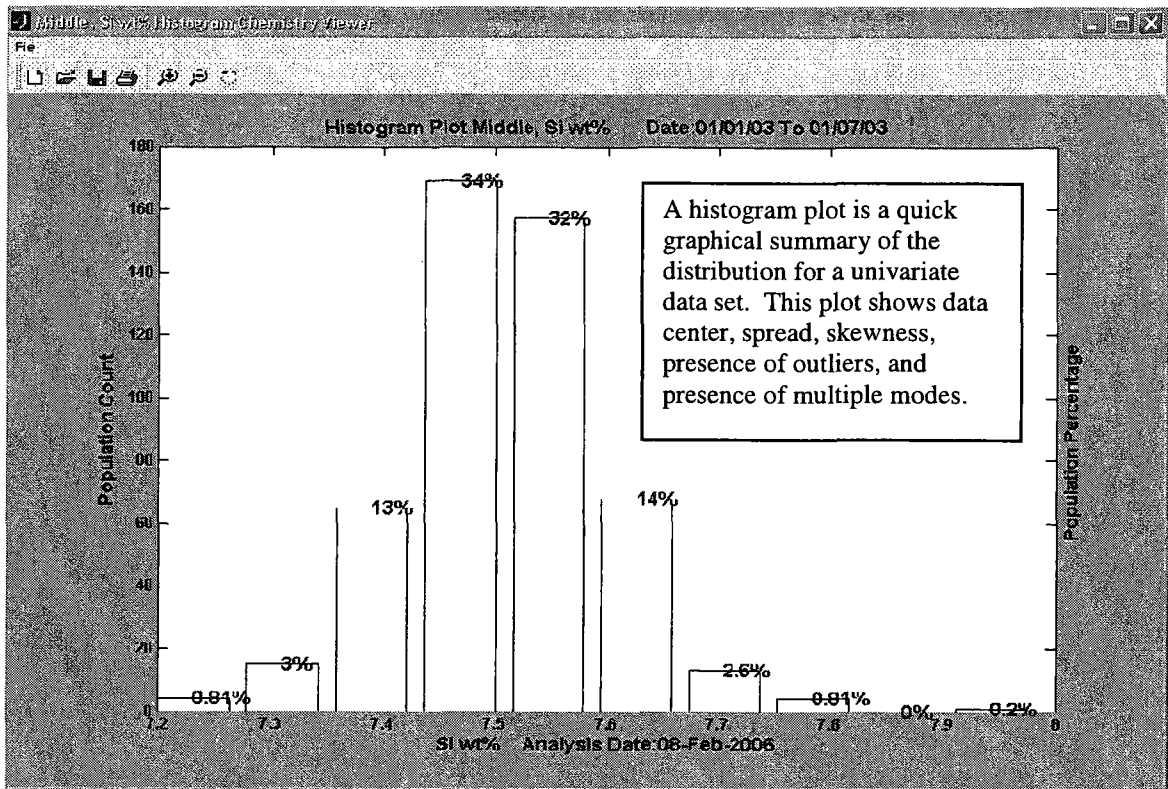


Figure 4.15. "Chemistry Viewer" Example of Histogram Plot.

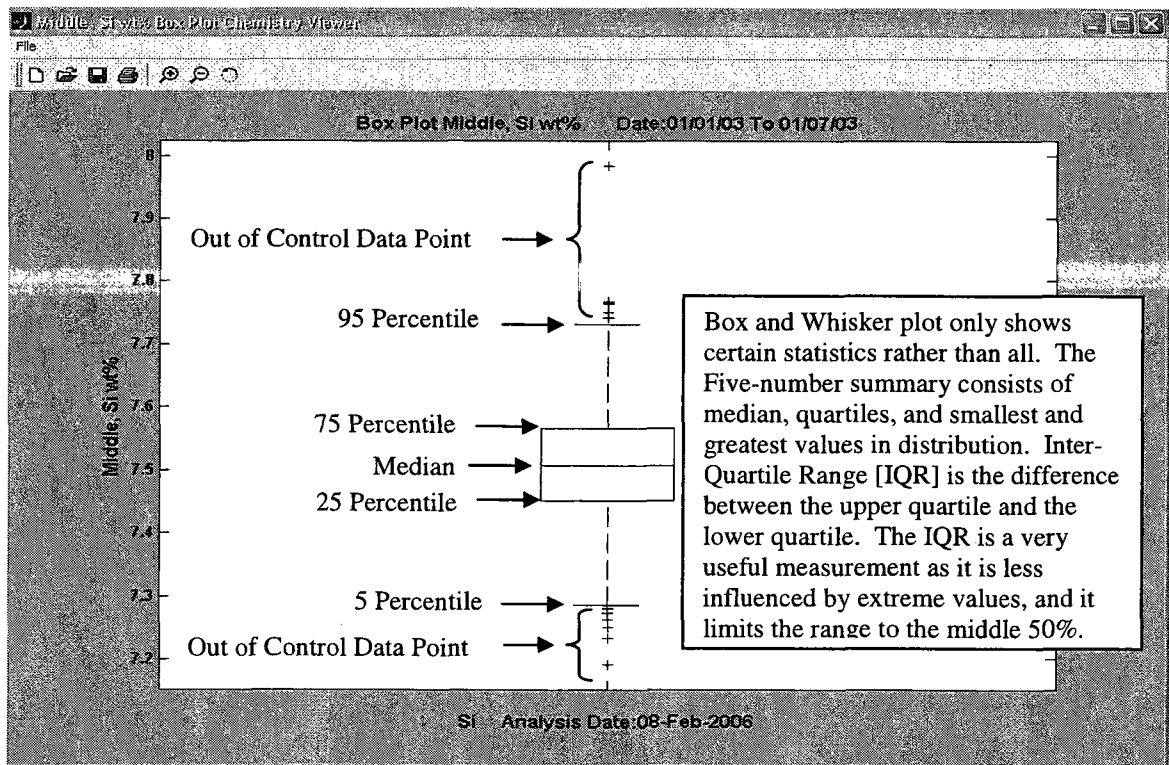


Figure 4.16. "Chemistry Viewer" Example of Box and Whisker Plot.

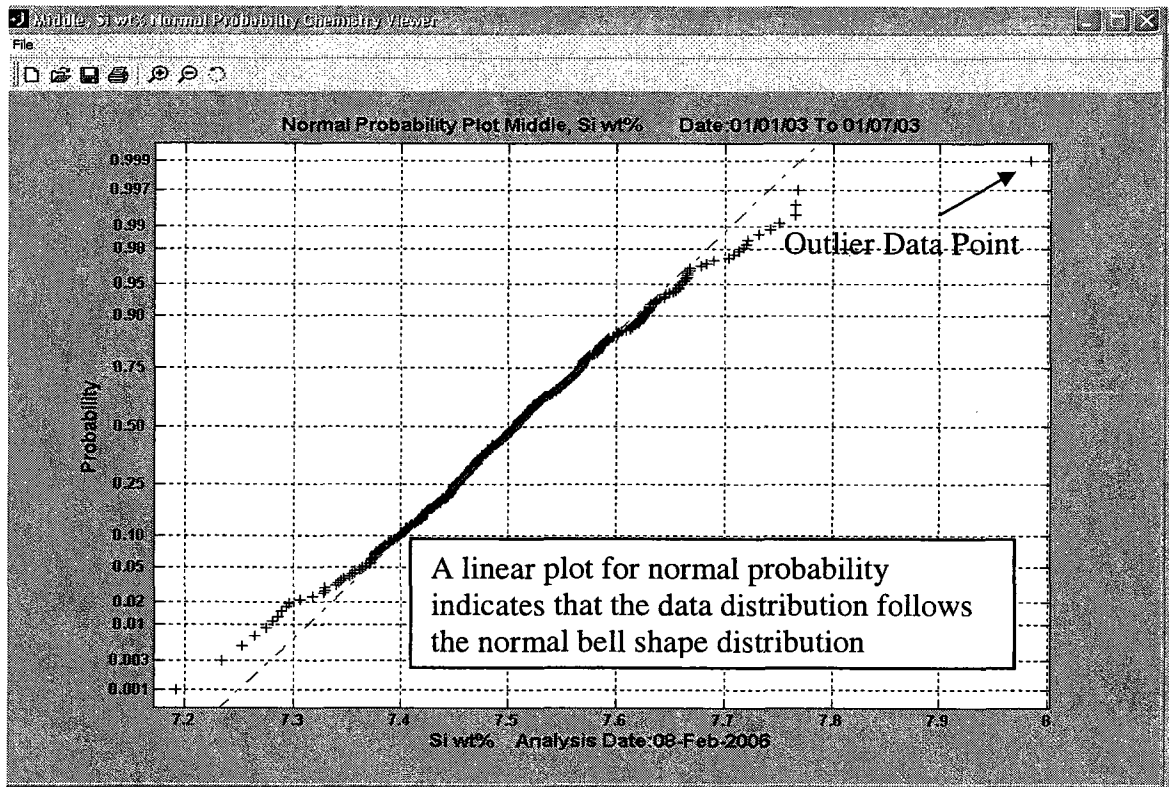


Figure 4.17. "Chemistry Viewer" Example of Histogram Plot.

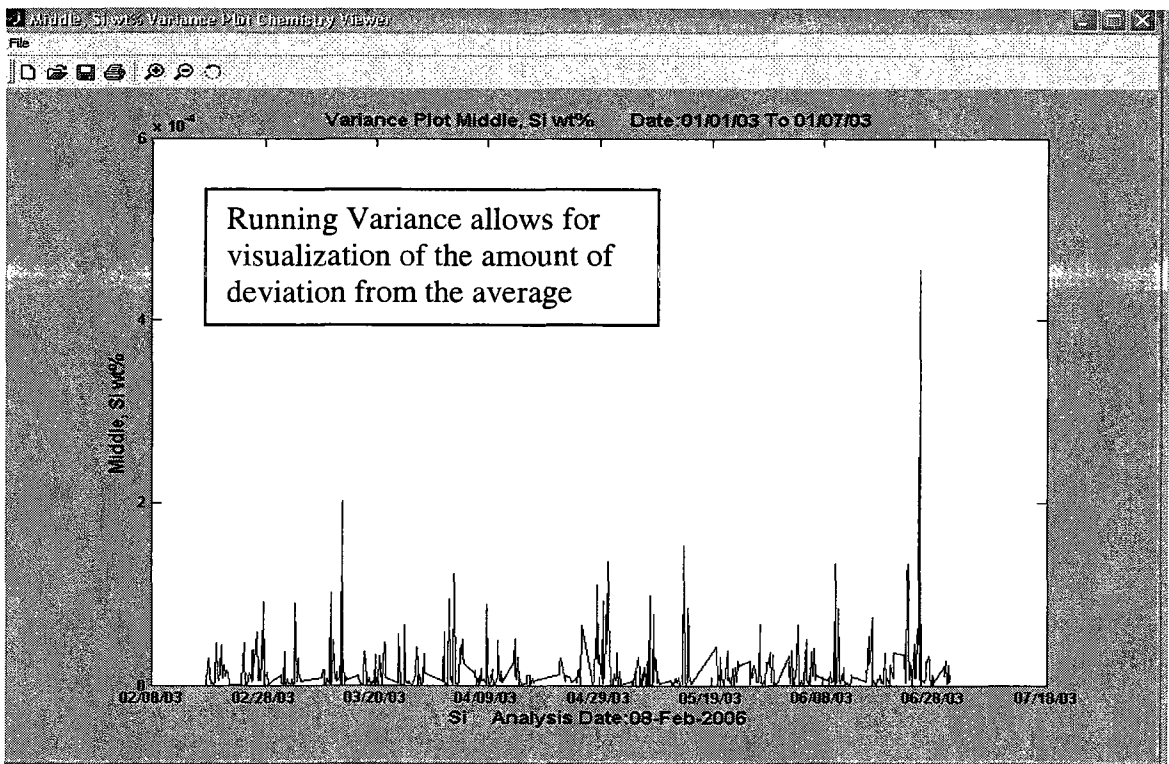


Figure 4.18. "Chemistry Viewer" Example of Running Variance Plot.



### 4.3 Development of Thermal Analysis “Filters” Software for 3XX Al Alloy(s)

Calculations performed as part of TA can become time consuming and tedious leaving less time for interpretation of the obtained results. The calculations involve filtering the noise from the recorded temperature signal and detecting critical solidification parameters. Accuracy and processing time can be greatly improved using software with a built in algorithm to perform cooling curve and its first derivative analysis leaving more time for interpretation of the obtained results. The “Filters” stand alone software was developed to automatically perform cooling curve analysis for 3XX Al Alloy(s), and to perform statistical analysis on archived cooling curve parameters. The solidification characteristics for a typical W319 Al Alloy cooling curve are described in Chapter Three. The algorithms built in “Filters” were either developed or selected based on the IRC’s extensive knowledge in this field. The sequence of calculations performed for cooling curve analysis is explained in Figure 4.19. The instructions for using the software are explained in Figure 4.20 and Figure 4.21. The “baseline” equation was developed by the IRC and the published in a paper that was awarded best paper by AFS in 1999 (Kierkus, et al., 1999). The Dendrite Coherency Point (DCP) was determined by using the IRC’s technique with only one thermocouple placed in the center of the sample (Jiang, et al., 1999). Copper enriched phases were quantified using the area fraction under the reaction peaks on the cooling rate vs. time plot developed by the IRC (Djurdjevic, et al., 2001). The recorded signal noise was removed using the Savitsky-Golay filter method, which essentially performs a local polynomial regression to determine the smoothed value for each data point. This method is superior to adjacent averaging because it tends to preserve signal features such as peak height and width that otherwise would be 'washed out' (OriginLab, 2006). Statistical Process Control (SPC) tools built into the “Filters” could be used to archive detected cooling curve characteristics, and perform statistical analysis.

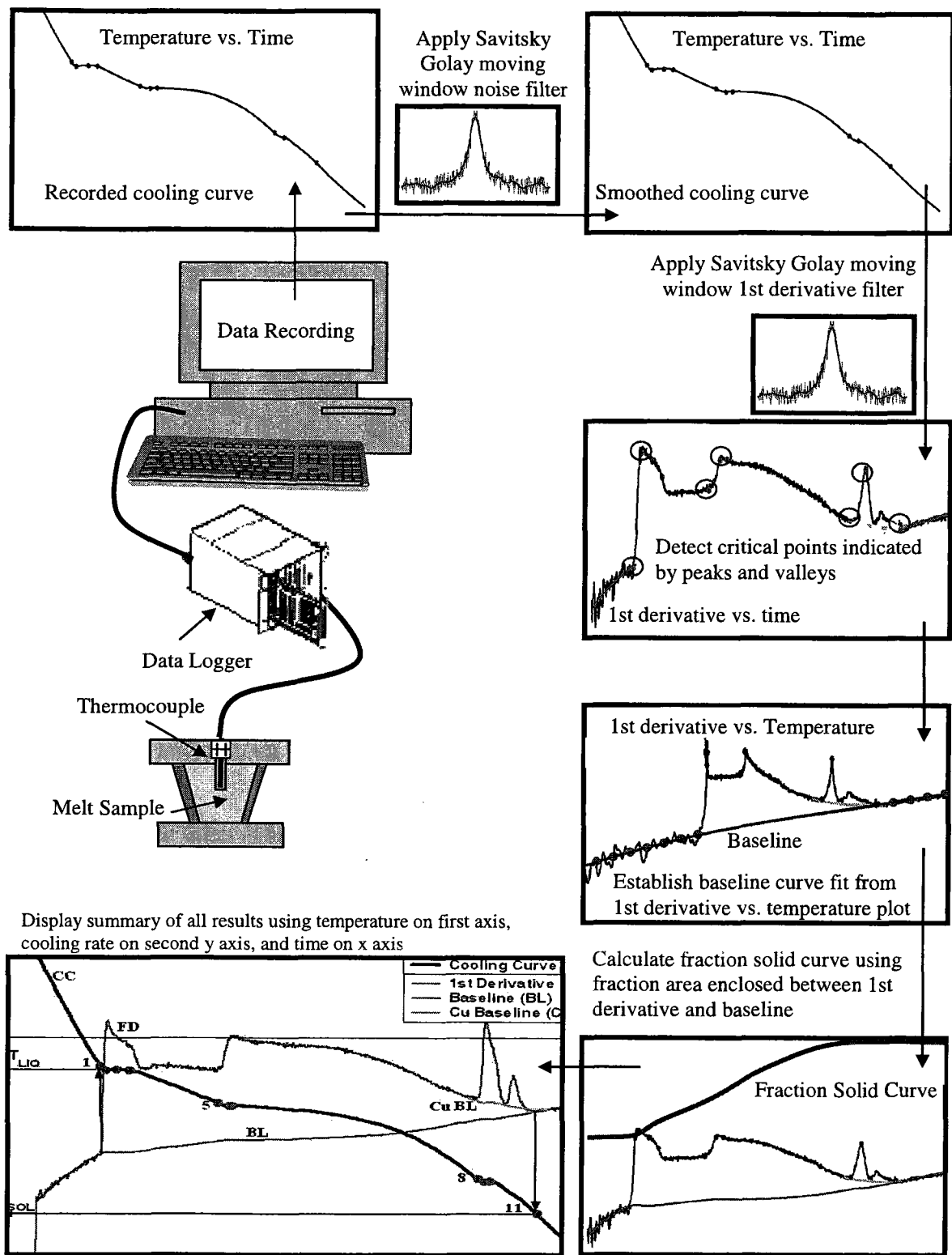
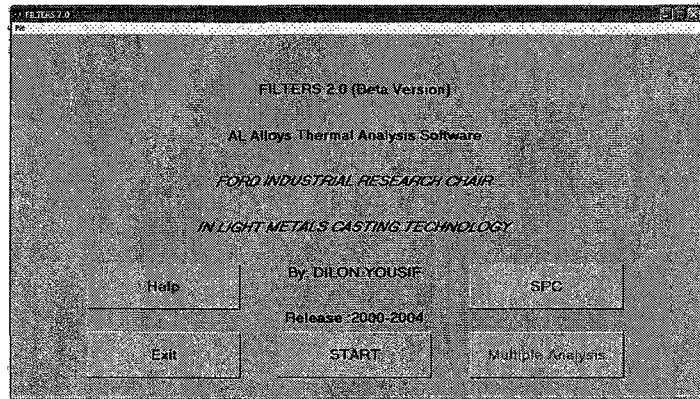
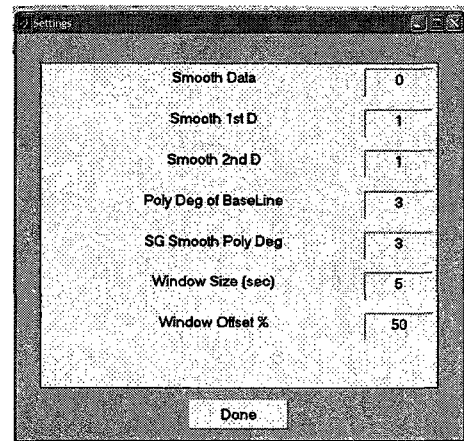


Figure 4.19. Procedure for Cooling Curve Analysis of Al-Si Alloys.

- Click on
- **START**: Perform cooling curve for a single file
  - **Multiple Analysis**: Perform cooling curve analysis for multiple files in a single folder
  - **SPC**: Perform statistical analysis on archived results, see Figure 84
  - **Help**: View user tips and instructions
  - **Exit**: Terminate the program



- Enter analysis settings and click Done
- **Smooth Data** Number of times to smooth recorded temperature signal
  - **Smooth 1<sup>st</sup> D** Number of times to smooth calculated first time derivative
  - **Smooth 2<sup>nd</sup> D** Number of times to smooth calculated second time derivative
  - **Poly Deg of BaseLine** Polynomial degree to calculate baseline fit
  - **SG Smooth Poly Deg** Polynomial degree for Savitsky-Golay smoothing filter
  - **Window Size [sec]** Width of moving window for signal filtering



- Browse and Open cooling curve input data file, and click on
- **Standard Plot**: Cooling curve, 1st derivative, fraction solid, baseline and summary table, example in Figure 4.22
  - **Cooling Rate vs. Time**: Cooling rate profile with zoom option, example in Figure 4.23
  - **File Save**: Export analysis results as a \*.CSV data file
  - **Cooling rate vs. Temp**: Cooling rate vs. Temperature with baseline line curve, see example in Figure 4.24
  - **Update Database** Archive detected characteristic points in user specified \*.CSV data file
  - **Temp vs. Time** Temperature vs. time cooling curve with zoom option, example in Figure 4.25
  - **Restart** Terminate program and start new analysis session
  - **Subplot**: Plot three separate plots in one single window including; temperature vs. time, cooling rate vs. time, and cooling rate vs. temperature, example in Figure 4.26

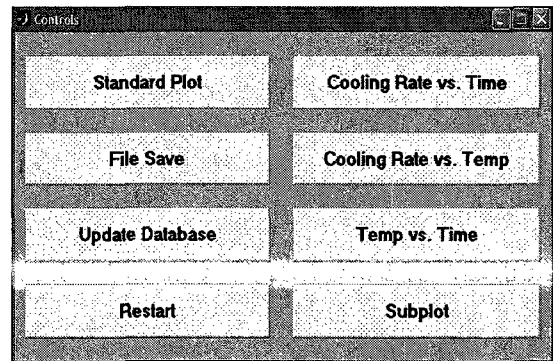


Figure 4.20. Quick Reference User Guide for “Filters” Software.

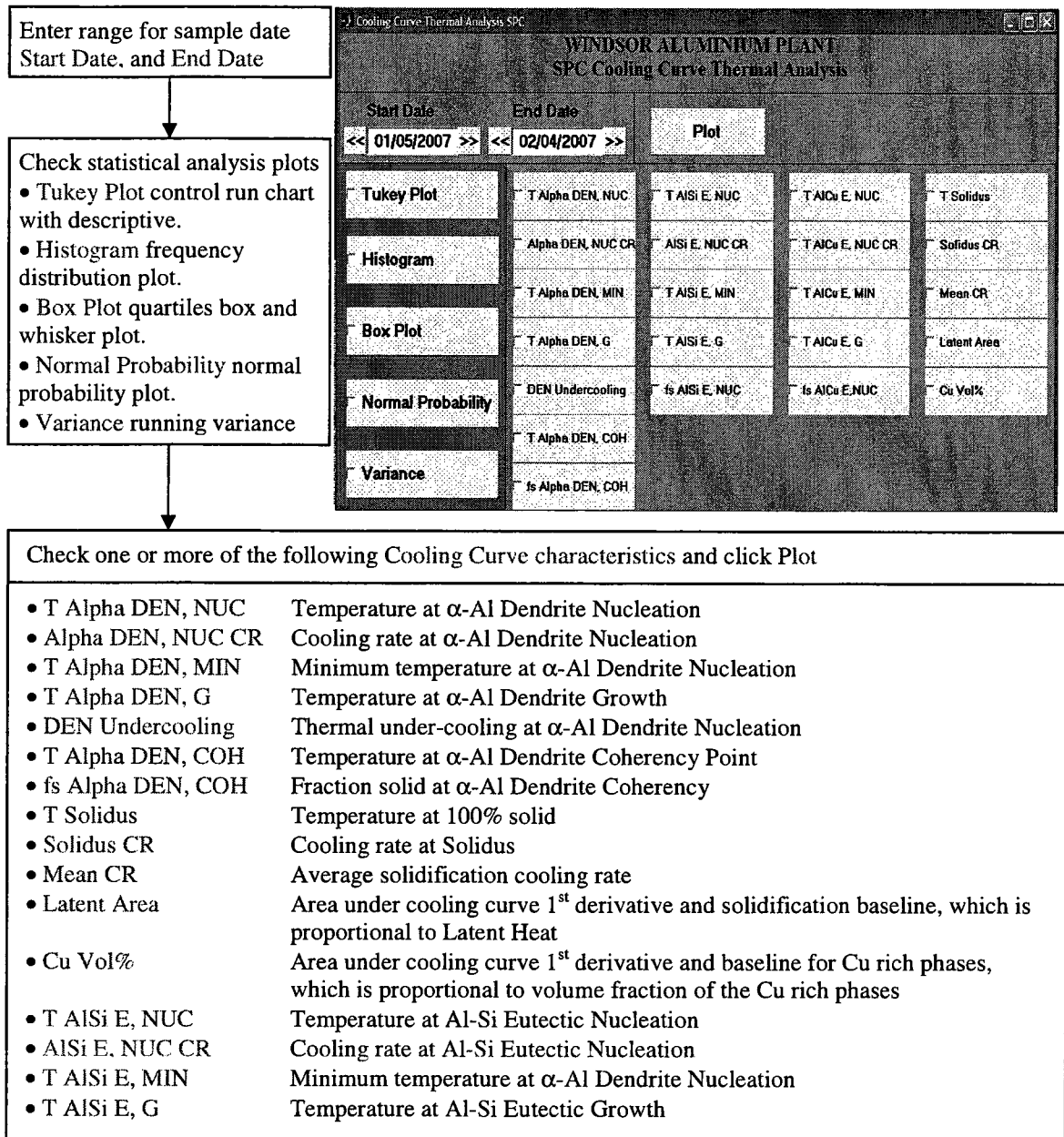


Figure 4.21. Control Window for SPC Analysis of Archived Cooling Curve Characteristics.

Results

T Alpha, DEN<sub>NUC</sub> = 601.7C  
 T Alpha, DEN<sub>MIN</sub> = 595C  
 T Alpha, DEN<sub>G</sub> = 596.7 C  
 Under Cooling = 1.73C  
 T Alpha, DEN<sub>CON</sub> = 595.5C/s  
 f<sub>s</sub> Alpha, DEN<sub>COH</sub> = 16%  
 CR = 0.68C/s

T AISi<sub>E,NUC</sub> = 568.7C  
 T AISi<sub>E,MIN</sub> = 564.9C  
 T AISi<sub>E,G</sub> = 565.3 C  
 f<sub>s</sub> AISi<sub>E,NUC</sub> = 35%  
 CR = 0.21C/s

T AICu<sub>E,NUC</sub> = 504.3C  
 T AICu<sub>E,MIN</sub> = 496.9C  
 T AICu<sub>E,G</sub> = 496.9 C  
 f<sub>s</sub> AICu<sub>E,NUC</sub> = 93%  
 CR = 0.22C/s

T SOL = 461.4C  
 CR = 0.29C/s

Total Area = 316C  
 AlCu %V = 4.31%  
 Latent Heat = 449KJ/Kg  
 CP = 1.42KJ/kg.K  
 Mean CR = 0.177

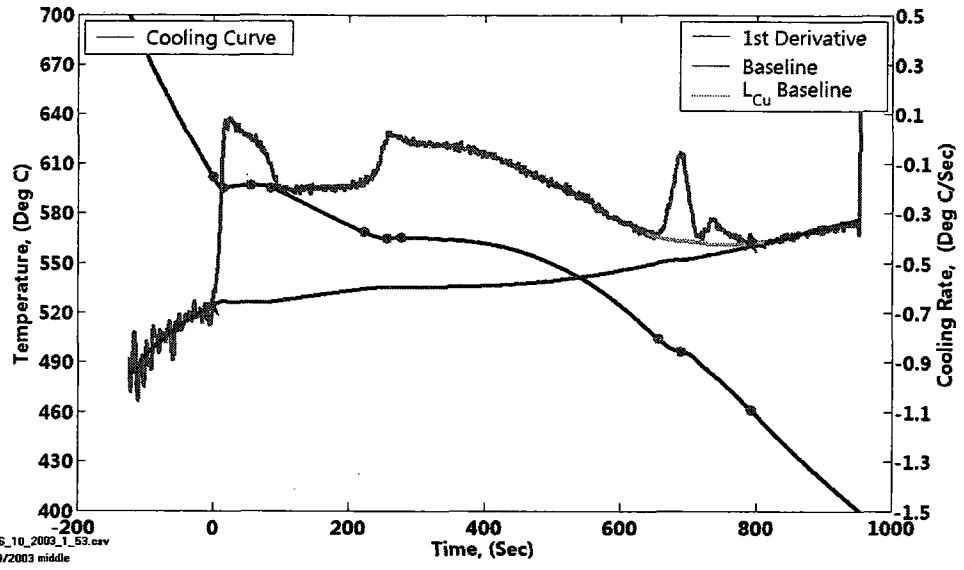


Figure 4.22. Cooling Curve Analysis Featuring Temperature – Time Plot (Left Y Axis) and Temperature 1<sup>st</sup> Derivative – Time Plot with Baseline (Right Y Axis), and Summary of the Solidification Characteristics.

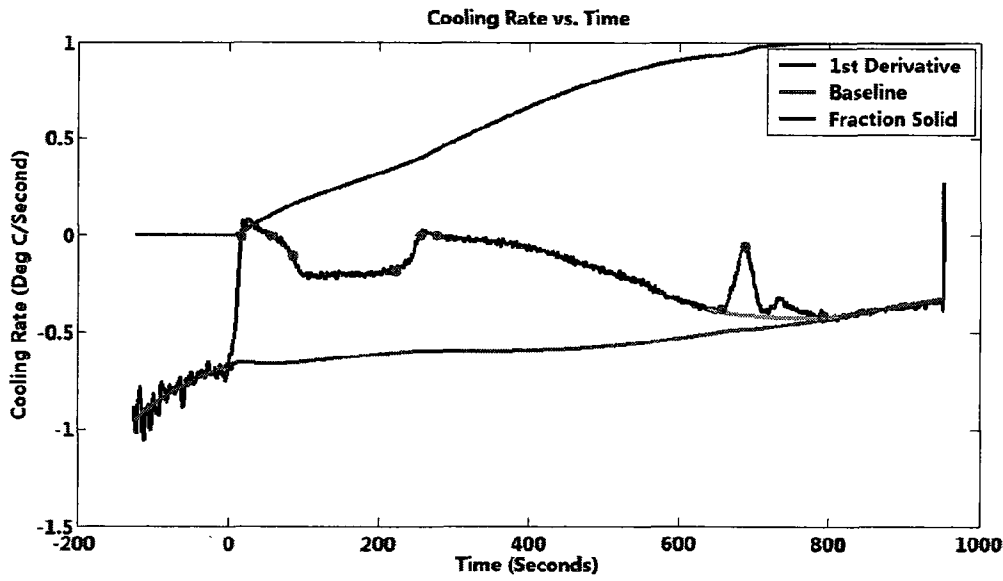


Figure 4.23. Cooling Curve Analysis Featuring Temperature 1<sup>st</sup> Derivative – Time Plot with Baseline and Fraction Solid – Time Plot.

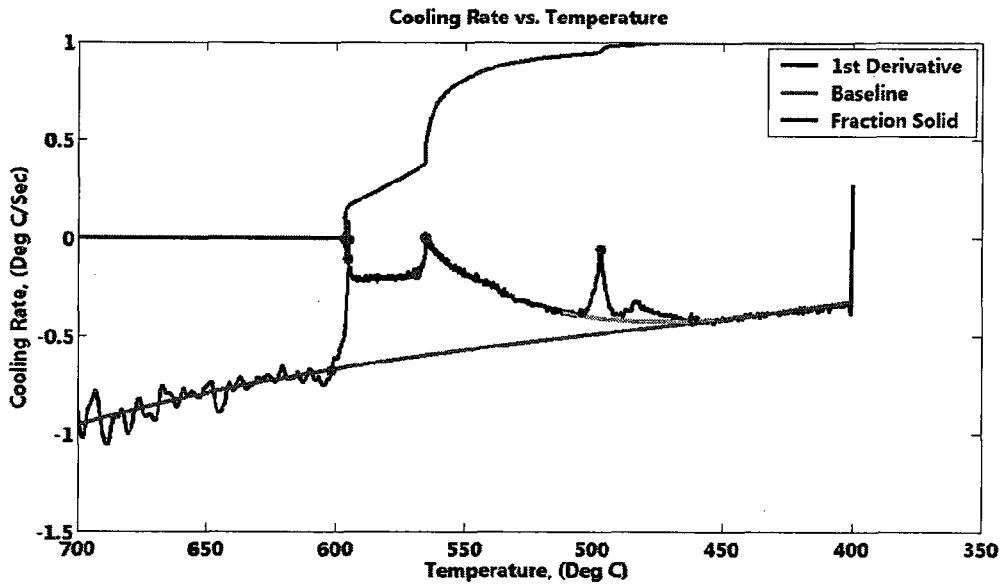


Figure 4.24. Cooling Curve Analysis Featuring Temperature 1<sup>st</sup> Derivative – Temperature Plot with Baseline and Fraction Solid – Temperature Plot.

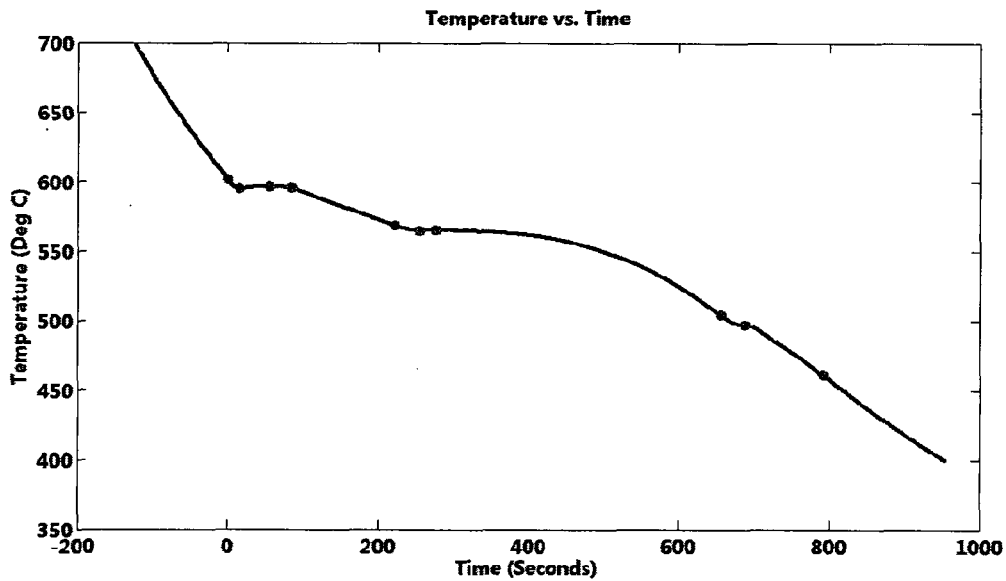


Figure 4.25. Cooling Curve Analysis Featuring Temperature - Time Plot.

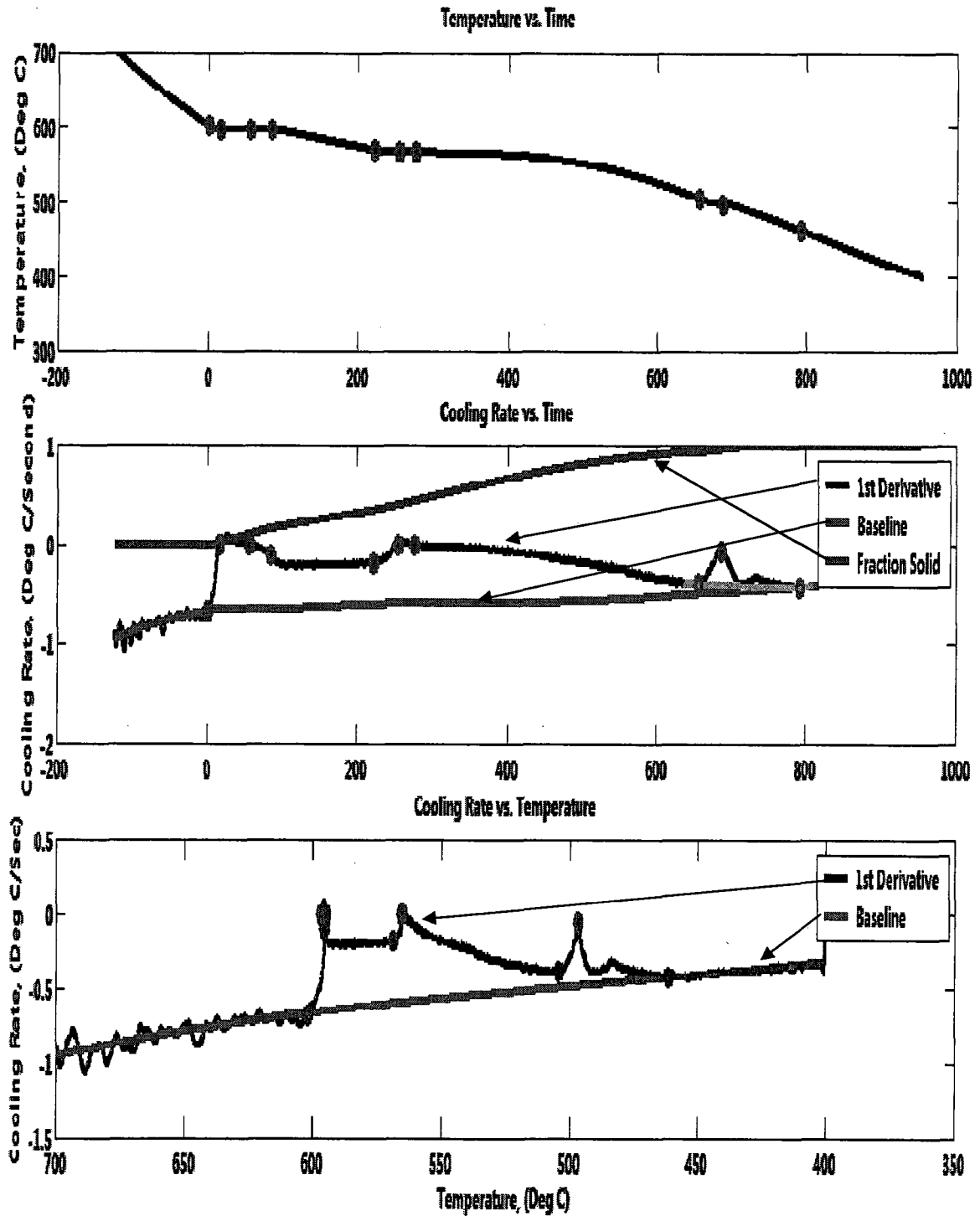


Figure 4.26. Cooling Curve Analysis with Time, Temperature, and Temperature Derivative.

#### 4.4 Development of Melt Sampling Device

The WAP QC procedure for cooling curve analysis for the WAP process melt was originally established using the Alu-Delta microprocessor based test equipment. Unfortunately, the Alu-Delta equipment using a thick wall sand test cup is considered outdated and only offers limited capabilities to perform grain structure analysis and determine the Silicon Modification Level. Limited analysis capabilities fail to fulfill the growing demands of the modern casting industry. Traditionally the melt sample must be manually transferred using a small ladle from the furnace to the test cup. Heat lost during ladle transfer results in a large melt temperature drop prior to the start of the cooling curve recording. The IRC developed the MSD, described in Chapter Three, to overcome limitations of traditional melt sampling techniques. The different designs were developed and built as part of this study to conduct cooling curve experiments at WAP. The design of the MSD introduces three significant advantages over traditional techniques. First, the melt sample could be collected from any desired depth with a minimum melt disturbance. Even with careful skimming the melt sampled from the top surface could be relatively more contaminated compared to the melt sampled from the lower depths. Second, the temperature of the solidifying melt sample could be recorded immediately after the filled test cup emerge above the furnace melt surface. This eliminates significant heat lost during traditional melt ladle transfer before cooling curve recording. Third, sensitivity of the recorded cooling curve temperature signal is greatly improved by using a low thermal mass steel sheath protected K-type thermocouple, and a thin wall steel test cup. The cooling curve recorded using In-Situ TA of the WAP V6 3.0L engine block casting is very similar to the cooling curve recorded using the MSD instead of the Alu-Delta as shown in Figure 4.27. The MSD test equipment design was based on recommendations documented in the IRC comparative study of cooling curve parameters for different thermal mass crucibles and thermocouple assemblies (Kierkus, et al., 2002). However more work is needed to further improve design reliability, and safety in order to be ready for commercial use on the production floor.



### Comparison of Cooling Curves for Different T.A Test Configurations

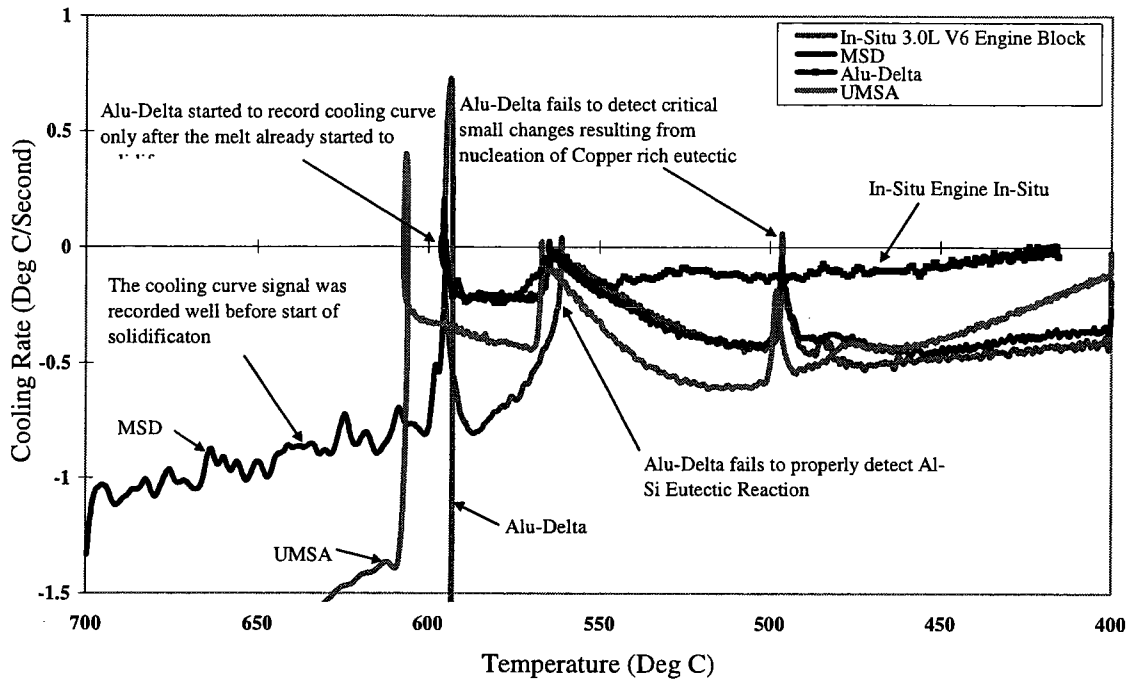


Figure 4.27. Comparison of the Cooling Curve Sensitivity Between the Alu-Delta TA System, the MSD developed by IRC, and the 3.0L Engine Block In-Situ TA.

## 4.5 Results Summary

Chemical elements in W319 Al Alloy with a control limit PI of less than 1.0 or higher than 3.5 were considered poor based on the literature recommendations. The control limits for the W319 chemical composition were recalculated to improve the limit performance. The W319 limits were recalculated such that the limit PI would be between 1.2 and 2.8.

The chemical analysis software “Chemistry Viewer” was developed and used for statistical analysis and silicon equivalency analysis of the W319 Al Alloy composition. The software was successfully implemented at WAP and could be potentially utilized at other foundries. The software features comprehensive statistical analysis capabilities as well as the unique  $Si_{EQ}$  to predict as cast material properties.

The Thermal Analysis software “Filters” was developed and used for cooling curve analysis of the W319 Al Alloy test samples. The software was successfully implemented to replace all manual calculations performed as part of the cooling curve analysis and could potentially be utilized at other foundries using Al-Si-Cu alloys. The software features comprehensive statistical analysis capabilities as well as the IRC methods to determine baseline, fraction solid, and latent heat.

The Melt Sampling Device was redesigned, constructed, and used to collect test samples from the WAP melt furnaces for cooling curve analysis. The prototype melt sampling device may require more design work before being ready for production floor applications.

## 5 CONCLUSIONS

The declared objectives of this thesis were achieved based on the following accomplishments that could be useful for improving QC at any Al Alloy(s) foundry:

1. Development of “Chemistry Viewer” software for statistical analysis of the chemical composition for multi-component Al Alloy(s). The software should also predict as cast material properties for the 3XX Al Alloy(s) using the  $Si_{EQ}$  technique.
2. Development of “Filters” software for cooling curve analysis of the 3XX Al Alloy(s). The software automatically detects characteristic points on the cooling curve and corresponding 1<sup>st</sup> derivative curve. The latent heat and fraction solid are calculated using the “baseline” techniques developed by the IRC.
3. Development of the MSD testing device for collecting melt furnace samples to perform online cooling curve analysis. The device overcomes limitations of traditional melt sampling techniques that use a steel ladle and sand test cup.

Other accomplishments achieved in the course of this study were:

1. Development of chemical control limits for the WAP in process W319 Al Alloy.
2. Development of cooling curve control limits for the WAP in process W319 Al Alloy.
3. Recommendation to recalculate control limits at least once a year or when a known change occurs that may impact quality.
4. Recommendation to properly distinguish between the control limits specific to one process and the limits in material specifications established for various applications.
5. Recommendation to use the UMSA for qualifying ingot suppliers to ensure that the start of melting and solidification characteristics satisfy the established control limits.

## APPENDIX I

### WAP Experimental Data

Please explore the content of the attached CD for all recorded measurement data that includes:

- Cooling curves of the in process W319 Al Alloy.
- Chemical Composition of the in process W319 Al Alloy.
- Brinell hardness readings of cast engine block - bulkhead sections.
- Porosity radiography ratings of the cast engine block - bulkhead sections.

## REFERENCES

- 1 ARL Thermo Electron Corporation, "SPC WinOE Software Product Specifications for Metal Analysis", online 2006, [www.thermo.com/com/cda/product/detail/0,1055,11445,00.html](http://www.thermo.com/com/cda/product/detail/0,1055,11445,00.html).
- 2 Bakhtiyarov, S. I., and Overfelt R. A., "Thermoviscoelastic Properties of Phenolic Resin/Polymeric Isocyanate Binders System", 14th Symposium on Thermophysical Properties, online 2000, [www.symp14.nist.gov/PDF/MET02BA2.PDF](http://www.symp14.nist.gov/PDF/MET02BA2.PDF).
- 3 Cáceres C. H., Sokolowski J. H. and Gallo P., "Effect of Ageing and Mg Content on the Quality Index of Two Model Al-Cu-Si-Mg Alloy", *Materials Science and Engineering A*, 1999, 53-61 [ISBN 0921-5093].
- 4 Campbell, J., "Castings Practice: The Ten Rules of Castings". 1 ed., 2004, Oxford England: Elsevier Butterworth-Heinemann. 205.
- 5 Cast Solutions "Computer Models Calculate Riser Size and Position to Reduce Porosity and Increase Metal Yield", Fall 2002 Design Successes, online 2006, [www.castolutions.com/archive/CastingSucesses/LCS1002\\_10.html](http://www.castolutions.com/archive/CastingSucesses/LCS1002_10.html).
- 6 CMI Novacast Inc, Electromagnetic Pump Operating Principle, online 2005, [www.cminovacast.com/CMIttechpaper1.html#fig3](http://www.cminovacast.com/CMIttechpaper1.html#fig3).
- 7 Cosworth Technology, "Cosworth Process: Zircon Sand", online 2005, [www.cosworth-technology.co.uk/400\\_castings/430\\_zircon.htm](http://www.cosworth-technology.co.uk/400_castings/430_zircon.htm).
- 8 Djurdjevic M. B., Kasprzak W., Kierkus C. A., Kierkus W. T. and Sokolowski J. H. "Quantification of Cu Enriched Phases in Synthetic 3XX Aluminum Alloy Using the TA Technique", American Foundry Society, 2001.
- 9 Djurdjevic, M. B., Kierkus, W. T., Byczynski, G. E. and Sokolowski, J. H. Calculation of Liquidus Temperature for the Aluminum 3XX Series of Alloy, *AFS Transactions*, 1998, v. 47, 143-147.
- 10 Djurdjevic, M. B., Mitrasinovic, A., Sokolowski, J. H., "Development of the Silicon Equivalent Algorithm and Its Application for the Calculation of the Characteristic Temperatures of Solidification of Multi-component 3XX Series of Al Alloy(s)", *Proceedings of the 15th International Conference and Exposition of the Foundry Industry*, Monterrey, Mexico, 2003.
- 11 DuPont, "DuPont Biasill Staurolite Sand", online 2006, [www.titanium.dupont.com](http://www.titanium.dupont.com)
- 12 Engineering Fundamentals efunda, "Brinell Hardness", online 2006, [www.efunda.com/units/hardness/convert\\_hardness.cfm](http://www.efunda.com/units/hardness/convert_hardness.cfm).
- 13 Guthy Hema V., "Evolution of the Eutectic Microstructure in Chemically Modified and Unmodified Aluminum Silicon Alloy", Worcester Polytechnic Institute, 2002.
- 14 i Six Sigma, "Recalculating Control Limits", online 2005, [www.isixsigma.com/library/content/c030306a.asp](http://www.isixsigma.com/library/content/c030306a.asp)
- 15 i Six Sigma, "Six Sigma DMAIC Roadmap", online 2006, [www.software.isixsigma.com/library/content/c020617a.asp](http://www.software.isixsigma.com/library/content/c020617a.asp)
- 16 Instron "Brinell Hardness Test", online 2006, [www.instron.us/wa/applications/test\\_types/hardness/brinell.aspx](http://www.instron.us/wa/applications/test_types/hardness/brinell.aspx).
- 17 Jiang H., Kierkus, W. T. and Sokolowski, J. H., "Determining Dendrite Coherency Point Characteristics of Al Alloy(s) using Single-Thermocouple Technique", *AFS Transactions*, 1999, v. 68, 169-172.
- 18 Kasprzak M., Kasprzak, W., Kierkus, W. T., and Sokolowski, J. H., "Method and Apparatus for Universal Metallurgical Simulation and Analysis", Patent, PCT/CA02/01903, Canada, 2002.

- 19 Kasprzak M., Kasprzak, W., Kierkus, W. T., and Sokolowski, J. H., "Method and Apparatus for Universal Metallurgical Simulation and Analysis", Patent, PCT/CA02/01903, Canada, 2002.
- 20 Kasprzak W., Kierkus C. A., Kierkus W. T. and Sokolowski J. H., "The Structure and Matrix Microhardness of the 319 Aluminum Alloy After Isothermal Holding During the Solidification Process", American Foundry Society, 2001.
- 21 Key to Metals, "Aluminum Alloy - Effects of Alloying Elements", online 2006, [www.key-to-metals.com/PrintArticle.asp?ID=55](http://www.key-to-metals.com/PrintArticle.asp?ID=55).
- 22 Kierkus, W. T., Djurdjevic, M. B., Sokolowski, J. H., "A Comparative Study of Cooling Curve Parameters for Different Thermal Mass Crucibles and Thermocouple Assemblies", IRC, June, 2002.
- 23 Kierkus, W. T., Sokolowski, J. H., "Recent Advances in Cooling Curve Analysis: A New Method for Determining the 'Baseline' Equation", AFS Transactions, 1999, V.107, pp.161-167.
- 24 Matweb, "Aluminum Alloy Temper Designations", online 2005, [http://www.matweb.com/reference/aluminum\\_temper.asp](http://www.matweb.com/reference/aluminum_temper.asp).
- 25 Mei, Li, Vijayaraghavan, Ravi, Prabhu, Eben, Xuming, Su, Singh, Gurinder, Zagajac, Jovan, and Allison, John E., "Development and Applications of OPTCAST –A Thermal Boundary Conditions and Casting Process Optimization Tool", International iSIGHT Automotive Conference, 2003.
- 26 Monroe, R., "Porosity in Castings", American Foundry Society, online 2005, [www.moderncasting.com/archive/WebOnly/0905/WebOnly0905.pdf](http://www.moderncasting.com/archive/WebOnly/0905/WebOnly0905.pdf)/Ultimate Tensile Strength vs Hydrogen Porosity for Cast Aluminum.
- 27 OriginLab Corporation, "Origin: Data Smoothing", online 2006, [www.originlab.com/index.aspx?s=8&lm=115&pid=109](http://www.originlab.com/index.aspx?s=8&lm=115&pid=109)
- 28 Pyrotek Inc, "STAR™ 3000 fixed degasser", online 2005, [www.metallics.com/star.html](http://www.metallics.com/star.html).
- 29 Roberts, S. G., "Aluminium, Magnesium and Titanium Alloys", Department of Materials Science and Engineering, Ohio State University. online 2006, [www.sgrgroup.materials.ox.ac.uk/lectures/alloy\\_handout\\_1.pdf](http://www.sgrgroup.materials.ox.ac.uk/lectures/alloy_handout_1.pdf).
- 30 Sehitoglu, H, Engler-Pinto Jr. Carlos C., Maier, Hans J., Foglesong, Tracy. J., "Thermo-Mechanical Fatigue of Cast Mechanical Fatigue of Cast 319 Aluminum Alloy", University of Illinois at Urbana, Ford Motor Company Universität-GH Paderborn, Exxon, online 2005, [www.mechse.uiuc.edu/media/pdfs/about/research/fcp/Sehitoglu\\_presentation.pdf](http://www.mechse.uiuc.edu/media/pdfs/about/research/fcp/Sehitoglu_presentation.pdf).
- 31 Sokolowski, J. H., and Kierkus, C. A., "The Effect of the 319 Aluminum Alloy Sample Preparation Technique on Optical Emission Spectrometer Response", Advanced Materials Processing Technology, 2001.
- 32 Sokolowski, J. H., Kierkus, C. A., Brosnan, B. and Evans, W. J., "What Causes Electromagnetic Pump Clogging", online 2005, [www.allbusiness.com/periodicals/article/448305-1.html](http://www.allbusiness.com/periodicals/article/448305-1.html).
- 33 Sparkman, D., Kearney, A. "Breakthrough in Aluminum Alloy TA Technology for Process Control" Transactions of the American Foundry Society, V102 , 1994, Paper 94-13, pp. 455-460. online 2006, [www.fissys.com/new-docs/default2.html](http://www.fissys.com/new-docs/default2.html).
- 34 Triveño Rios, C.; Caram, R.; Bolfarini, C.; Botta, W.J. F. and Kiminami, C.S., "Intermetallic Compounds In The Al-Si-Cu System", V12, No. 1 acta microscopica. 2003.

35 WAP, Nematik of Canada Windsor Aluminum Plant, Personal Communication, 2004.

### VITA AUCTORIS

Dilon Yousif was born in Baghdad, Iraq in 1978. He moved to Canada in 1996 and graduated from Catholic Central High School in 1997. From there he went on to the University of Windsor, Ontario, where he obtained a BAsC. in Mechanical Engineering with a Materials Option Co-op in 2001.